NBER WORKING PAPER SERIES

ENVIRONMENTAL DRIVERS OF AGRICULTURAL PRODUCTIVITY GROWTH: CO_2 FERTILIZATION OF US FIELD CROPS

Charles A. Taylor
Wolfram Schlenker

Working Paper 29320
http://www.nber.org/papers/w29320

NATIONAL BUREAU OF ECONOMIC RESEARCH
1050 Massachusetts Avenue
Cambridge, MA 02138
October 2021, Revised December 2025

We would like to thank seminar participants at the Harvard Agriculture and Climate Workshop, Agricultural & Applied Economics Association (AAEA) annual meeting, Auburn University, University of British Columbia, UC Berkeley, Yale University, and the University of California (UC-wide) environmental economics seminar for useful comments. We thank Anika Fergusson and Sherry Tang for their research assistance. This work was supported by USDA National Institute of Food and Agriculture, Grant No. 2022-67023-36400. The views expressed herein are those of the authors and do not necessarily reflect the views of the National Bureau of Economic Research.

Environmental Drivers of Agricultural Productivity Growth: CO_2 Fertilization of US Field Crops

Charles A. Taylor and Wolfram Schlenker

NBER Working Paper No. 29320
October 2021, Revised December 2025
JEL No. N52, Q11, Q54

ABSTRACT

We present a novel methodology to estimate the CO_2 fertilization effect on crop yields using data from NASA's Orbiting Carbon Observatory satellites. Our study complements field and chamber experiments by examining county-level crop yields under actual growing conditions across the majority of US cropland. For identification, we utilize remotely sensed, year-to-year CO_2 anomalies from county-specific trends and further instrument for these anomalies using wind patterns. We find a CO_2 fertilization effect greater than that reported in most field and chamber experiments. In a thought exercise, we apply the CO_2 fertilization effect estimated in our sample from 2015–2022 backward to 1940. Assuming no other limiting factors, we find that rising CO_2 was a major driver of past yield growth, particularly for wheat—with important implications for estimates of future climate change damages.

Charles A. Taylor
Harvard University
Harvard Kennedy School
and NBER
ctaylor@hks.harvard.edu

Wolfram Schlenker
Harvard University
Harvard Kennedy School
and NBER
wolfram_schlenker@hks.harvard.edu

An understanding of the drivers of agricultural productivity is critical for explaining patterns of economic growth within the farm sector and across other sectors of the economy. For example, the adoption of high-yield varieties had significant positive economic spillovers in India (Gollin et al., 2021) and other countries more generally (McArthur and McCord, 2017).

The "Green Revolution" brought about a massive increase in crop yields across the world. In the US, for example, corn yields increased sixfold since 1940, while soybean and wheat yields increased by a factor of three. Prior to this point, however, yields fluctuated around a constant mean, as shown in Figure 1. By extension, productivity of the agricultural sector increased rapidly (Jorgenson and Gollop, 1992). Before 1950, US farm sector productivity growth was half that of the non-farm sector, but afterwards the relationship reversed, with farm productivity growth exceeding the non-farm sector by 62% (Pardey and Alston, 2021). Factors such as increased input usage, mechanization, irrigation, and improved crop genetics all contributed to yield growth (Wang et al., 2015). But since aggregate US farm output increased several-fold while the aggregate quantity of inputs (land, capital, labor, and materials) stayed flat, technology is generally seen as the main driver of agricultural productivity growth.

This paper argues that carbon dioxide (CO_2) fertilization[1] may help illuminate the puzzling conclusion of Jorgenson and Gollop (1992): why did productivity growth explain over 80% of agriculture's postwar growth but less than 15% in the non-farm economy? During this time, both atmospheric CO_2 and crop yields were steadily increasing as shown in Figure 1. The physiological response of plants to CO_2 is well-known: CO_2 drives photosynthesis and has long been used as a greenhouse input to boost yields. Over the last 40 years, half of the world's vegetated area has undergone greening, of which 70% is attributed to elevated CO_2 (Zhu et al., 2016).[2]

Our paper investigates the extent to which elevated CO_2 contributed to the observed increase in US crop yields over time. Establishing a causal link between two trending variables is statistically challenging. CO_2 has risen smoothly in tandem with crop yields as well as other factors such as mechanization and input use. Industrialization, both in agriculture and other sectors, could have independently increased CO_2 levels as well as yields—making it difficult to disentangle CO_2 fertilization from other productivity drivers.

[1]The CO_2 fertilization effect is defined in the scientific literature as the increase in photosynthetic activity in response to elevated CO_2. In this paper, we use the term more specifically to refer to an outcome of increased crop yields.

[2]That paper defines "greening" as an increase in the growing season integrated leaf area index.

We develop a new approach to estimate the effect of CO_2 on crop yields that relies on neither process-based models nor localized field experiments, while enabling analysis of most US cropland. We use observed ambient CO_2 data from NASA's Orbiting Carbon Observatory (OCO) satellites (OCO-2 and OCO-3) and link it to county-level crop yield data in the United States. The OCO satellites detect changing ambient CO_2 levels that occur within and across locations and the growing season (Crisp, 2015). While CO_2 mixes in the atmosphere, there are temporal and spatial deviations due to variance in CO_2 sources and sinks and changing atmospheric conditions and wind patterns (see Appendix Figure D1 for an illustration from 2019). We focus on the US as it is the largest producer of corn and soybeans, accounting for 33% of global production (FAOSTAT) over our sample time frame, and 7% of global wheat production.

We use several empirical approaches that isolate both time-series and cross-sectional variation in CO_2 levels. In assessing causal impacts, a major identification concern involves the potential correlation of CO_2 anomalies with other factors that influence crop yields. One could imagine several such confounders related to agricultural practices, fossil fuel production, urbanization, and large-scale weather systems. While we control for such factors when possible, we employ an instrumental variables approach that leverages wind variation. We instrument for CO_2 exposure in a county using upwind CO_2 concentrations. Our results are robust to myriad sensitivity checks, i.e., the functional form (logarithmic versus levels), whether the temporal trend is by state or county, sample selection, and the choice of controls for co-occurring air pollutants. We bolster our findings with a national-level time series analysis using Mauna Loa measurements from 1958–2024, which produces consistent estimates of the CO_2 fertilization effect, particularly for wheat.

We consistently find significant CO_2 fertilization effects on US yields: a 1 part per million (ppm) increase in CO_2 equates to yield increases of 0.17%, 0.20%, and 0.55% for corn, soybeans, and winter wheat, respectively, in our preferred IV model.[3] Our estimates are on the higher end of those found in the agronomic literature, a fact we discuss in more detail in Section 5. We see the major contributions as follows:

First, this paper provides an example of how satellite-based measures of CO_2 can complement field experiments to ensure external validity of CO_2's effect on agriculture and ecosystem functioning at a global scale. We measure the effect under real-world growing conditions.

[3]This is after adjusting by a scaling factor to account for the fact that CO_2 varies more at ground level than it does across the total air column observed by the satellite, further explained in equation (3) below.

Second, our finding that CO_2 fertilization has driven a significant portion of the historical increase in crop yields—particularly for wheat—has implications for how we think about the drivers of agricultural productivity growth, which has very large economic spillovers (Gollin et al., 2021), and the contribution of environmental factors versus technological change to this growth.

Third, our results shed light on a driver of yield growth that is usually taken as exogenous. The recent literature has used panel variation to estimate climate change damages by relating outcomes to random exogenous year-to-year weather fluctuations (Dell et al., 2014). This approach, which relies on annual variation in weather, does not take into account longer-term dynamics that are correlated with climate change. Consequently, part of the estimated damages may be offset by yield gains from rising CO_2.

Fourth, our results are relevant for estimating the impact of climate change on agriculture. There is a disconnect between process-based studies of climate change, which incorporate CO_2 fertilization, and statistical studies, which tend to omit this factor (Lobell and Asseng, 2017). As a result, estimates of climate impacts can vary widely. For example, one study finds that the net welfare effect on agriculture is negative in the absence of CO_2 fertilization but negligible when fertilization is included (Moore et al., 2017a).[4]

Fifth, as many previous studies have suggested, the CO_2 fertilization effect varies across crop types and environmental conditions, raising the possibility that global inequalities could be exacerbated, since the welfare effects of climate change on agriculture vary across regions even before considering CO_2 fertilization (Nath, 2025; Hultgren et al., 2025). The implication is that yields in areas with few limiting conditions (e.g., nutrient deficiency)—which tend to be higher to begin with—might grow more than in areas facing greater constraints. This would widen the yield gap and alter the comparative advantage between countries (Costinot et al., 2016). The importance of the CO_2 fertilization effect was also emphasized in a recent report on the economic costs of climate change in the US,[5] which argued that US agriculture could benefit from climate change (U.S. Department of Energy, 2025).[6]

[4]Recent research places the social cost of carbon (SCC) at \$185 per ton CO_2, with agricultural impacts contributing \$84 per ton—almost half the total—in one model. However, the uncertainty surrounding the interactions between CO_2, temperature, and crop yields produces a wide confidence interval for agriculture's contribution to the SCC, ranging from -\$23 to \$263 per ton CO_2 (Rennert et al., 2022; Moore et al., 2017b). Hultgren et al. (2025) estimates a partial SCC from agriculture between \$1 and \$49 per ton CO_2, depending on modeling assumptions.

[5]The report cited an earlier version of this paper. The principal change since that version is that we now scale our estimates by the factor κ, as specified in equation (3).

[6]Some argue that CO_2 fertilization is understood well enough to be directly included in global climate models and impact projections (Toreti et al., 2020; Rezaei et al., 2023; Makowski et al., 2020).

Finally, we emphasize that the strong fertilization effect we observe occurs under current day CO_2 levels and environmental conditions. The experimental evidence indicates a tapering of the CO_2 fertilization effect at higher concentrations, so any linear extrapolation of our estimates into the future should be approached with caution. While previous studies have projected weather changes into the future—justified in part by the observation that existing cross-sectional yield differences across climates resemble those identified from weather variation in panel data (Schlenker and Roberts, 2009)—a similar approach is not warranted for CO_2. In other words, while we can currently observe hot locations (which provide a useful counterfactual for warming's impact on cooler locations), we do not have equivalent real-world data for places with substantially higher CO_2 concentrations.

Our paper proceeds as follows: Section 1 provides some background on the CO_2 fertilization effect and current estimates. Section 2 describes how we construct our CO_2 anomaly measure from the OCO-2 satellite data product, as well as the other datasets used in this analysis. Section 3 describes our identification strategies and empirical approaches before Section 4 presents our regression results along with robustness tests. The implications of these results are discussed in Section 5 by exploring the scientific and policy implications of our study before Section 6 concludes the paper.

1 Background on CO_2 Fertilization

Plants respond directly to rising CO_2 through photosynthesis and stomatal conductance, which is the basis for the fertilization effect (Long et al., 2004; Ainsworth and Rogers, 2007). This response has been known for over 200 years. The role of CO_2 in plant growth was first demonstrated in 1796 by Swiss botanist Jean Senebier, and CO_2 gas has long been pumped into greenhouses to spur photosynthesis and increase the yield of horticultural crops, especially during daytime hours, when photosynthesis reduces the amount of available CO_2 in the greenhouse. The fact that greenhouse operators pay to pump CO_2 into their chambers showcases that CO_2 is an input that meaningfully enhances yields. Optimal levels are reported to be in the range of 800-1000 ppm, more than twice the current atmospheric CO_2 concentrations of 420 ppm (Wang et al., 2022).

The fertilization process varies by crop type. For C3 crops like soybeans, wheat, and rice, mesophyll cells containing RuBisCO are in direct contact with the air. RuBisCO is an enzyme that fixes atmospheric CO_2 during photosynthesis. Thus, higher ambient CO_2 increases photosynthetic CO_2 uptake because RuBisCO is not CO_2-saturated at today's atmospheric

levels (Long et al., 2004). For C4 crops like corn, on the other hand, RuBisCO is located in bundle sheath cells, where CO_2 levels are several times higher than atmospheric levels. At this concentration, RuBisCO is CO_2-saturated and a direct photosynthetic response to changing atmospheric CO_2 levels is limited. However, C4 yields respond indirectly to elevated CO_2, mainly through increased water use efficiency driven by reduced stomatal conductance (Long et al., 2006). All things being equal, one would expect a larger CO_2 fertilization effect for wheat and soybeans than for corn.

Historical estimates of yield responses to CO_2 came from controlled experiments in laboratories and greenhouses, where CO_2 levels can easily be controlled. There are clear advantages to such experiments, i.e., the ability to isolate change in one variable: CO_2. This approach, however, faces challenges of its own. The conditions in a well-controlled experiment might not be indicative of real-world farming conditions. Large regional differences in crop responses to CO_2 reflect geographic variation in crop distribution and environmental conditions (McGrath and Lobell, 2013). CO_2 fertilization may be negligible in the presence of limiting factors such as nutrient deficiency (Kimball et al., 2001; Hungate et al., 2003; Reich et al., 2006; Ziska and Bunce, 2007). The effect is generally stronger under water deficit conditions (Ottman et al., 2001; Leakey et al., 2006; Keenan et al., 2013; Morgan et al., 2011), with the exception of soybeans (Gray et al., 2016) and possibly rice (Zheng et al., 2020). Elevated CO_2 may also increase high temperature stress due to stomatal closure (Batts et al., 1997).

Differences in observed outcomes across field experiments suggest that the CO_2 fertilization effect crucially depends on other limiting factors and field conditions; yet, there is only one major agriculture-focused CO_2 enrichment experiment in the breadbasket of the US, the Midwest: SOYFACE, which is located at the University of Illinois and focuses mainly on soybeans. Whether this experiment station is representative of diverse real-world growing conditions is doubtful.

There are other downsides of controlled field experiments: they can suffer from significant measurement error due to the difficulty of controlling elevated CO_2 concentrations in turbulent air (Allen et al., 2020). In other words, the CO_2 that is pumped into the experimental plots might dissipate too quickly or lead to large pulses in CO_2 rather than achieve the permanent level of elevated CO_2 the experiment is designed to simulate. Although CO_2 enrichment experiments have generated important insights into the physiological channels of the fertilization effect and its environmental interactions, they are limited in the extent to which they reflect growing conditions on commercial farms at a large geographic scale, as

well as the background process of gradually increasing ambient CO_2.

We next turn to the range of estimates found in field and chamber experiments. An early survey concluded that doubling ambient CO_2 increased yields by 24-43% for C3 crops in the context of full water and nutrient availability (Kimball, 1983), which aligned with USDA reporting a 33% increase in yields for most crops under similar settings (Allen Jr et al., 1996). Another study estimated that CO_2 could have accounted for 15% US soybean yield growth from 1972 to 1997 (Specht et al., 1999).

In recent decades, free-air concentration enrichment (FACE), a process involving a series of pipes in fields that emit CO_2, has allowed for larger-scale trials under more realistic crop-growing conditions. A survey of over 25 years of FACE experiments concludes that increasing CO_2 from 353 to 550 ppm results in 19% higher C3 yields, on average, while C4 crops were only affected under conditions of water scarcity (Kimball, 2016). FACE experiments tend to show a lower fertilization effect than laboratory or greenhouse enclosure studies (Long et al., 2006). However, recent work has pointed out potential measurement error, arguing that FACE estimates may need to be adjusted upward by 18-50% to account for the effect of air turbulence and short-term CO_2 fluctuations, whereby crops in FACE experiments experience a 10-times greater range in CO_2 fluctuations compared to crops under natural conditions (Allen et al., 2020, 2025).

Given the heterogeneous CO_2 fertilization effect, which varies according to other limiting factors, an outstanding question pertains to the external validity of these field experiments—specifically, what the correct average effect is under real-world growing conditions. This issue is especially pertinent because the geographic extent of FACE experiments is limited: there are only two long-standing agricultural FACE sites in the US—Arizona FACE in Maricopa, AZ, and SOYFACE in Champaign, IL—with only the latter located in the traditional Midwestern breadbasket. This motivated us to use satellite data to measure the effect under actual growing conditions. We note other recent work using OCO-2 satellite data to estimate the impact of the 2019 Midwestern floods on CO_2 uptake and crop productivity (Yin et al., 2020).

2 Data

Yield Data

Our dependent variables are county-level crop yields for corn, soybeans, and winter wheat and were obtained from USDA's National Agricultural Statistics Service. Note that the USDA stopped reporting county-level wheat yields after 2023. See Figure A4 for the number of counties that report yields in our datasets.

CO_2 Data

Our primary measure of atmospheric CO_2 comes from two Orbiting Carbon Observatory (OCO) products, OCO-2 and OCO-3. Launched in 2014, OCO-2 is NASA's first satellite specifically designed to measure atmospheric CO_2 with the aim of better understanding the geographic distribution of CO_2 sources and sinks and their changes over time. We downloaded the bias-corrected OCO-2 LITE Level 2 v11 product, specifically the dry-air mole fraction of CO_2 averaged over the atmospheric column (XCO2) in parts per million (ppm). The satellite has a sun-synchronous orbit with an equatorial crossing time at 13:30 hours and a repeat cycle of 16 days. Each frame records eight adjacent footprints ($\sim$1.29 $\times$ 2.25 km), yielding a swath $\sim$10 km wide. A typical daily output contains over 150,000 XCO2 global readings, including the latitude-longitude point. About 50% of readings have quality flags, which we exclude from our analysis.

We also incorporate CO_2 data from OCO-3, which was launched in 2019. This spectrometer is similar to OCO-2 and produces comparable XCO2 retrievals, but was mounted on the International Space Station (ISS). Because the ISS flies a precessing orbit between 52°S and 52°N, OCO-3 samples a range of local times from dawn to dusk in contrast to the fixed early afternoon sampling of OCO-2. As an added feature, OCO-3 has a two-axis pointing mirror that allows for dense scans of areas of interest, such as cities and point sources.

In our baseline analysis, we pool readings from OCO-2 and OCO-3 to calculate the annual crop-specific CO_2 measure for each county and crop from 2015 to 2022. A detailed description of the aggregation procedure is given in Appendix A.

Figure A3 displays the resulting number of observations per county in the dataset, i.e., where CO_2 readings and annual crop yield data are available over the eight years from 2015 to 2022. Given the satellites' high resolution, the relatively long revisit time (16-days for OCO-2), and the size of the median US county (1,610 km^2), CO_2 readings are not obtained for each US county in each year. Since we include both county fixed effects and county-specific annual time trends, we need at least three degrees of freedom per county, i.e., we can

only include counties with at least 3 observations in our regressions. The resulting average number of counties with observations per year is 1196 for corn, 1064 for soybeans, and 747 for wheat.

Flux Tower Data

Our analysis uses satellite-derived measures of CO_2 levels in the air column below it. A common issue with remotely-sensed products is whether the data captured across the entire column is indicative of the conditions found at the ground level, in our case, the crop canopy. We examine this issue using *in situ* flux towers from the AmeriFlux network, which, importantly for us, measure CO_2 levels at various heights of the tower. Appendix C outlines our steps: we first compute year-to-year CO_2 anomalies accounting for annual time trends. We then calculate the standard deviation of these anomalies across flux towers and at different instrument heights, which can be visualized in Figure C2.

We then contrast the average flux tower variability with OCO satellite variability at the same locations, as reported in Table 1. The standard deviation calculation for OCO mirrors the processing of the flux tower data. Specifically, we select all OCO readings within a 0.1° radius of each flux tower. We processed these readings following the steps in Appendix A, which include averaging seasonally-adjusted values over April–September and accounting for a location-specific fixed effect and location-specific linear time trend. Across flux towers with overlapping data, the standard deviation at 2 m (closest to ground level) is about 4.5 times larger, on average, than the variability in the OCO satellite column average.

Weather Data

For weather, we use a recalculated version of the fine-scale PRISM data at the same 2.5-minute resolution, or 4.5 km by 4.5 km, that maintains the set of weather stations constant over time. We follow the approach of Schlenker and Roberts (2009), which found that four weather variables (two temperature, two precipitation) are good predictors of crop yields. The two temperature variables are degree days 10-29°C (moderate degree days) and degree days above 29°C (extreme degree days) for corn. The upper bound is slightly higher for soybeans, resulting in degree days 10-30°C and degree days above 30°C. We use the same degree day variables for winter wheat as for soybeans. In each regression, we also include a quadratic of season-total precipitation. Precipitation and degree days are summed across the six-month growing season from April to September and spatially averaged using the same PRISM grid weights as for the CO_2 data based on USDA's Cropland Data Layer for each

county.

Air Pollution Data

Air pollution data come from the EPA's national network of pollution monitors. We use hourly data from the EPA's Pre-Generated Data Files[7] for five major pollutants: Ozone O_3 (44201), sulfur dioxide SO_2 (42401), carbon monoxide CO (42101), nitrogen dioxide NO_2 (42602), and particulate matter PM_{10} Mass (81102). We use the spatial interpolation approach of Boone et al. (2019) to get the pollution variables at the PRISM grid, and then take the crop area-weighted average (again using the Cropland Data Layer, similar to what was used for CO_2 and weather) of all grids in a county across the six-month growing season from April to September.

Additional Data

For the analysis of long-term trends in vegetation density, we use NOAA's Advanced Very High Resolution Radiometer (AVHRR) satellite measure of Normalized Difference Vegetation Index (NDVI) at 0.05° resolution, or 5.6 km at the equator (Vermote et al., 2014). Accessed through Google Earth Engine, the advantage of AVHRR relative to MODIS and other, more recent, remote sensing products is its three-decade time span encompassing growing seasons from 1982 to 2013.

In a sensitivity check in Appendix B we focus on innovations in the annual time series of growing season CO_2 levels as recorded at Mauna Loa Observatory, Hawaii.

There are other potential CO_2 data sources: the OCO-2 GEOS Level 3 daily product, which gap-fills observations in time and space using short transport simulations from the GEOS atmospheric model (Weir and Ott, 2022) and is utilized for the monthly visualization of CO_2 anomalies in Figure D1. Another is NOAA's CarbonTracker, which is based on air sample measurements across 460 global sites and an inverse model of atmospheric CO_2 that adjusts surface-level uptake and releases to align with observational constraints (Jacobson et al., 2020). We prefer the OCO-2 and OCO-3 Level 2 satellite products due to their minimal processing, thus avoiding endogeneity concerns arising from the modeling assumptions behind the OCO-2 Level 3 and CarbonTracker products in relation to weather and vegetation dynamics, or ground-level confounders such as local pollution and economic activity. Further, reanalysis products may suffer from the promulgation of interpolation errors (Parker, 2016).[8]

[7] Available `https://aqs.epa.gov/aqsweb/airdata/download_files.html`

[8] Nevertheless, we replicate our main analysis using CarbonTracker data and find a statistically significant

3 Model and Empirical Strategy

To estimate the CO_2 fertilization effect across US croplands, we first need to link OCO satellite data with US county-level yield data. The latter is observed once per year and we hence need to aggregate the CO_2 exposure to the annual level. There are several identification challenges to address. While gaseous CO_2 ultimately diffuses across space and becomes uniformly distributed in the atmosphere,[9] this process occurs over weeks to months and is affected by specific emission events, local CO_2 sources and sinks, as well as wind and weather dynamics (Hakkarainen et al., 2016; Massen and Beck, 2011). Spatial variation in CO_2 exposure at any given time is driven by such disturbances. Figure D1 visualizes this variation across the US during each month of the growing season in an example year, 2019. Taking Nebraska as an example, we see that in April, CO_2 exposure is low compared to the US average, high in May, lower in June, neutral in July, high in August, and lower in September.

Our empirical approach links local variation (i.e., anomalies) in CO_2 around its location-specific trend to fluctuations in crop yields. We combine the CO_2 and yield data at the county-year level with weather outcomes for the areas where corn, soybeans, and winter wheat are grown within each county, respectively. All models use CO_2 anomalies in parts per million (ppm), adjusted for seasonality and annual trends as described in Appendix A, and the natural logarithm of county-level yields as the outcome variable, unless otherwise noted.

Focusing on the US, a top global agricultural producer, our primary analysis encompasses counties east of the 100° meridian for corn and soybeans—the same set of counties used in Schlenker and Roberts (2009). Because winter wheat is grown farther west, we use all states east of the Rocky Mountains as the baseline for wheat. These areas account for the vast majority of US row crop production. As a sensitivity check, we conduct our analysis on the entire continental US and other subsamples, as visualized in Figure A3.

Panel model

The setup of our panel model is similar to empirical specifications that link annual crop yields to weather and pollution outcomes. Specifically, we regress log yields on CO_2, while

CO_2 fertilization effect at the county level in the US (available upon request). They are larger for corn than what we find in the analysis using satellite data, and smaller for wheat.

[9] The spatial diffusion of CO_2 is what makes climate change a global public goods problem. It also allows scientists to rely on singular sources of long-term CO_2 measurements, such as the Mauna Loa Observatory, to estimate global CO_2 levels, which are then incorporated into global process-based models.

controlling for the four weather variables that were found to best predict corn and soybean yields (Schlenker and Roberts, 2009), as well as criteria air pollutants (CO, NO_2, O_3, PM_{10}, SO_2). The panel model includes county fixed effects to account for differences in average yields across counties driven by factors such as soil quality and average climate, as well as county-specific time trends to account for local trends in yields—helping to guard against spurious correlation with trending variables such as CO_2. Figure 2 illustrates the variation leveraged in the panel model, highlighting the correlation in Macoupin County, Illinois, which is downwind from St. Louis. The panel model specification is:

$$y_{it} = \alpha_{i0} + \alpha_{i1} t + \beta \; c_{it} + \boldsymbol{\gamma} \mathbf{W}_{it} + \boldsymbol{\delta} \mathbf{P}_{it} + \epsilon_{it} \tag{1}$$

where y_{it} is the log crop yield in county i and year t; α_{i0} is a county fixed effect; α_{i1} is a county-specific time trend; β measures the observed CO_2 fertilization effect from the CO_2 anomaly c_{it} in county i in year t;[10] and $\boldsymbol{\gamma}$ is a vector of coefficients for weather variables $\mathbf{W}_{it}$ (which includes two temperature degree day variables, precipitation, and precipitation squared, all summed over the six-month growing season, fixed as April–September for all crops); $\boldsymbol{\delta}$ is a vector of coefficients for the five criteria air pollutants $\mathbf{P}_{it}$ (CO, NO_2, O_3, PM_{10}, SO_2), calculated as daily means averaged over the growing season April-September. The error terms, ϵ_{it}, are clustered at the state level to account for spatial correlation and common state-level policy.

The effect of year-to-year weather fluctuations on annual yield outcomes are clearly visible in Figure 1, where, for example, there is a significant reduction in national corn yields in 2012, when the Corn Belt experienced a major extreme heat event.

Identification remains challenged by several factors. There is the possibility that local drivers of CO_2 anomalies could also affect yields. For example, intense agricultural activity, fossil fuel production, or nearby urbanization might correlate with both higher CO_2 and higher yields, potentially biasing estimates upward. However, we expect downward biases to dominate for two reasons: first, reverse causality implies that higher yields (and thus higher photosynthetic activity) reduce local atmospheric CO_2, creating a negative correlation; second, CO_2 anomalies often co-vary with yield-damaging pollutants, further contributing to a downward bias in our estimates. While we control for confounders where possible, we next adopt an instrumental variables approach that uses CO_2 anomalies in upwind counties to

[10]The Frisch–Waugh–Lovell theorem implies that including α_{i0} and α_{i1} is equivalent to first regressing both the dependent and all independent variables on α_{i0} and α_{i1}, and then using the resulting residuals (i.e., anomalies around a trend) in the regression equation.

ensure that local CO_2 levels are not driven by local conditions. Given the likely net downward bias, we would expect the estimates to increase once we employ our IV setup.

Wind instrument

Wind direction is often employed in health economics to obtain exogenous variation in pollution exposure (Schlenker and Walker, 2016; Deryugina et al., 2019). In the context of our study, CO_2 levels and fluxes are related to the wind direction at localized CO_2 emission sources (Coutts et al., 2007; Massen and Beck, 2011; García et al., 2012; Xueref-Remy et al., 2018). And while there are non-wind drivers of CO_2 anomalies, like power plants, vegetation, and geysers, these features vary far less over time and space than the relatively random atmospheric phenomena that influence wind patterns.

One limitation of this instrument is that wind-driven CO_2 exposure could also be correlated with other co-occurring pollutants. We try to address this by explicitly controlling for the five criteria air pollutants. In any case, given the negative effect of pollutants like ozone on crop yield (Boone et al., 2019), this would likely bias our estimates downward.

Figure 3 shows our approach to deriving a wind instrument that follows Braun and Schlenker (2023) by pairing a county with the neighbor that is most frequently upwind during the growing season April-September. We outline the exact procedure in Appendix A.2.

The strength of the upwind relationship is an important consideration. Figure 4 displays the number of hours that the "upwind" county is actually upwind in a given year for each crop. A lower number of hours indicates that wind direction varies across many upwind counties over the growing season. For example, a value of 1,000 hours means that the county most frequently upwind is in fact upwind 23% of the time.[11] In our IV regression, we vary the minimum number of upwind hours required for a county to be considered "upwind" and thus included in our sample. Summary statistics relating to the IV setup are presented in Table A1. The wind IV implies the following first stage:

$$c_{it} = a_{i0} + a_{i1}t + b\, c_{it}^{[upwind]} + \boldsymbol{\eta}\mathbf{W}_{it} + \boldsymbol{\theta}\mathbf{P}_{it} + e_{it} \tag{2a}$$

$$y_{it} = \alpha_{i0} + \alpha_{i1}t + \beta\ c_{it} + \boldsymbol{\gamma}\mathbf{W}_{it} + \boldsymbol{\delta}\mathbf{P}_{it} + \epsilon_{it} \tag{2b}$$

where items are defined as in equation (1) for the panel model, except that β measures the observed CO_2 fertilization effect from the instrumented CO_2 value (c_{it}), and $c_{it}^{[upwind]}$ is the

[11] 23% equals 1,000 divided by the 4,392 hours in the growing season.

instrument using the CO_2 value from the county that is most frequently upwind in that year based on the hourly wind data. Note that the upwind county can change year-to-year.

Variation in CO_2 Anomalies in the Crop Canopy versus Satellites

Before we present the results of our empirical analysis linking county-level crop yields in commercially-farmed fields in the US to satellite measurements of CO_2, we discuss a scaling issue to adjust for the different variances of CO_2 anomalies in the crop canopy compared to what is measured by satellites in the entire air column.

CO_2 levels vary not only in space but also with altitude. Our remotely-sensed data come from satellites that measure CO_2 across the entire atmospheric column, i.e., the air mass between the satellite and the ground. What matters for plants, however, is the variation in CO_2 within the canopy at ground level, not at higher altitudes.

Concentrations across the air column are related through diffusion processes. Temporary CO_2 disturbances at ground level due to ground sources dissipate with altitude. As a result, the variation observed in the satellite data is likely smaller than the actual ground-level variation (Keppel-Aleks et al., 2011; Broquet et al., 2018), which can lead to an upward bias in the estimated CO_2 fertilization coefficient.

An example may illustrate this point: assume that CO_2 anomalies in the crop canopy have a standard deviation of $\sigma_{\text{fluxTower}}$ =4.5 ppm, an amount which boosts crop yields by 1%. The CO_2 fertilization effect would then be $\frac{1\%}{4.5\,\text{ppm}} = 0.22$ percent per ppm. However, ground-level shocks dissipate with altitude. For illustrative purposes, suppose the 4.5 ppm anomaly at ground level is reduced to an additional 1.5 ppm at 100 meters and declines exponentially at higher altitudes. Assume the variation detected by the satellite, averaged across altitudes, is thus only σ_{OCO} =1 ppm for the original 4.5 ppm ground-level anomaly. Using the uncorrected satellite reading would upwardly bias the CO_2 fertilization effect to $\frac{1\%}{1\,\text{ppm}} = 1$ percent per ppm. To address this, we scale (multiply) by the ratio of the variation in CO_2 observed across the atmospheric column to the variation at ground level, which in this case would be by multiplying by the factor $\frac{1}{4.5} = \frac{2}{9}$.[12] More specially, the scaling factor is:

$$\kappa = \frac{\sigma_{\text{OCO}}}{\sigma_{\text{fluxTower}}} \tag{3}$$

Figure C2 shows that the standard deviation—i.e., the variability—of CO_2 anomalies indeed decreases with altitude using data from AmeriFlux towers, as described in the Data

[12]The general concern about how well remotely-sensed measurements capture ground-level conditions is increasingly addressed in the economics literature; see, e.g., Fowlie et al. (2019); Proctor et al. (2023).

Section and Appendix C. The results hold whether we use all towers or only those over cropland areas. We derive the standard deviation in the crop canopy as the predicted value at a height of 2 meters, which roughly matches the average height of weather stations that measure temperature.

We next compute the variation in CO_2 satellite readings at the locations of the flux towers.[13] Table 1 presents results for all flux towers (first two columns) and just those located in cropland areas (last two columns). Since our empirical analysis focuses on US crop yields, we provide results for both the entire world and for towers located only in the United States. Panel A displays the variability observed in the remotely-sensed satellite data, while Panel B shows the results using flux tower data. The different sub-panels vary the selection of locations, for example, including (i) any location where a tower ever reported data; (ii) restricting to only the years used in our analysis, 2015–2022; or (iii) restricting to locations present in both datasets.

Two findings emerge: first, the standard deviation in our county-level satellite measure of CO_2, σ_{OCO}, ranges from 1.01 for wheat to 1.16 for soybeans, matching the value observed in Panel A2 around flux tower locations. In other words, the satellite-measured variation at flux tower sites is representative of the satellite-measured variation across US counties more generally. Second, we obtain an average $\sigma_{\text{fluxTower}}$ of 4.5 when including all global flux towers or cropland towers. Subsetting the data to include only US towers, or restricting to a subset of years, reduces the number of observations and yields a noisier signal, which can sometimes be larger or smaller, but on average remains close to 4.5.

When taking the ratio of these standard deviations ($\kappa = \sigma_{\text{OCO}}/\sigma_{\text{fluxTower}}$), we obtain a value of approximately 1/4.5 (see Table 1). This implies that the variation at ground level is about 4.5 times larger than what is observed in the atmospheric column. Since the OCO satellite detects a dampened signal, the raw regression coefficients will be inflated by this same factor. Thus, going forward we scale all our regression results by multiplying by κ (equivalent to dividing by 4.5) to recover the crop canopy level effect of CO_2 fertilization.

[13] The calculation of σ_{OCO} mirrors that of $\sigma_{\text{fluxTower}}$. Specifically, we select all OCO readings within a 0.1° radius of each flux tower, seasonally adjusted readings following the steps in Appendix A, average them over April–September of each year, and then account for linear time trends.

4 Results

Panel Regression

The results of our panel model testing the relationship between CO_2 anomalies and county-level crop yields in the US are presented in Table 2. We present three specifications: column (a) includes only county fixed effects and county-specific time trends, column (b) adds the four weather variables ($\mathbf{W}_{it}$ in equation (1)), and column (c) adds five criteria air pollutants ($\mathbf{P}_{it}$ in equation (1)). Our preferred model specification is the full model in column (c); however, we find a statistically significant CO_2 fertilization effect in all specifications for all three crops.

When moving from column (a) to (b), the CO_2 fertilization effect increases for all three crops. This finding is consistent with our hypothesis that omitting weather variables will downwardly bias the results, as weather influences yields, which in turn affects photosynthesis and CO_2 levels. This creates a negative feedback loop between yields and CO_2 levels, as higher yields imply lower CO_2 concentrations. The effect is more pronounced for corn and soybeans, as our weather measures are tailored to those crops, while the effects of weather on wheat yields vary across seasons in more complex ways (Tack et al., 2015).[14]

Finally, when also controlling for pollution in column (c), the CO_2 fertilization effect increases very slightly for corn and soybeans, and decreases for wheat. We find that a 1 ppm increase in CO_2 equates to yield increases for corn, soybeans, and winter wheat of 0.12%, 0.13%, and 0.19%, respectively. The fertilization effect is smaller for corn (a C4 crop) and greater for soybeans and winter wheat (C3 crops), consistent with findings from controlled experiments. The weather controls in columns (b) and (c) confirm that moderate degree days are generally yield-enhancing, while extreme heat (measured by extreme degree days) is highly detrimental. Similarly, the quadratic term for precipitation is hill-shaped, suggesting that a moderate amount of precipitation is generally optimal. Other pollutants besides CO_2 tend to reduce yields (i.e., they have negative and sometimes significant coefficients).

These results do not appear to be driven by outliers: Figure A5 plots the anomalies for CO_2 anomalies after controlling for all covariates in the preferred panel model shown in columns (c) of Table 2.[15] Note that we observe both positive and negative anomalies within

[14] We experimented with more disaggregated weather measures for wheat yields but did not find significant results. This is likely due to the fact that Tack et al. (2015) use data from field trials that allow for better matching than what is possible with county-level aggregates.

[15] By the Frisch–Waugh–Lovell theorem, our panel regression is equivalent to first regressing both the log of yields and our satellite measure of CO_2 on all covariates, and then regressing the residual from the former on the residual from the latter. The figure displays the variation in these latter residuals, i.e., the CO_2

each year across counties, and only a few outliers. This ensures that our results are not driven by common year-to-year macroeconomic shocks or by individual outliers.

Wind IV

Table 3 presents the results from the IV model in which CO_2 levels are instrumented by those of the upstream neighbor. All columns report the full model specification, including weather and pollution controls—that is, the same as in column (c) of Table 2. While our panel model included all counties with at least three CO_2 and yield observations, the wind IV approach further requires at least three observations in which both the county itself and its upwind neighbor have CO_2 measurements available.[16] This requirement further reduces the sample size. To account for this, the table first replicates the panel regression results for the restricted sample in the top row, columns (b), (c), and (d), and then reports the IV results for the same sample in the bottom row. This approach ensures that any differences can be attributed to the IV strategy rather than changes in sample composition.

As described in the modeling section, any feedback mechanism—whereby higher yields remove CO_2 from the atmosphere through increased photosynthesis—would induce a downward bias in our estimates, manifesting as a negative correlation. We would thus expect the coefficient to increase when we instrument with upwind CO_2 levels, which is indeed what we observe. Compared to the OLS panel estimates, the coefficients for corn, soybeans, and winter wheat are larger by factors of 1.4, 1.7, and 2.7, respectively, when averaged across columns (b), (c), and (d). These relative ratios, reported in the second-to-last row, are robust to varying the stringency of the upwind county definition—that is, whether we require the most frequent upwind county to be at least 0, 1,000, or 1,500 hours upwind during the growing season. Further restricting our dataset to counties with more consistent wind patterns—where the upwind county is even more frequently the same—shifts the sample towards the drier western regions of the US, particularly the Great Plains, where a strong north–south wind pattern prevails. As a result, the sample becomes less representative of average conditions across the US. Our preferred specification, columns (c), uses a 1,000 hour

anomalies used for identification.

[16]Recall that the CO_2 exposure of the upwind county is measured over the entire county area and not just cropland area; i.e., the measure will exist even if the county is urban, as long as there are satellite readings.

cutoff to balance these tradeoffs.[17]

Sensitivity Checks

We perform a number of sensitivity checks that produce largely similar results. First, we run our analyses across different US geographies, as visualized by the colored regions in Figure A3. Our primary analysis encompasses counties east of the 100° meridian (excluding Florida) for corn and soybeans—an area accounting for the vast majority of US production of these crops—as well as counties east of the Rocky Mountains for wheat. Figure A6 presents results for samples comprising the entire contiguous US, counties east of the Rockies, and counties east of the 100° meridian where row crop agriculture is primarily rainfed. The results are again fairly stable, mitigating concerns that the observed relationship is driven by regional dynamics such as irrigation. Note that the color coding of geographic subsets in this figure matches the map in Figure A3.

The bottom of Figure A6 displays the fraction of US production covered by our analysis, based on the sample of counties with at least one OCO-satellite reading; in all cases our analysis encompasses over half of total US production, with the exception of wheat grown east of the 100° meridian—but this fraction increases when considering the contiguous US. The wind IV approach reduces the sample size further by requiring not only an OCO-satellite reading over a county, but also a reading over its upwind neighbor (used in the first-stage regression 2a).[18]

Second, we vary the time trends to allow for the possibility that the upward-trending relationship between CO_2 and crop yields may occur at a geographic level different from the county, for example, if state-level policies drive both energy and agricultural production. Figure A7 plots the CO_2 coefficient for all the panel and IV models, alternately using no

[17]By focusing on areas with dominant wind directions, we also limit the number of times the upwind county changes from year to year. Identification therefore relies on two sources of variation: (i) temporal fluctuations in the CO_2 anomaly of a stable upwind neighbor, and (ii) changes in the identity of the upwind neighbor. As Table A1 shows, the upwind neighbor remains constant for the majority of observations, and thus the temporal channel is the primary source of variation.

[18]An alternative way to address concerns about missing data is to use a reanalysis product that fills in missing observations. We replicate our main analysis using CO_2 from NOAA's CarbonTracker release CT2019B (Jacobson et al., 2020), selecting the measurement level closest to the ground, which corresponds to 25 m above the Earth's surface. The data are available for the years 2000–2018. We consistently find significant CO_2 fertilization effects at the county-year level (results are available upon request), although the effects for corn become larger. Since interpolated reanalysis data products like CarbonTracker involve many modeling assumptions, we prefer our less processed OCO satellite measurements—especially in relation to our instrumental variables approach where spatially-interpolated data may mechanically produce a significant first stage.

time trend, a common national trend, state-level trends, and county-level trends. All point estimates are positive. While there is some variation in the panel or IV setup when using a common national time trend or omitting trends altogether, the granularity of the time trend (state-specific versus county-specific) does not have a substantial effect.

Third, we vary the end year used in our analysis. USDA stopped reporting county-level wheat yields after 2023, in part due to a continuous decline in the response rate to USDA-NASS surveys (Johansson and Coble, 2017). There was even consideration of ending all county-level yield reporting in 2024. The year 2023 saw significant wildfire smoke over the central United States,[19] which led to substantial CO_2 and particulate matter emissions—the latter being far outside the normal range, risking bias in our pollution control. As a result, we end our baseline analysis in 2022. Figure A8 varies the last year between 2020 and 2024. The results are fairly stable for the first three years—i.e., we get very similar results whether we end the analysis in 2020, 2021, or 2022, but estimates start to become smaller in magnitude and less significant if we include data from 2023 or 2024, coinciding with declining response rate to USDA-NASS surveys, and hence fewer counties reporting yields as shown in Figure A4. Panel estimates remain significant for corn and soybeans, while the results from the wind IV remain significant for wheat.

Fourth, our baseline analysis uses a longitudinal setting, observing around a thousand counties each year. Since there is a large amount of spatial correlation—a fact our wind IV specifically relies on since CO_2 levels are in part determined by upwind CO_2 levels—we supplement our panel setting with a national-level time series analysis in Appendix B, where we rely on one observation per year. We follow the approach of Bilal and Känzig (2024) and construct CO_2 innovations from an autoregressive process, which we use to explain aggregate crop yields in the US. A benefit of this approach is that we can go back in time before the 2015 launch of the OCO-2 satellite: we use CO_2 measurements from the Mauna Loa Observatory in Hawaii, which started year-round reporting in 1958, giving us a sample from 1958–2024 (67 years). But going from the county level to national level results in much fewer observations, and the confidence intervals become larger. They are highly significant for wheat, marginally significant for corn, and not significant for soybeans. However, in the case of soybeans, the results are also not significantly different from our baseline estimates. We find it reassuring that this entirely different approach—using *in situ* rather than remotely-sensed data—also points toward sizable CO_2 fertilization effects.

Fifth, we vary the model specification to test for non-linear effects. Our baseline model

[19] For example, see Figures 2 and 3 in Lee and Jaffe (2024).

links log yields to CO_2 levels, assuming that a 1 ppm change in CO_2 has the same *relative* (percent) effect on yields. Figure A9 compares the effect of the main specification (log-linear) to other functional form combinations: linear-linear (constant absolute effect), log-log (constant elasticity), and linear-log. To make the results comparable, we do not show the coefficients directly; instead, we present the effect of a 1 ppm increase in CO_2 on corn yields in each case, along with the 90% confidence interval. The figure displays results for both the panel regression and the wind IV. The results are similar, which is not surprising given that we have only eight years of data, during which CO_2 varies by about 20 ppm; over such a limited range, all specifications provide local linear approximations, making it difficult to detect non-linear relationships. It is important to note, however, that in our thought exercise in the next section—where we extend the coefficient backward to 1940 to simulate earlier CO_2 effects—the functional form makes a large difference, as it would when projecting several decades into the future.

5 Discussion

Global ambient CO_2 levels have increased by 2 to 2.5 ppm per year on average since 2000. Our preferred IV models estimate yield responses between 0.2% and 0.6% per 1 ppm CO_2. These estimates, which are at the higher end of the range found in the literature, imply that CO_2 fertilization was a major contributor to recent crop productivity in the US. That is, yields may have increased 0.5% to 1.5% per year due to CO_2 in recent years, fully accounting for observed yield increases in the case of wheat.

Looking further back in time, Figure 1 shows that since 1940, corn yields have increased by 500%, while soybean and winter wheat yields have increased by 200%. This was during a time when ambient CO_2 levels rose by about 100 ppm. We can conduct a back-of-the-envelope counterfactual in which we hold CO_2 constant at 1940 levels while everything else remains constant. We assume that the CO_2 fertilization effect estimated using 2015–2022 data can be applied from 1940 to the present. Admittedly, this is a strong assumption, as previous studies (see Section 1) have shown that the CO_2 fertilization effect may diminish under stressors such as nutrient or water deficiencies. If crops suffered from such limiting factors, the CO_2 fertilization effect might have been weaker. Moreover, the climate in recent decades would not be the same if atmospheric CO_2 had remained at 1940 levels. Nevertheless, we find it useful to run this thought experiment to highlight the possible magnitude of the CO_2 fertilization effect. Figure 5 shows the results, implying that CO_2 fertilization may be

responsible for a substantial share of past productivity growth, especially for wheat.

How could this have occurred? One source of insight is the period before 1940, when crop yields were largely stagnant despite rapid industrialization and economic growth. Olmstead and Rhode (2002) argue that from 1800 to 1940, "wheat production witnessed wholesale changes in varieties and cultural practices... without these changes, vast expanses of the wheat belt could not have sustained commercial production and yields everywhere would have plummeted due to the increasing severity of insects, diseases, and weeds." What if this same dynamic persisted after 1940, such that agricultural innovation mainly served to protect crops against loss rather than to increase yields? One-third of all crop seed patents are related to crop pests or pathogens (Moscona and Sastry, 2025), and many agricultural technologies are focused on crop resilience to extreme weather (e.g., flood and drought tolerance). Furthermore, only a small share of yield gains since 2005 can be attributed to genetic improvements (Rizzo et al., 2022). Taken together, if CO_2 had remained static, wheat yields could have conceivably grown only modestly over time—especially given that extreme weather and pest pressures have increased with globalization and climate change (Bebber et al., 2014; Deutsch et al., 2018).

Notwithstanding these explanatory factors, how do these results compare with existing CO_2 fertilization estimates? Most FACE experiments raise CO_2 levels by 190 to 200 ppm over a 350 ppm baseline, typically showing yield responses of 18–19% (Kimball, 2016; Ainsworth and Long, 2021), or approximately 0.1% per ppm. Our estimates of 0.2–0.6% per ppm are thus 2 to 6 times larger. However, the average effect from the literature conceals significant variation across crops, locations, and growing conditions. For example, a FACE study of dryland wheat in Australia showed that a 180 ppm increase in CO_2 was associated with yield increases of 24% and 53% in two sites, with some yield responses reaching 79% (Fitzgerald et al., 2016). The latter estimate, equivalent to 0.44% per ppm, is closer to what we find for wheat. Similarly, under varying environmental conditions, yield responses have been observed above 35% for corn, rice, cotton, as well as various leguminous and root crops (Kimball, 2016; Ainsworth and Long, 2021). Given such variation in FACE results and the complexities of environmental interactions, it is difficult to benchmark our results precisely.

FACE experiments are likely to underestimate the effect of CO_2 fertilization due to measurement error related to the difficulty of maintaining elevated gas concentrations in open-air settings. FACE experiments regulate CO_2 through a series of pipes that inject the gas at high velocity in response to sensor feedback. CO_2 concentrations in FACE experiments fluctuate widely due to air turbulence, varying 10 times more than what plants experience

under natural conditions (Kimball, 2016; Allen et al., 2020). When elevated CO_2 is supplied in cycles or pulses, crop responses are lower than if CO_2 is supplied more steadily (Bunce, 2012).[20] Just as CO_2 can be better controlled in chamber studies than in FACE experiments, our study's smaller absolute variation in ambient CO_2 would also imply less fluctuation. A recent review of FACE experiments by USDA researchers found that they underestimate yield responses due to CO_2 fluctuations by 18–50% (Allen et al., 2020, 2025). Our estimates point in the same direction.

It is worth noting that there are only two long-standing FACE experiments in the US that focus on agriculture: the Arizona FACE in Maricopa, AZ, and SOYFACE at the University of Illinois in Champaign, IL (Ainsworth and Long, 2021). Other FACE experiments study non-cropland ecosystems like forests, grasslands, and tundra, as well as crops in other countries. Only SOYFACE in Illinois has the potential to approximate agricultural conditions in the Midwest, where most US crop production occurs—though SOYFACE's primary focus on soybeans limits what can be said about other crops. Moreover, SOYFACE consists of 16 octagonal experimental sites, each 20 m wide (283 m^2), covering over 4,500 m^2 in total, or slightly more than one acre. For comparison, the average farm in the US is 445 acres (USDA ERS), which raises questions about the generalizability of the results—especially considering the large variation in crop yields across counties and even within fields (Lobell and Azzari, 2017).

Therefore, it is possible that FACE experiments do not reflect the growing conditions and farming practices of the major growing regions. Given the well-documented interactions between CO_2 and environmental conditions,[21] CO_2 fertilization effects could vary between FACE experiments and commercial agricultural operations in response to differing fertilization and input regimes, soil and water management practices, and local air pollution and climate anomalies across regions—as well as conditions that vary over time. Our experimental design, utilizing OCO satellite measurements of ambient CO_2, allows us to account for this variation across thousands of US counties and across multiple years of observations.

Nevertheless, we offer another potential explanation for why our estimated CO_2 fertilization effects are higher than those generally found in the literature. Our study focuses only

[20] Short-term fluctuations in CO_2 can affect photosynthetic activity, in part because leaves have little storage capacity for gaseous CO_2 and the half-life of CO_2 in the gas space is short, e.g., 0.20 seconds for wheat (Hendrey et al., 1997).

[21] Including nutrient availability (Kimball et al., 2001; Hungate et al., 2003; Reich et al., 2006; Ziska and Bunce, 2007), water availability (Ottman et al., 2001; Leakey et al., 2006; Keenan et al., 2013; Morgan et al., 2011; Zheng et al., 2020; Gray et al., 2016), and combined nutrient-water-CO_2 interactions (Markelz et al., 2011).

on small increases in CO_2, and it may be inappropriate to extrapolate the fertilization effect to much higher CO_2 concentrations if there are diminishing returns. Most studies (including FACE, open-top chamber, and greenhouse experiments) involve large increases in CO_2 (200 ppm or more) over ambient levels. In contrast, our analysis relies on variation in the range of 20 ppm during the OCO timeline from 2015 to 2022. Such marginal increases could produce relatively higher fertilization effects, as the photosynthetic response curve of plants to elevated CO_2 is diminishing. For example, the rate of CO_2 assimilation in C4 plants is approaching saturation at current global CO_2 concentrations (Lambers and Oliveira, 2019). Our results may reflect higher yield responses around current ambient CO_2 levels, which occur on a steeper part of the response curve. This same dynamic could explain part of the observed decline in the global carbon fertilization effect (Wang et al., 2020).

More generally, a strong positive relationship between CO_2 and yields should not be surprising. CO_2 is a purchased input in many agricultural settings. As mentioned earlier, the gas has long been pumped into greenhouses to spur photosynthesis and increase the yield of horticultural crops. Optimal CO_2 concentrations of 900 ppm have been suggested, which is more than twice current ambient levels (Mortensen, 1987). It has also been argued that rising CO_2 levels were a necessary condition for the emergence of agriculture in the Holocene (Richerson et al., 2001).

An alternative way to contextualize our results is to examine trends in non-cropland vegetation in the US. As mentioned earlier, studies have documented a global greening trend associated with CO_2 fertilization (Zhu et al., 2016). In a similar vein, Figure D2 analyzes trends in NDVI—a measure of vegetative density—over 32 years from 1982 to 2013 using AVHRR satellite data. We find that NDVI increases by 0.48% per year, on average, across the entire US. Focusing on forested land, which is still subject to CO_2 fertilization but less actively managed than cropland, NDVI growth is 0.64% per year. This is in line with our estimates of the crop yield response of 0.2–0.6% per CO_2 ppm, or 0.5–1.5% per year.[22] We can further restrict the sample to isolated and protected forests like the Adirondacks or the Ozarks to limit ourselves to locations largely untouched by agricultural innovation. The bottom panel shows that several of these locations experienced an even higher greening trend, closer to 1% per year. Acknowledging that vegetation indices are not the same as

[22]Caution is warranted when comparing NDVI and crop yields, which are correlated but inherently different measures. Forest growth can also reflect the aggregate impact of CO_2 and factors like forest succession and climate change. Nevertheless, the higher forestland average aligns with evidence from FACE experiments showing trees to be more responsive than herbaceous species (e.g., row crops) to elevated CO_2 (Ainsworth and Long, 2005).

crop yields, this analysis suggests that CO_2 fertilization likely played a material role in greening forestlands near US croplands in a way that cannot be attributed to technology-driven productivity drivers, and on an order of magnitude similar to what we find in managed croplands.

6 Conclusion

We find a significant and robust CO_2 fertilization effect by linking satellite-measured CO_2 fluctuations to yield fluctuations of corn, soybeans, and winter wheat from 2015 to 2022. Our study spans more than half of commercially farmed production for these crops in the US and offers a test of whether the fertilization effects found in controlled experiments can be verified under real-world growing conditions. While panel models linking weather and yield anomalies have shown the possible detrimental effect of extreme heat on yield, the same setup can be used to show that localized CO_2 anomalies drive significant yield changes—a finding that is confirmed when relying on upwind CO_2 levels as an instrumental variable. Our results suggest that CO_2 is an important driver of past agricultural productivity growth.

Our paper illustrates how satellite-based measures of CO_2 can be useful in complementing FACE field experiments, especially in the context of ensuring external validity of estimates for the effect of CO_2 on agriculture and ecosystem functioning at large scales. The approach can be extended to study real-world crop responses globally. Our results also merit consideration in the context of climate models used to estimate climate change impacts and the social cost of carbon, though we caution against extrapolating the fertilization effect far into the future, which requires further assumptions about the functional form, the extent of diminishing returns to additional CO_2, and ongoing uncertainty about future environmental interactions.

Relatedly, our analysis is focused on the US, and it is possible that fertilization effects will differ greatly across countries based on prevailing crops and environmental conditions (McGrath and Lobell, 2013), especially as climate change alters the coupling of temperature, soil moisture, and precipitation that determine crop yields (Proctor et al., 2022). Under future climate change, such heterogeneity could exacerbate spatial inequalities (Cruz and Rossi-Hansberg, 2024) and alter the comparative advantage of different crops and regions (Costinot et al., 2016; Nath, 2025), with potentially large welfare effects that are worth investigating. While recent research has shown that mechanization significantly increases productivity and welfare (Caunedo and Kala, 2022), as do well-functioning credit markets (Wüpper et al., 2023), we argue that environmental factors like CO_2 also play a crucial role.

We would like to close by stressing that the overall effect of climate change will consist of the positive effect of CO_2 fertilization net of the effect of extreme heat, which is highly significant in our regression tables and predicted to rise with ongoing climate change. Moreover, CO_2-driven yield increases may be offset by effects on food nutrition and quality (Loladze, 2002; Taub and Allen, 2008; Myers et al., 2014). Nevertheless, this paper demonstrates that marginal increases in CO_2 have a strong countervailing fertilization effect, and that such effects may account for a material proportion of historical productivity improvements in wheat yields.

References

Ainsworth, Elizabeth A, and Stephen P Long. 2005. "What have we learned from 15 years of free-air CO2 enrichment (FACE)? A meta-analytic review of the responses of photosynthesis, canopy properties and plant production to rising CO2." *New phytologist* 165 (2): 351–372.

Ainsworth, Elizabeth A., and Stephen P. Long. 2021. "30 years of free-air carbon dioxide enrichment (FACE): What have we learned about future crop productivity and its potential for adaptation?" *Global Change Biology* 27 (1): 27–49.

Ainsworth, Elizabeth A., and Alistair Rogers. 2007. "The response of photosynthesis and stomatal conductance to rising CO_2: mechanisms and environmental interactions." *Plant, Cell & Environment* 30 (3): 258–270.

Allen Jr, L Hartwell, Jeff T Baker, and Ken J Boote. 1996. "The CO_2 fertilization effect: higher carbohydrate production and retention as biomass and seed yield." *Global climate change and agricultural production. Direct and indirect effects of changing hydrological, pedological and plant physiological processes.*

Allen, Leon H, Bruce A Kimball, James A Bunce, Kenneth J Boote, and Jeffrey W White. 2025. "Metrics of plant response to CO2 Enrichment." *Agricultural and Forest Meteorology* 370 110557.

Allen, LH, BA Kimball, JA Bunce, M Yoshimoto, Y Harazono, JT Baker, KJ Boote, and JW White. 2020. "Fluctuations of CO2 in Free-Air CO2 Enrichment (FACE) depress plant photosynthesis, growth, and yield." *Agricultural and Forest Meteorology* 284 107899.

Batts, G.R., J.I.L. Morison, R.H. Ellis, P. Hadley, and T.R. Wheeler. 1997. "Effects of CO_2 and temperature on growth and yield of crops of winter wheat over four seasons." *European Journal of Agronomy* 7 (1-3): 43–52.

Bebber, Daniel P, Timothy Holmes, and Sarah J Gurr. 2014. "The global spread of crop pests and pathogens." *Global Ecology and Biogeography* 23 (12): 1398–1407.

Bilal, Adrien, and Diego R. Känzig. 2024. "The Macroeconomic Impact of Climate Change: Global vs. Local Temperature." *NBER Working Paper 32450.* https://doi.org/10.3386/w32450.

Boone, Christopher, Wolfram Schlenker, and Juha Siikamäki. 2019. "Ground-Level Ozone and Corn Yields in the United States." *CEEP Working Paper 7*.

Braun, Thomas, and Wolfram Schlenker. 2023. "Cooling Externality of Large-Scale Irrigation." *Working Paper*.

Broquet, Grégoire, François-Marie Bréon, Emmanuel Renault et al. 2018. "The potential of satellite spectro-imagery for monitoring CO¡ sub¿ 2¡/sub¿ emissions from large cities." *Atmospheric Measurement Techniques* 11 (2): 681–708.

Bunce, J.A. 2012. "Responses of cotton and wheat photosynthesis and growth to cyclic variation in carbon dioxide concentration." *Photosynthetica* 50 (3): 395–400.

Caunedo, Julieta, and Namrata Kala. 2022. "Mechanizing Agriculture." *Working Paper*.

Costinot, Arnaud, Dave Donaldson, and Cory Smith. 2016. "Evolving comparative advantage and the impact of climate change in agricultural markets: Evidence from 1.7 million fields around the world." *Journal of Political Economy* 124 (1): 205–248.

Coutts, Andrew M, Jason Beringer, and Nigel J Tapper. 2007. "Characteristics influencing the variability of urban CO2 fluxes in Melbourne, Australia." *Atmospheric Environment* 41 (1): 51–62.

Crisp, David. 2015. "Measuring atmospheric carbon dioxide from space with the Orbiting Carbon Observatory-2 (OCO-2)." In *Earth Observing Systems XX*, Volume 9607. 960702.

Cruz, José-Luis, and Esteban Rossi-Hansberg. 2024. "The economic geography of global warming." *Review of Economic Studies* 91 (2): 899–939.

Dell, Melissa, Benjamin F. Jones, and Benjamin A. Olken. 2014. "What Do We Learn from the Weather? The New Climate-Economy Literature." *Journal of Economic Literature* 53 (3): 740–798.

Deryugina, Tatyana, Garth Heutel, Nolan H Miller, David Molitor, and Julian Reif. 2019. "The mortality and medical costs of air pollution: Evidence from changes in wind direction." *American Economic Review* 109 (12): 4178–4219.

Deutsch, Curtis A, Joshua J Tewksbury, Michelle Tigchelaar, David S Battisti, Scott C Merrill, Raymond B Huey, and Rosamond L Naylor. 2018. "Increase in crop losses to insect pests in a warming climate." *Science* 361 (6405): 916–919.

Etheridge, David M, LP Steele, R Ll Langenfelds, Roger J Francey, J-M Barnola, and VI Morgan. 1996. "Natural and anthropogenic changes in atmospheric CO2 over the last 1000 years from air in Antarctic ice and firn." *Journal of Geophysical Research: Atmospheres* 101 (D2): 4115–4128.

Fitzgerald, Glenn J., Michael Tausz, Garry O'Leary et al. 2016. "Elevated atmospheric CO_2 can dramatically increase wheat yields in semi-arid environments and buffer against heat waves." *Global Change Biology* 22 (6): 2269–2284.

Fowlie, Meredith, Edward Rubin, and Reed Walker. 2019. "Bringing satellite-based air quality estimates down to earth." In *AEA Papers and Proceedings*, Volume 109. 283–88.

García, Ma Ángeles, Ma Luisa Sánchez, and Isidro A Pérez. 2012. "Differences between carbon dioxide levels over suburban and rural sites in Northern Spain." *Environmental Science and Pollution Research* 19 (2): 432–439.

Gollin, Douglas, Casper Worm Hansen, and Asger Mose Wingender. 2021. "Two Blades of Grass: The Impact of the Green Revolution." *Journal of Political Economy* 129 (8): 2344–2384. https://doi.org/10.1086/714444.

Gray, Sharon B, Orla Dermody, Stephanie P Klein et al. 2016. "Intensifying drought eliminates the expected benefits of elevated carbon dioxide for soybean." *Nature Plants* 2 (9): 1–8.

Hakkarainen, Janne, Iolanda Ialongo, and Johanna Tamminen. 2016. "Direct space-based observations of anthropogenic CO2 emission areas from OCO-2." *Geophysical Research Letters* 43 (21): 11–400.

Hendrey, GR, SP Long, IF McKee, and NR Baker. 1997. "Can photosynthesis respond to short-term fluctuations in atmospheric carbon dioxide?" *Photosynthesis Research* 51 (3): 179–184.

Hultgren, Andrew, Tamma Carleton, Michael Delgado et al. 2025. "Impacts of climate change on global agriculture accounting for adaptation." *Nature* 642 (8068): 644–652.

Hungate, Bruce A., Jeffrey S. Dukes, M. Rebecca Shaw, Yiqi Luo, and Christopher B. Field. 2003. "Nitrogen and climate change." *Science* 302 (5650): 1512–1513.

Idso, Sherwood B, Craig D Idso, and Robert C Balling Jr. 2002. "Seasonal and diurnal variations of near-surface atmospheric CO2 concentration within a residential sector of the urban CO2 dome of Phoenix, AZ, USA." *Atmospheric environment* 36 (10): 1655–1660.

Jacobson, Andrew R., Kenneth N. Schuldt, John B. Miller et al. 2020. "CarbonTracker CT2019B." https://doi.org/10.25925/20201008.

Johansson, Robert, and Anne Effland and Keith Coble. 2017. "Falling Response Rates to USDA Crop Surveys: Why It Matters." *farmdoc daily* 7 (9): , `https://farmdocdaily.illinois.edu/2017/01/falling-response-rates-to-usda-crop-surveys.html`.

Jorgenson, Dale W., and Frank M. Gollop. 1992. "Productivity Growth in U.S. Agriculture: A Postwar Perspective." *American Journal of Agricultural Economics* 74 (3): 745–750, `http://www.jstor.org/stable/1242588`.

Keenan, Trevor F., David Y. Hollinger, Gil Bohrer, Danilo Dragoni, J. William Munger, Hans Peter Schmid, and Andrew D. Richardson. 2013. "Increase in forest water-use efficiency as atmospheric carbon dioxide concentrations rise." *Nature* 499 (7458): 324–327.

Keppel-Aleks, G, PO Wennberg, and T Schneider. 2011. "Sources of variations in total column carbon dioxide." *Atmospheric Chemistry and Physics* 11 (8): 3581–3593.

Kimball, B. A., C. F. Morris, P. J. Pinter Jr et al. 2001. "Elevated CO_2, drought and soil nitrogen effects on wheat grain quality." *New Phytologist* 150 (2): 295–303.

Kimball, Bruce A. 1983. "Carbon Dioxide and Agricultural Yield: An Assemblage and Analysis of 430 Prior Observations." *Agronomy Journal* 75 (5): 779–788.

Kimball, Bruce A. 2016. "Crop responses to elevated CO_2 and interactions with H_2O, N, and temperature." *Current Opinion in Plant Biology* 31 36–43.

Lambers, Hans, and Rafael S. Oliveira. 2019. "Photosynthesis, Respiration, and Long-Distance Transport: Photosynthesis." In *Plant Physiological Ecology*, 11–114, Springer.

Leakey, Andrew D.B., Martin Uribelarrea, Elizabeth A. Ainsworth, Shawna L. Naidu, Alistair Rogers, Donald R. Ort, and Stephen P. Long. 2006. "Photosynthesis, Productivity, and Yield of Maize Are Not Affected by Open-Air Elevation of CO_2 Concentration in the Absence of Drought." *Plant Physiology* 140 (2): 779–790.

Lee, Haebum, and Daniel A. Jaffe. 2024. "Wildfire Impacts on O3 in the Continental United States Using PM2.5 and a Generalized Additive Model (2018–2023)." *Environmental Science & Technology* 58 (33): 14764–14774. 10.1021/acs.est.4c05870, Publisher: American Chemical Society.

Lobell, David B., and Senthold Asseng. 2017. "Comparing estimates of climate change impacts from process-based and statistical crop models." *Environmental Research Letters* 12 (1): 015001.

Lobell, David B, and George Azzari. 2017. "Satellite detection of rising maize yield heterogeneity in the US Midwest." *Environmental Research Letters* 12 (1): 014014.

Loladze, Irakli. 2002. "Rising atmospheric CO_2 and human nutrition: toward globally imbalanced plant stoichiometry?" *Trends in Ecology & Evolution* 17 (10): 457–461.

Long, Stephen P., Elizabeth A. Ainsworth, Andrew D. B. Leakey, Josef Nösberger, and Donald R. Ort. 2006. "Food for Thought: Lower-Than-Expected Crop Yield Stimulation with Rising CO_2 Concentrations." *Science* 312 (5782): 1918–1921.

Long, Stephen P., Elizabeth A. Ainsworth, Alistair Rogers, and Donald R. Ort. 2004. "Rising atmospheric carbon dioxide: plants FACE the future." *Annual Review of Plant Biology* 55 591–628.

Makowski, David, Elodie Marajo-Petitzon, Jean-Louis Durand, and Tamara Ben-Ari. 2020. "Quantitative synthesis of temperature, CO2, rainfall, and adaptation effects on global crop yields." *European Journal of Agronomy* 115 126041.

Markelz, R. J. Cody, Reid S. Strellner, and Andrew D. B. Leakey. 2011. "Impairment of C_4 photosynthesis by drought is exacerbated by limiting nitrogen and ameliorated by elevated CO_2 in maize." *Journal of Experimental Botany* 62 (9): 3235–3246.

Massen, Francis, and Ernst-Georg Beck. 2011. "Accurate estimation of CO 2 background level from near ground measurements at non-mixed environments." In *The Economic, Social and Political Elements of Climate Change*, 509–522, Springer.

McArthur, John W, and Gordon C McCord. 2017. "Fertilizing growth: Agricultural inputs and their effects in economic development." *Journal of Development Economics* 127 133–152.

McGrath, Justin M., and David B. Lobell. 2013. "Regional disparities in the CO_2 fertilization effect and implications for crop yields." *Environmental Research Letters* 8 (1): 014054.

Moore, Frances C, Uris Baldos, Thomas Hertel, and Delavane Diaz. 2017b. "New science of climate change impacts on agriculture implies higher social cost of carbon." *Nature communications* 8 (1): 1–9.

Moore, Frances C., Uris Lantz C. Baldos, and Thomas Hertel. 2017a. "Economic impacts of climate change on agriculture: a comparison of process-based and statistical yield models." *Environmental Research Letters* 12 (6): 065008.

Morgan, Jack A., Daniel R. LeCain, Elise Pendall et al. 2011. "C4 grasses prosper as carbon dioxide eliminates desiccation in warmed semi-arid grassland." *Nature* 476 (7359): 202–205.

Mortensen, Leiv M. 1987. "CO_2 Enrichment in Greenhouses. Crop Responses." *Scientia Horticulturae* 33 (1-2): 1–25.

Moscona, Jacob, and Karthik Sastry. 2025. "Inappropriate Technology: Evidence from Global Agriculture." *Working Paper*.

Myers, Samuel S., Antonella Zanobetti, Itai Kloog et al. 2014. "Increasing CO_2 threatens human nutrition." *Nature* 510 (7503): 139–142.

Nath, Ishan. 2025. "Climate change, the food problem, and the challenge of adaptation through sectoral reallocation." *Journal of Political Economy* 133 (6): 1705–1756.

Olmstead, Alan L, and Paul W Rhode. 2002. "The red queen and the hard reds: Productivity growth in American wheat, 1800–1940." *The Journal of Economic History* 62 (4): 929–966.

Ottman, M. J., B. A. Kimball, P.J. Pinter et al. 2001. "Elevated CO_2 increases sorghum biomass under drought conditions." *New Phytologist* 150 (2): 261–273.

Pardey, Philip G, and Julian M Alston. 2021. "Unpacking the Agricultural Black Box: The Rise and Fall of American Farm Productivity Growth." *The Journal of Economic History* 81 (1): 114–155.

Parker, Wendy S. 2016. "Reanalyses and observations: What's the difference?" *Bulletin of the American Meteorological Society* 97 (9): 1565–1572.

Proctor, Jonathan, Tamma Carleton, and Sandy Sum. 2023. "Parameter recovery using remotely sensed variables."Technical report, National Bureau of Economic Research.

Proctor, Jonathan, Angela Rigden, Duo Chan, and Peter Huybers. 2022. "More accurate specification of water supply shows its importance for global crop production." *Nature Food* 3 (9): 753–763.

Reich, Peter B., Sarah E. Hobbie, Tali Lee et al. 2006. "Nitrogen limitation constrains sustainability of ecosystem response to CO_2." *Nature* 440 (7086): 922–925.

Rennert, Kevin, Frank Errickson, Brian C Prest et al. 2022. "Comprehensive evidence implies a higher social cost of CO2." *Nature* 610 (7933): 687–692.

Rezaei, Ehsan Eyshi, Heidi Webber, Senthold Asseng, Kenneth Boote, Jean Louis Durand, Frank Ewert, Pierre Martre, and Dilys Sefakor MacCarthy. 2023. "Climate change impacts on crop yields." *nature reviews earth & environment* 4 (12): 831–846.

Richerson, Peter J, Robert Boyd, and Robert L Bettinger. 2001. "Was agriculture impossible during the Pleistocene but mandatory during the Holocene? A climate change hypothesis." *American antiquity* 66 (3): 387–411.

Rizzo, Gonzalo, Juan Pablo Monzon, Fatima A Tenorio, Réka Howard, Kenneth G Cassman, and Patricio Grassini. 2022. "Climate and agronomy, not genetics, underpin recent maize yield gains in favorable environments." *Proceedings of the National Academy of Sciences* 119 (4): e2113629119.

Schlenker, Wolfram, and Michael J. Roberts. 2009. "Nonlinear Temperature Effects Indicate Severe Damages to U.S. Crop Yields under Climate Change." *Proceedings of the National Academy of Sciences* 106 (37): 15594–15598.

Schlenker, Wolfram, and W Reed Walker. 2016. "Airports, Air Pollution, and Contemporaneous Health." *Review of Economic Studies* 2 (83): 768–809.

Specht, JE, DJ Hume, and SV Kumudini. 1999. "Soybean yield potential—a genetic and physiological perspective." *Crop science* 39 (6): 1560–1570.

Tack, Jesse, Andrew Barkley, and Lawton Lanier Nalley. 2015. "Effect of Warming temperatures on US Wheat Yields." *Proceedings of the National Academy of Sciences* 112 (22): 6931–6936.

Taub, Daniel R., and Brian Millerand Holly Allen. 2008. "Effects of elevated CO_2 on the protein concentration of food crops: a meta-analysis." *Global Change Biology* 14 (3): 565–575.

Toreti, Andrea, Delphine Deryng, Francesco N. Tubiello et al. 2020. "Narrowing uncertainties in the effects of elevated CO_2 on crops." *Nature Food* 1 (12): 775–782.

U.S. Department of Energy. 2025. "A Critical Review of Impacts of Greenhouse Gas Emissions on the U.S. Climate."Technical report, U.S. Department of Energy.

Vermote, Eric, Chris Justice, Ivan Csiszar et al. 2014. "NOAA Climate Data Record (CDR) of Normalized Difference Vegetation Index (NDVI), Version 4." https://doi:10.7289/V5PZ56R6.

Wang, Anran, Jianrong Lv, Jiao Wang, and Kai Shi. 2022. "CO2 enrichment in greenhouse production: Towards a sustainable approach." *Frontiers in Plant Science* 13. https://doi.org/10.3389/fpls.2022.1029901.

Wang, Songhan, Yongguang Zhang, Weimin Ju et al. 2020. "Recent global decline of CO_2 fertilization effects on vegetation photosynthesis." *Science* 370 (6522): 1295–1300.

Wang, Sun Ling, Paul Heisey, David Schimmelpfennig, and V. Eldon Ball. 2015. "Agricultural Productivity Growth in the United States: Measurement, Trends, and Drivers." *Economic Research Service, Paper No. 189.*

Weir, Brad, and Lesley Ott. 2022. "OCO-2 GEOS Level 3 daily, 0.5x0.625 assimilated CO2 V10r." https://doi.org/10.5067/Y9M4NM9MPCGH.

Wüpper, David, Wolfram Schlenker, Meha Jain, Haoyu Wang, and Robert Finger. 2023. "Institutions and Global Crop Yields." *Working Paper.*

Xueref-Remy, Irène, Elsa Dieudonné, Cyrille Vuillemin et al. 2018. "Diurnal, synoptic and seasonal variability of atmospheric CO 2 in the Paris megacity area." *Atmospheric Chemistry and Physics* 18 (5): 3335–3362.

Yin, Yi, Brendan Byrne, Junjie Liu et al. 2020. "Cropland carbon uptake delayed and reduced by 2019 Midwest floods." *AGU Advances* 1 (1): e2019AV000140. https://doi.org/10.1029/2019AV000140.

Zheng, Yunpu, Chunlin He, Lili Guo, Lihua Hao, Dongjuan Cheng, Fei Li, Zhengping Peng, and Ming Xu. 2020. "Soil water status triggers CO_2 fertilization effect on the growth of winter wheat (Triticum aestivum)." *Agricultural and Forest Meteorology* 291 108097.

Zhu, Zaichun, Shilong Piao, Ranga B. Myneni et al. 2016. "Greening of the Earth and its Drivers." *Nature climate change* 6 (8): 791–795.

Ziska, Lewis H., and James A. Bunce. 2007. "Predicting the impact of changing CO_2 on crop yields: some thoughts on food." *New Phytologist* 175 (4): 607–618.

Figures and Tables

Figure 1: Agricultural Yields and CO_2 Levels

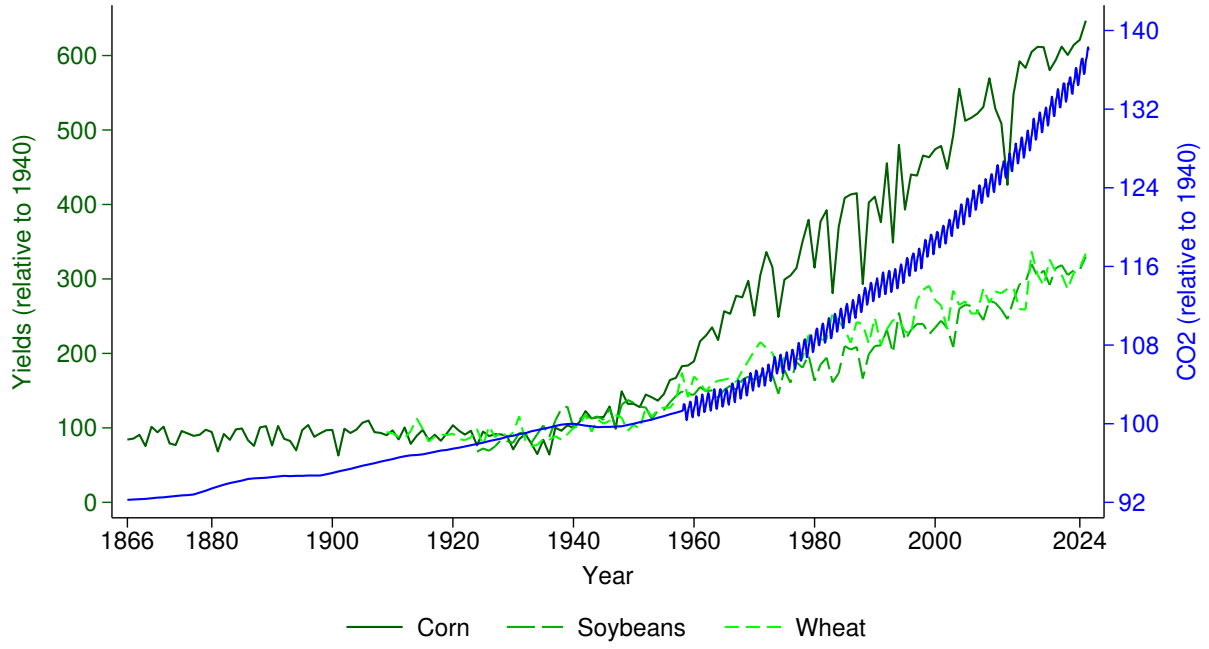

Notes: The figure displays the evolution of yearly aggregate US yields (left axis) and annual CO_2 averages (right axis). Each time series is normalized relative to 1940 (value = 100). Aggregate US corn yields are shown in dark green from 1866–2024, aggregate US soybean yields in green from 1924–2024, and aggregate US winter wheat yields in light green from 1909–2024, corresponding to the years for which data are reported by USDA. Monthly CO_2 readings at Mauna Loa Observatory are shown from March 1958 onward in blue, while earlier years use annual averages from ice cores (Etheridge et al., 1996) as provided by NASA (link).

Figure 2: Yield and CO_2 Anomalies in Macoupin County, Illinois

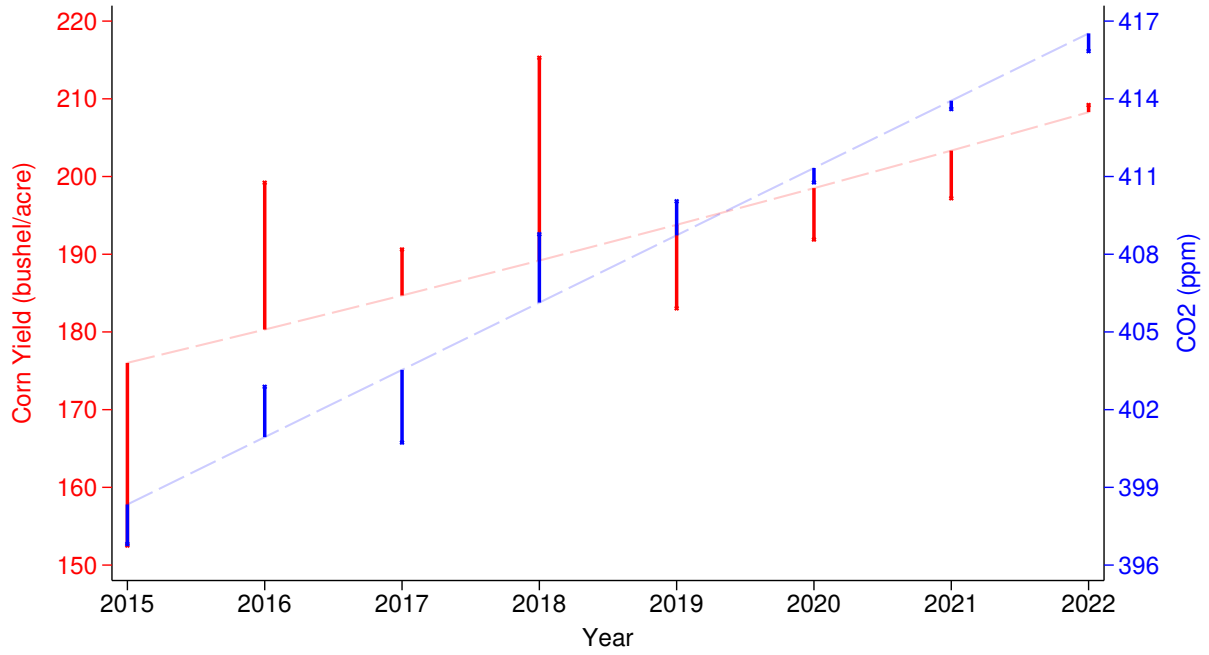

Notes: The figure displays corn yields (left axis, shown in red) and CO_2 levels (right axis, shown in blue) in Macoupin County, Illinois, which is also shown in Figure 3. Dashed lines represent the county-specific time trend over the eight-year period (2015–2022), while solid lines show anomalies (annual deviations from the trend). The correlation between corn yield anomalies and CO_2 anomalies is 0.55.

Figure 3: IV Setup

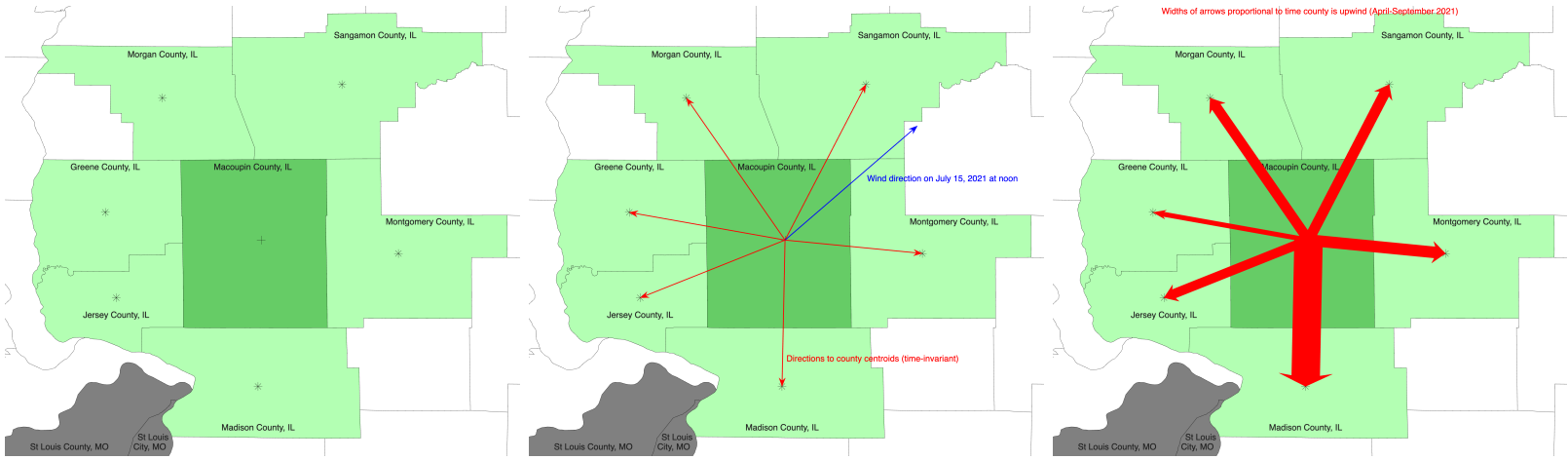

Notes: The figure outlines the construction of the wind instrument, using Macoupin County, Illinois (FIPS code 17117) as an example. The **left panel** demonstrates the first step: we derive the centroid (shown as +) for Macoupin County (shown in dark green) as the cropland-weighted average of all grids in the county. The weight is the combined corn, soybean, and winter wheat acreage from the Cropland Data Layer. We pair Macoupin's centroid with the centroids of all its six neighbors (shown as $*$), which are *not* cropland-area weighted, as we are including all CO_2 readings as part of our instrument, not just those over cropland. The **middle panel** demonstrates how we determine the upwind county: the red arrows show the direction in which neighbor centroids are located, which are time-invariant. The blue arrow shows the wind direction at 12 noon on July 15, 2021. This is constructed from hourly NLDAS data, using the cropland-area weighted average of all NLDAS grid cells in Macoupin County. At each hour, we compute the cosine between the direction of neighboring counties (red arrows) and the wind direction (blue arrow), and record which neighbor is "upwind"—the one with a cosine closest to -1. The **right panel** shows how often a neighboring county is "upwind" during the 4,392 hours in April–September of a year, with the widths of the arrows proportional to frequency. For example, CO_2 readings over Madison County (entire county, not just agricultural area) are used as an instrument for CO_2 over the agricultural area of Macoupin County in 2021, as it is upwind 1,659 hours (38% of the time). Both counties are downwind from the city of St. Louis (shown in gray). Note that the "upwind" county can change year to year.

Figure 4: Histogram of Hours a County is Upwind

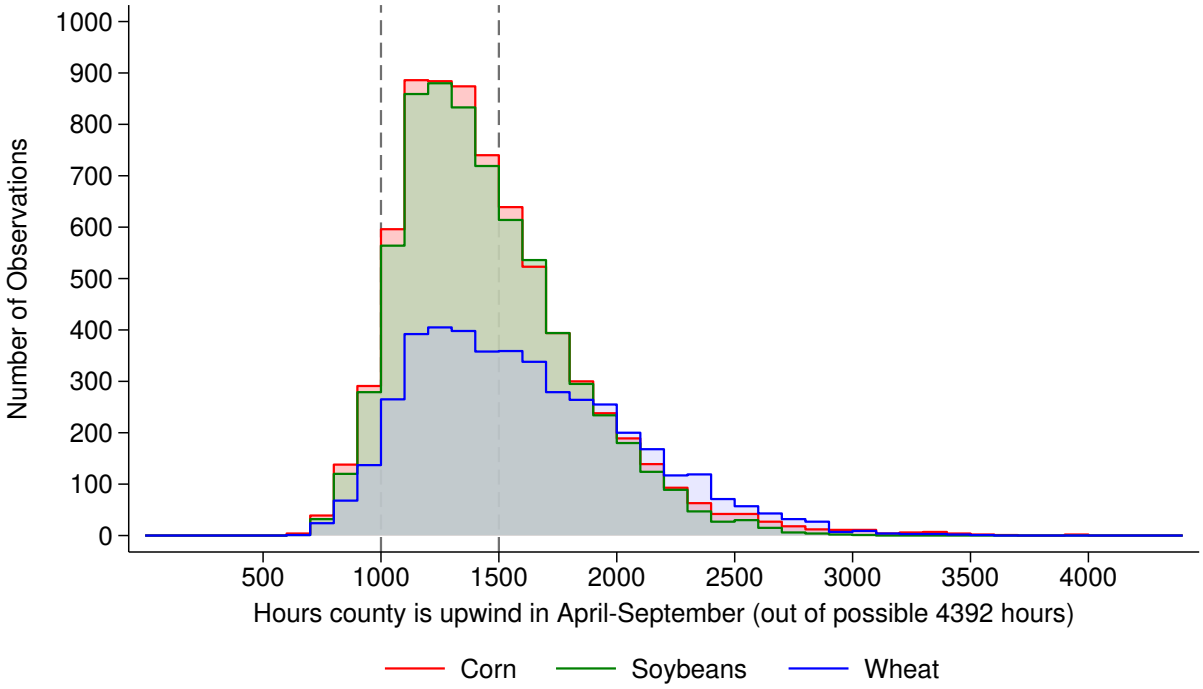

Notes: The figure displays histograms of the number of hours the county used as the IV is upwind (out of a possible 4,392 hours in April–September of a year). Data are shown for counties east of the 100° meridian for corn and soybeans (shown in green in Figure A3), and east of the Rocky Mountains for winter wheat (shown in green and blue in Figure A3).

Figure 5: Counterfactual if CO_2 Remained at 1940 Levels

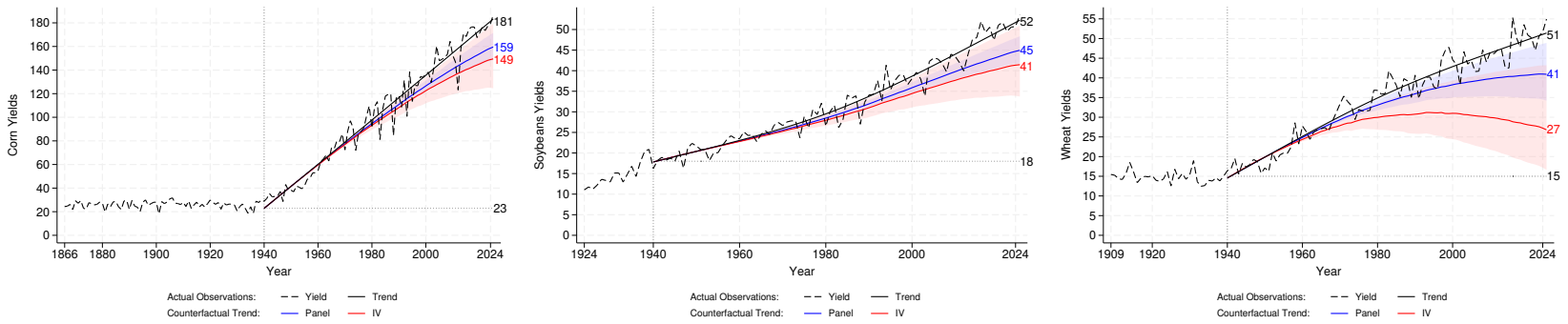

Notes: The figure displays the evolution of yearly aggregate US yields as a dashed black line. Yield trends (estimated using restricted cubic splines with three knots) since 1940 are shown as a solid black line. The graph adds counterfactuals where CO_2 levels are kept constant at the 1940 value, assuming the CO_2 fertilization effect estimated from 2015–2022 data applies throughout the 1940–2024 period. The blue line uses the coefficient estimates from columns (c) of the panel regressions in Table 2. The red line uses the IV estimates from the columns (c) of the wind IV regressions in Table 3. We adjust the yield trend only by the difference between actual CO_2 and CO_2 in 1940, leaving all other factors, notably realized weather, unchanged. The 95% confidence bands are shown as shaded areas.

Table 1: Standard Deviation of Annual CO_2 Anomalies in Satellite and FluxTower Data

	All flux towers		Cropland flux towers	
	World	US	World	US
	Panel A: OCO Reading Around Tower Location			
	A1: Location of towers across all years			
σ_{OCO}	1.30	1.29	1.40	1.37
N_{tower}	[375]	[317]	[93]	[91]
	A2: Location of towers with 2015-2022 data			
σ_{OCO}	1.21	1.25	1.21	1.21
N_{tower}	[96]	[90]	[20]	[20]
	Panel B: Flux Tower at 2 m Height			
	B1: All years			
$\sigma_{\text{fluxTower}}$	5.83	5.28	6.35	5.91
N_{tower}	[287]	[226]	[48]	[42]
	B2: 2015-2022			
$\sigma_{\text{fluxTower}}$	5.36	4.88	6.07	5.64
N_{tower}	[206]	[178]	[36]	[32]
	B3: 2015-2022 with OCO data			
$\sigma_{\text{fluxTower}}$	4.94	4.91	6.97	6.97
N_{tower}	[96]	[90]	[20]	[20]
Ratio $\kappa = \frac{A1}{B1}$	$\frac{1}{4.49}$	$\frac{1}{4.09}$	$\frac{1}{4.55}$	$\frac{1}{4.30}$
Ratio $\kappa = \frac{A2}{B3}$	$\frac{1}{4.10}$	$\frac{1}{3.91}$	$\frac{1}{5.74}$	$\frac{1}{5.74}$

Notes: The table displays the year-to-year standard deviation of CO_2 anomalies from OCO satellite readings (σ_{OCO} in Panel A) and at flux towers ($\sigma_{\text{fluxTower}}$ in Panel B). The second row of each panel gives the number of towers (locations) included in the dataset. OCO readings are averaged within a 0.1-degree longitude/latitude radius around each flux tower location. The combined cropland area in the 2022 USDA Census of Agriculture was 382 million acres, equating to an average of 118,000 acres (or 184 square miles) across 3,244 US counties. For comparison, the area of a 0.1-degree circle is 150 square miles at the equator, which is roughly comparable. Panel A1 uses all flux tower locations (including those without height information for CO_2 measurements), while Panel A2 only uses flux tower locations with CO_2 data from 2015–2024 that report the height of the instrument. Panels B1-B3 fit a restricted cubic spline to estimate σ_{CO_2} as a function of measurement height and evaluates it at 2 m. Panel B1 uses data across all years (observations start in 1993 for all towers, and 2001 for cropland towers). Panel B2 is restricted to locations with flux towers that have CO_2 data from 2015–2024. Panel B3 only includes flux towers where there is also CO_2 data from OCO. Panels B3 and A1 therefore use the same locations. The final two rows report the ratio $\kappa = \frac{\sigma_{\text{OCO}}}{\sigma_{\text{fluxTower}}}$ using the standard deviations from Panels A1 and B1 (second to last row), as well as standard deviations from Panels A2 to B3 (last row). An average baseline scaling factor of $\kappa = \frac{1}{4.5}$ is obtained when using all available data, $\frac{\text{A1}}{\text{B1}}$, or when using all towers in the world (first column) or just cropland towers (third column). For simplicity in the text we may refer to the reciprocal of this scaling factor, $1/\kappa \approx 4.5$, which represents the factor by which ground-level variation exceeds the satellite variation.

Table 2: Baseline Panel Regression

	Corn			Soybeans			Winter Wheat		
	(1a)	(1b)	(1c)	(2a)	(2b)	(2c)	(3a)	(3b)	(3c)
CO_2 (ppm)	0.071**	0.118***	0.118***	0.087**	0.113***	0.128***	0.238**	0.293**	0.194**
	(0.030)	(0.029)	(0.031)	(0.038)	(0.038)	(0.032)	(0.113)	(0.115)	(0.077)
Moderate DDay		0.277***	0.282***		0.295**	0.557***		0.024	0.178
		(0.097)	(0.082)		(0.109)	(0.097)		(0.238)	(0.232)
Extreme DDay		-0.396***	-0.395***		-0.601***	-0.593***		-0.262**	-0.278**
		(0.070)	(0.070)		(0.096)	(0.092)		(0.115)	(0.107)
Precipitation		0.525***	0.547***		0.478**	0.476**		1.052*	0.773
		(0.176)	(0.181)		(0.178)	(0.190)		(0.545)	(0.508)
Prec. squared		-0.443***	-0.457***		-0.348***	-0.368***		-0.971**	-0.836**
		(0.114)	(0.118)		(0.112)	(0.132)		(0.377)	(0.355)
Mean CO			-0.001			-0.574*			0.006
			(0.286)			(0.295)			(0.514)
Mean NO_2			-0.007			-0.024*			0.018
			(0.012)			(0.013)			(0.016)
Mean O_3			-0.032			-2.447***			-0.320
			(0.693)			(0.575)			(1.303)
Mean PM_{10}			0.151			0.284			-1.948***
			(0.500)			(0.316)			(0.627)
Mean SO_2			-0.008			-0.037***			-0.011
			(0.017)			(0.013)			(0.014)
R^2	0.8230	0.8533	0.8535	0.8203	0.8559	0.8651	0.8347	0.8509	0.8559
Observations	8337	8337	8337	7918	7918	7918	4990	4990	4990

Notes: The table regresses log yields on CO_2 from OCO satellite readings between 2015 and 2022. Reported coefficients are multiplied by 100 so that estimates represent the percentage yield change per 1 ppm increase in CO_2. All regressions include county fixed effects and county-specific time trends. Columns (b) further include four weather variables: moderate degree days ×1000 (degree days 10–29°C for corn and 10–30°C for soybeans and winter wheat), extreme degree days ×100 (degree days above 29°C for corn and above 30°C for soybeans and winter wheat), and a quadratic in precipitation (in meters). Columns (c) include the mean pollution levels of five criteria air pollutants: CO (in ppm), NO_2 (in ppm), O_3 (in 100 ppb), PM_{10} (in 100 $\mu g/m^3$), and SO_2 (in ppm). All weather and pollution variables are constructed over the growing season (April–September). Corn and soybean regressions use counties east of the 100° meridian (green in Figure A3), while wheat regressions include all counties east of the Rocky Mountains (green and blue in Figure A3). CO_2 coefficients were scaled by $\kappa = \frac{1}{4.5}$ as outlined in equation (3) and Table 1. Standard errors are clustered at the state level. Stars indicate significance levels: * 10%, ** 5%, *** 1%.

Table 3: IV Regression using Upwind CO_2

	Corn				Soybeans				Winter Wheat			
	(1a)	(1b)	(1c)	(1d)	(2a)	(2b)	(2c)	(2d)	(3a)	(3b)	(3c)	(3d)
Min hours	-	0	1000	1500	-	0	1000	1500	-	0	1000	1500
					OLS Regression							
CO_2 (ppm)	0.118***	0.127***	0.135***	0.175*	0.128***	0.124***	0.132***	0.207***	0.194**	0.191*	0.180	0.352**
	(0.031)	(0.038)	(0.042)	(0.100)	(0.032)	(0.035)	(0.039)	(0.065)	(0.077)	(0.100)	(0.115)	(0.149)
					IV Regression							
CO_2 (ppm)		0.177**	0.174**	0.288*		0.209**	0.197**	0.416***		0.533***	0.555***	0.798***
		(0.076)	(0.079)	(0.166)		(0.086)	(0.090)	(0.117)		(0.190)	(0.207)	(0.281)
F (1st stage)		16.33	16.07	11.08		15.94	15.62	9.89		13.89	13.71	7.24
Ratio IV/OLS		1.39	1.29	1.65		1.68	1.49	2.00		2.80	3.08	2.27
Observations	8337	7219	6641	2436	7918	6885	6354	2288	4990	4406	4117	2173

Notes: The table regresses log yields on CO_2 ($\times 100$) from OCO satellite readings between 2015 and 2022.

The table regresses log yields on CO_2 from OCO satellite readings between 2015 and 2022. Reported coefficients are multiplied by 100 so that estimates represent the percentage yield change per 1 ppm increase in CO_2. Each coefficient is from a separate regression. Column (a) replicates the specification from column (c) in Table 2. Columns (b), (c), and (d) replicate the same OLS regression for the set of observations included in the IV regression in the second row, where CO_2 readings are instrumented with the CO_2 reading (averaged over the entire county, not just the agricultural area) from the predominant upwind county. Columns (b), (c), and (d) differ in how the upwind county is classified for the IV: column (b) uses the county most frequently upwind during April–September as measured from hourly wind data from NLDAS (a total of 4,392 hours in April–September); columns (c) and (d) include counties only if they are upwind for at least 1,000 or 1,500 hours, respectively. All regressions include county fixed effects, county-level time trends, and controls for four weather and five pollution variables. CO_2 coefficients were scaled by $\kappa = \frac{1}{4.5}$ as outlined in equation (3) and Table 1. Standard errors are clustered at the state level. Stars indicate significance levels: * 10%, ** 5%, *** 1%.

Appendix - For Online Publication

Environmental Drivers of Agricultural Productivity Growth: CO_2 Fertilization of US Field Crops

Charles A. Taylor[1] and Wolfram Schlenker[2]

List of Figures

List of Tables

[1] Harvard Kennedy School and NBER: ctaylor@hks.harvard.edu

[2] Harvard Kennedy School, NBER and CEPR: wolfram_schlenker@hks.harvard.edu

Appendix A Analysis Using OCO Satellite Data

Appendix A.1 Derivation of County-level CO_2 Exposure

To derive county-level CO_2 exposure, we first independently aggregate the raw OCO readings (Level 2) to the county-month level. For both OCO-2 and OCO-3, we follow a procedure that closely mirrors how the corresponding weather variables are constructed, before averaging across the two data sources and then across month of the growing season. The specific steps are:

1) **Seasonality Adjustment**: Since observations over a given county occur at different times of the crop-growing season, reflecting the satellite's revisit timing and the presence of quality flags, we adjust CO_2 values to make them comparable by accounting for the annual pattern in which ambient CO_2 concentrations decrease in the spring and summer, when plants are actively photosynthesizing in the Northern hemisphere, and increase in the fall and winter, when plants are respiring on net.

   We seasonally adjust the CO_2 readings for a common within-year seasonality, converting each reading to its equivalent value as of July 1st of the same year. The seasonal pattern is shown in Figure A1, where we fit a 4^{th}-order Chebyshev Polynomial over the year, which we normalize to [-1,1] by transforming January 1st to equal -1 and December 31st to equal 1.[A1] We restrict the seasonality so the value on January 1 (time -1) equals the value on December 31 (time 1). We further include a time trend to account for annual increases in CO_2 at the global level. For example, if the average CO_2 level on April 1st is 2.2 ppm higher than on July 1st, we subtract 2.2 ppm to all observations from April 1st.[A2]

2) **Link with PRISM grid**: Each longitude-latitude coordinate from a seasonality-adjusted OCO reading in step (1) is linked to the PRISM grid cell in which it falls. The PRISM grid is a $\frac{1}{24}$ degree raster in both longitude and latitude. For each day, we average all readings within a given grid. This results in a daily grid-level CO_2 measure.

3) **CO_2 by county-crop-month**: We derive a monthly county-level CO_2 exposure that varies by crop, since different crops may be grown in different areas within a county.

   3a) For each month, we compute the weighted average CO_2 exposure across all daily PRISM grids from step (2) within a county to derive the crop-specific exposure.

[A1] This normalization is necessary as leap years have an additional day.

[A2] CO_2 also exhibits strong diurnal within-day variation (Idso et al., 2002; Xueref-Remy et al., 2018). The OCO-2 satellite is sun-synchronous and revisits points at the same time each day, so diurnal variation is not a concern. For OCO-3, we average across readings that cycle through the sunlit hours at regular and repeating intervals, thus not producing any location-specific diurnal biases.

The weights are given by the crop-specific average growing area, as reported in the Cropland Data Layer by USDA (2015-2024), which specifies for each 30 m grid cell what crop is grown. We sum all pixels growing either corn, soybeans, or wheat to obtain the growing area for each crop in the PRISM grid (roughly 4.5 km resolution), *i.e.*, by counting how many of the 30 m $\times$ 30 m pixel centroids within a PRISM grid cell are classified as each crop. For example, if one grid grows twice as much corn as a neighboring grid, it receives twice the weight in the average.

We also average all readings within a month, without adjusting for the frequency of readings in a grid cell. As a result, if a grid has readings on two days and another on one, the first grid effectively receives twice the weight as we have a clearer (less noisy signal).

3b) Additionally, we retain the sum of the grid-cell specific growing area across all grids and days in a county and month, which reflects how representative the exposure measure is—either because readings are taken from grids with significant crop coverage, or because certain grids are sampled more frequently. We need this measure as weight in the next step.

4) **Aggregating monthly OCO-2 and OCO-3 data**: We average the OCO-2 and OCO-3 measures derived in step (3a), weighting them according to the coverage measure from step (3b). Intuitively, if OCO-2 has more readings, or readings from areas with more crop coverage than OCO-3, its monthly average receives a higher weight. See Figure A2 for a cross-plot of observations.

5) **CO_2 over growing season**: We then average the monthly values from step (4) over the period April–September, giving each month equal weight. We do not weight by the number of readings in a month, since there is high serial correlation in the data, and readings from different months convey more information than the same number of readings within the same month.

6) **Derivation of CO_2 Anomalies**: Our baseline regressions use the values of step (5) while including county fixed effects and county-specific linear time trends as outlined in equation (1). However, for the scaling factor κ in equation (3) we require the standard deviation of the anomalies, which we compute as residuals after fitting a linear model with county fixed effects and county-specific linear time trends to match the variation used in the regressions.

Appendix A.2 Derivation of Upwind Neighbor

Neighboring counties are derived using the following four steps:

1) **Cropland-weighted centroid**: We first calculate the centroid of a county as the cropland-weighted average of all grids within the county, weighting by the average acreage of corn, soybeans, and winter wheat from the Cropland Data Layer for 2015–2024. This provides a time-invariant measure of where the cropping area is, on average, located within each county.

2) **Pairing with unweighted centroids of neighboring counties**: We begin by pairing each county's cropland-weighted centroid with the unweighted centroids of all its neighboring counties, since we use all CO_2 sources as instruments, not only those over agricultural areas. The direction to each neighboring county is time-invariant and calculated once.

3) **Hourly wind direction and upwind neighbor**: Hourly wind data are obtained from the North American Land Data Assimilation System (NLDAS),[A3] using the cropland-area-weighted average of all NLDAS grid cells within each county. We determine which county is "upwind" by calculating the cosine of the angle between the wind direction and the direction to each neighboring county, identifying the county whose cosine is closest to -1.

4) **Cumulative time county is upwind**: For each neighboring county, we then sum the number of hours it is "upwind" of our target county over the 4,392 hours that comprise the growing season (April to September) in a given year. The neighboring county that is most frequently upwind is thus categorized as the "upwind" county for that year, which can vary from year to year. We then instrument each county's CO_2 anomaly with that of its most frequently upwind neighbor in the given year.

[A3] The data is available at https://hydro1.gesdisc.eosdis.nasa.gov/data/NLDAS/NLDAS_FORA0125_H.2.0/

Figure A1: Seasonality in CO_2

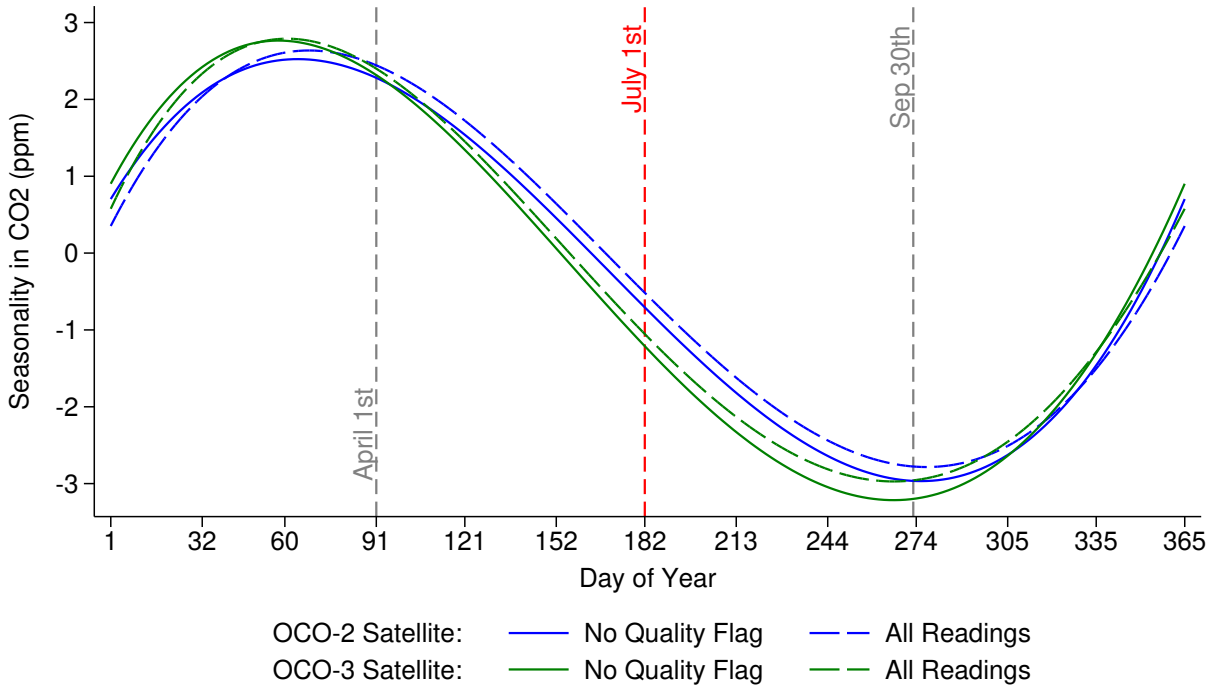

Notes: The chart displays the seasonality in CO_2 concentrations. To make readings comparable and compute average CO_2 levels at the county-year level, satellite readings are seasonally adjusted to July 1 (red dashed line) of each given year; that is, each reading is corrected by the difference between the July 1 value of the fitted seasonality curve and the value of the curve on the day of measurement. We fit a 4^{th}-order Chebyshev polynomial in the day of year and a linear time trend across years to the unbalanced daily time series of CO_2 satellite readings. Since years have different numbers of days, we normalize January 1 to -1 and December 31 to 1. The seasonality regression is constrained so that the value at the end of the year (December 31) equals the value at the beginning of the year (January 1). The seasonality curves used in the analysis (solid lines) are estimated using readings without quality flags across the contiguous US. For comparison, the dashed lines use all observations across the US, including those with flags. The main growing season for corn and soybeans (April–September) is indicated by gray dashed lines.

Figure A2: Comparing Observations in OCO-2 and OCO-3

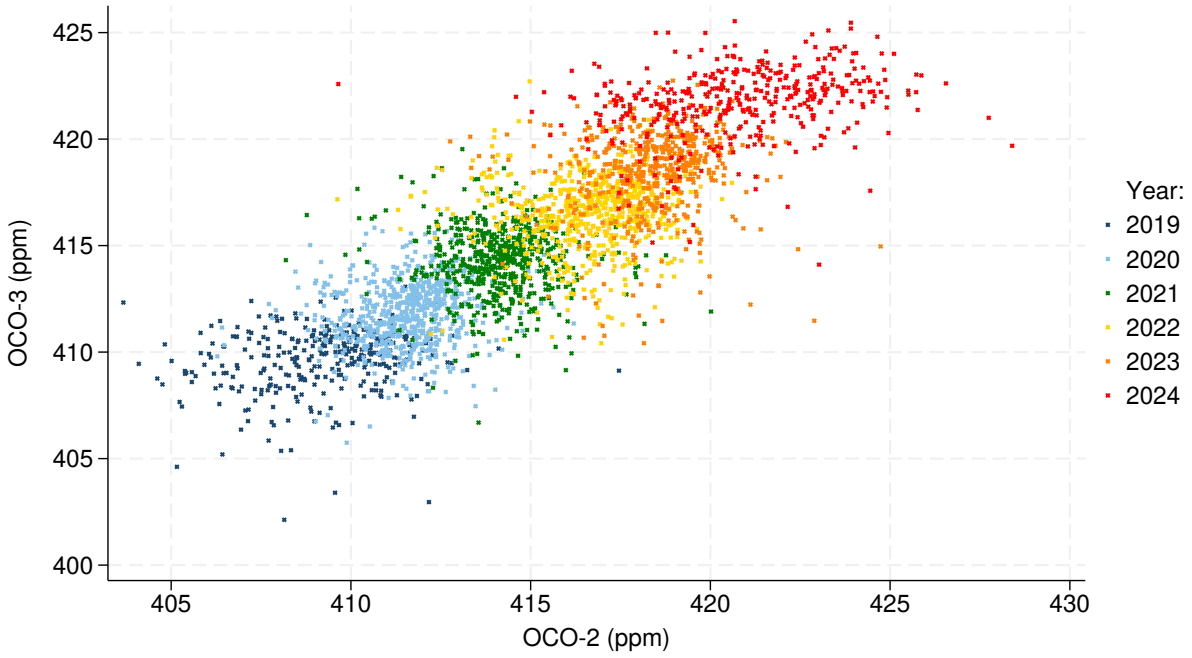

Notes: The chart displays county-level measures of CO_2 from OCO-2 (x-axis) and OCO-3 (y-axis) in our corn sample for the years in which both satellites report data (2019–2024). If the measurements were in perfect agreement, all points would lie on the 45-degree line. Some divergence between the two measures is expected, as the satellites operate at different frequencies and times, and the data inherently include sampling noise. To mitigate this noise and provide the most reliable signal, we average readings from both satellites.

Figure A3: Number of Observations per County in 2015-2022

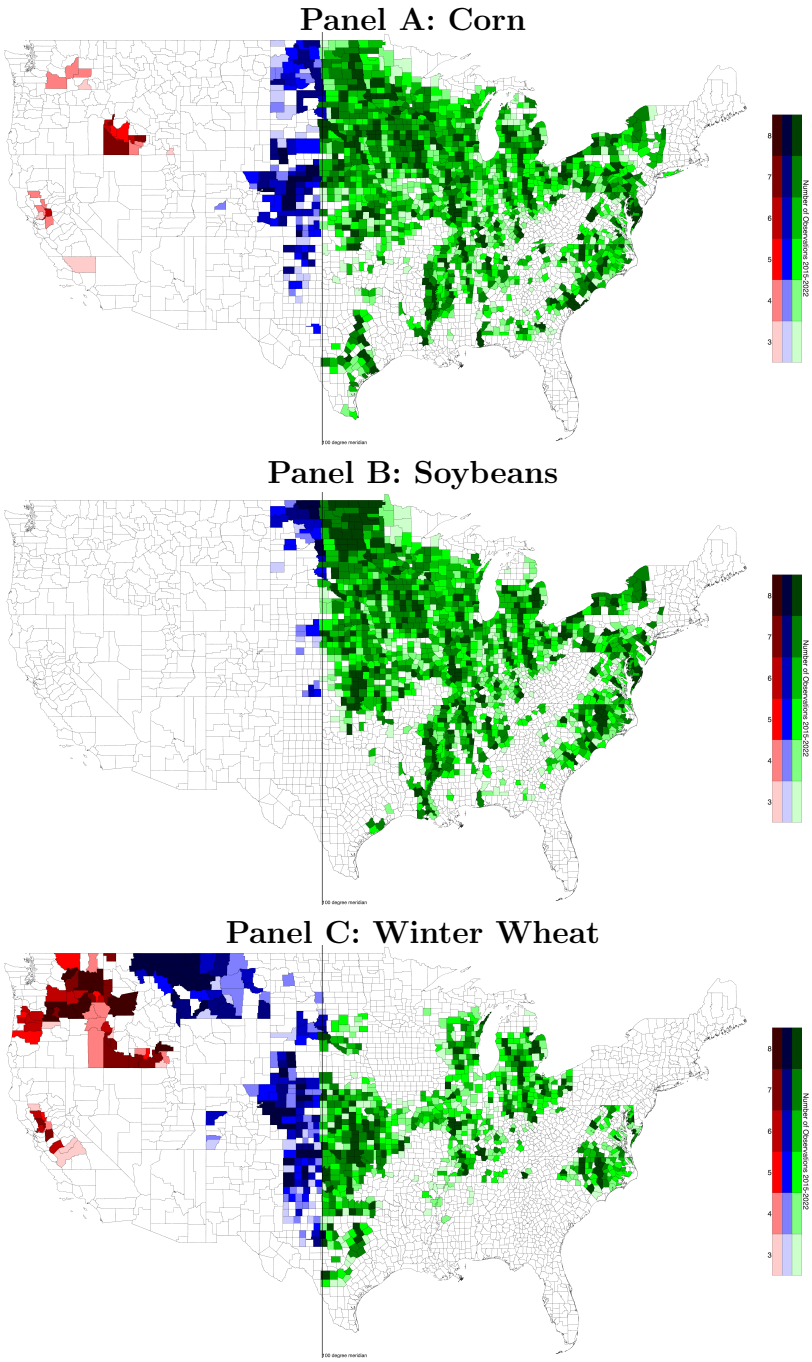

Notes: The figure displays the number of observations per county in the dataset, i.e., counties where yield, weather, air pollution, and CO_2 data (from either OCO-2 or OCO-3) are available over the sample period used in the baseline regression, 2015–2022. The analysis is split into three geographic subsets: east of the 100° meridian excluding Florida (Schlenker and Roberts, 2009) (shown in shades of green); inter-mountain states east of the Rocky Mountains (shown in blue); and western states (Arizona, California, Idaho, Nevada, Oregon, Utah and Washington; shown in red). Since the specification includes county fixed effects and county-specific time trends, at least three observations are required for a county to be included in the analysis.

Figure A4: Number of Counties Reporting Yields in 2015-2024

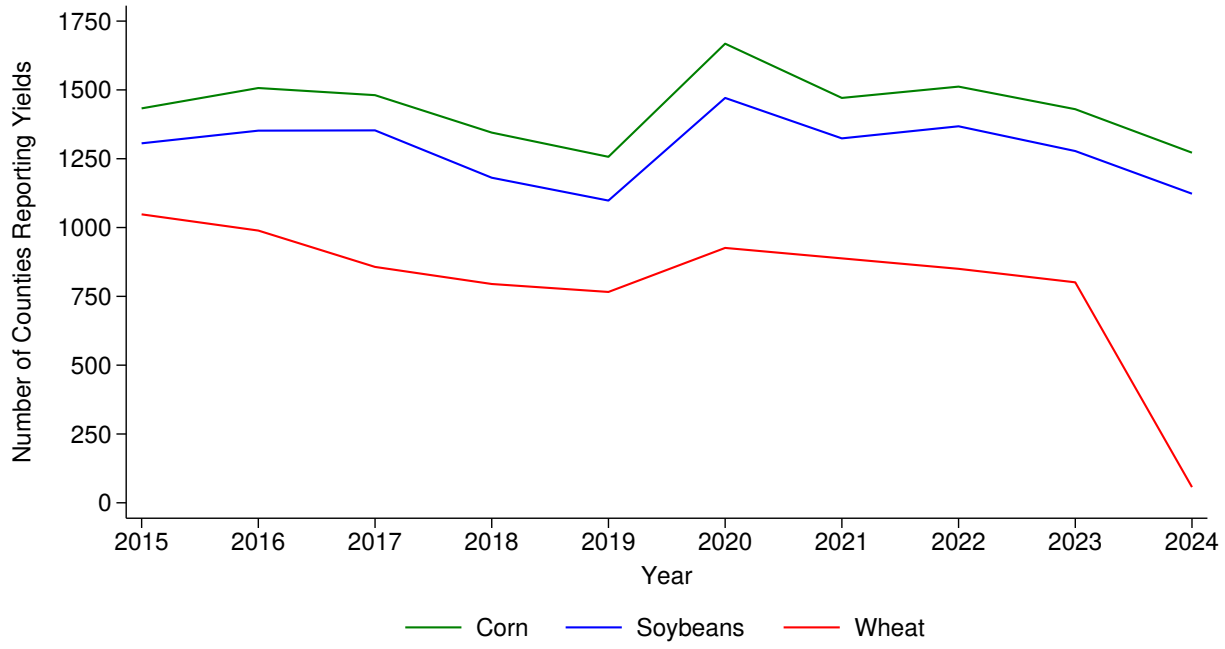

Notes: The figure displays the number of counties reporting yields in the National Agricultural Statistics Service (NASS) dataset. These include counties in all states and territories, and are not confined to specific geographic subsets. Note the precipitous drop in 2024, when the USDA stopped reporting county-level crop yields for several commodities, including wheat.

Figure A5: Variation in CO_2 Anomalies

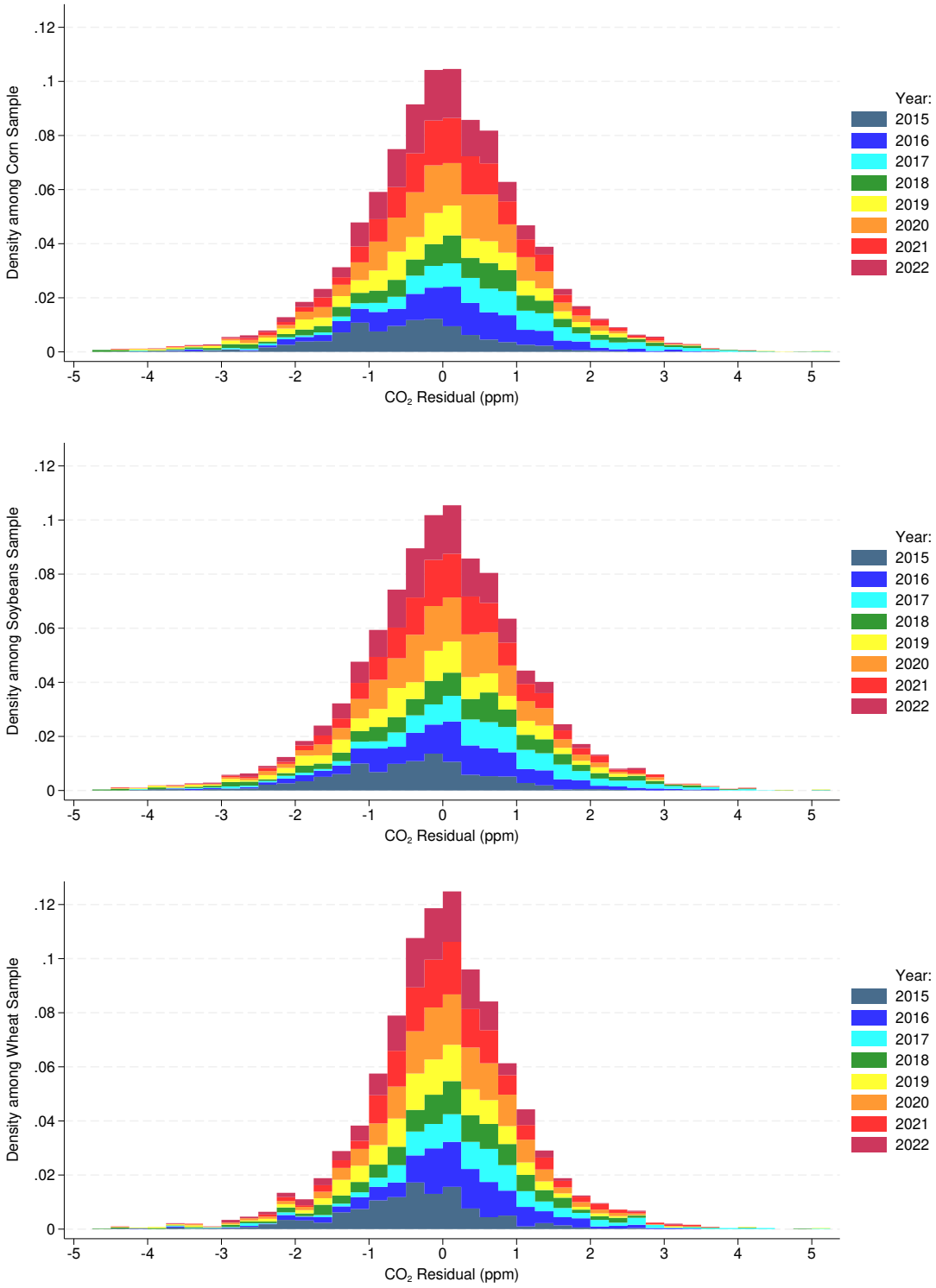

Notes: The graphs display histograms of the variation in CO_2 anomalies (after controlling for all covariates) by year for corn, soybeans, and wheat, respectively. Each histogram shows the fraction of anomalies falling within each 0.25 ppm bin. The leftmost bin is bottom-coded to include all anomalies below -5 ppm, while the rightmost bin is top-coded to include all anomalies above 5 ppm.

Figure A6: Sensitivity to Geographic Subset

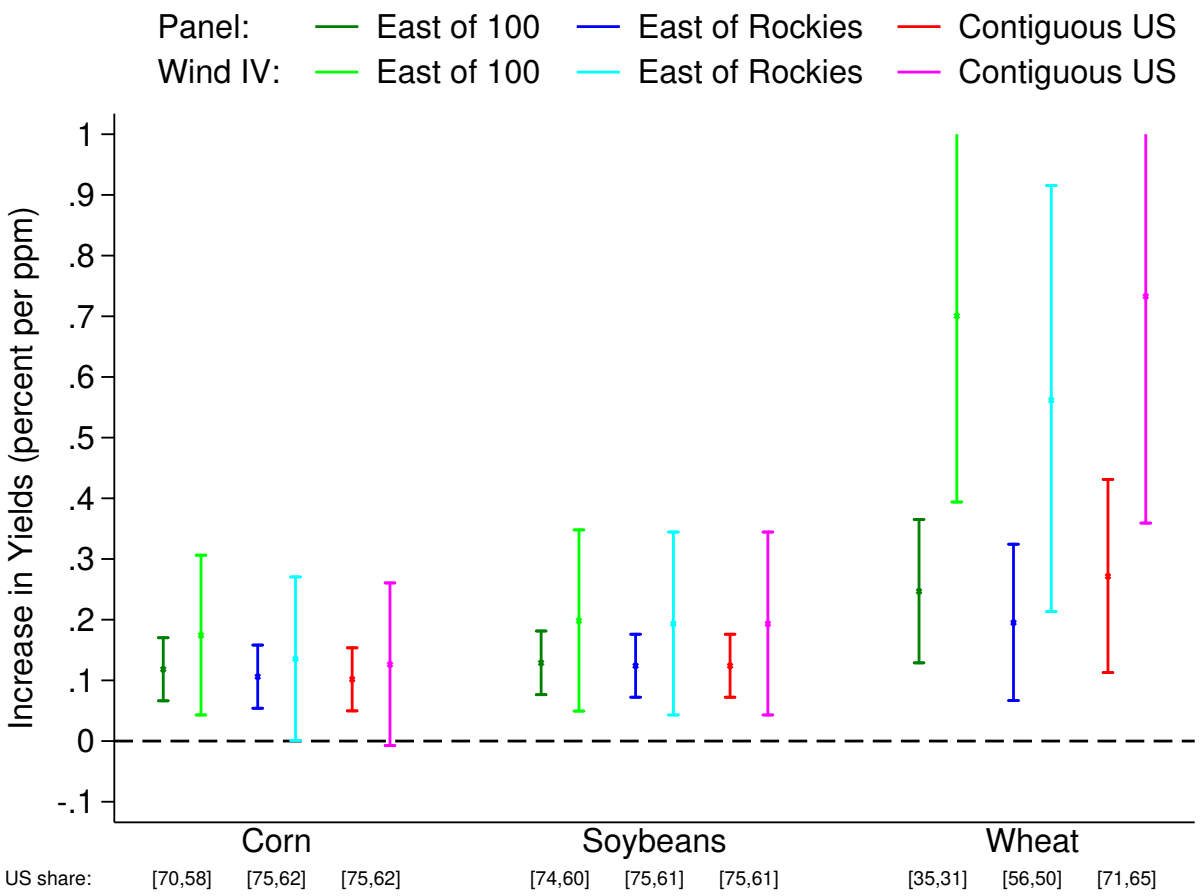

Notes: The figure displays the sensitivity of the results to the geographic subset used in the estimation, as shown in Figure A3. The "East of 100" sample includes all counties whose centroid is east of the 100° meridian (shown in green in Figure A3). The "East of Rockies" sample includes all counties east of the Rocky Mountains (shown in green or blue in Figure A3). The "Contiguous US" sample includes all counties in the continental US (shown in green, blue, or red in Figure A3). In each case, a county must report yields in at least three years to be included, as our specification has county fixed effects as well as county-specific time trends. Using the baseline period from 2015–2022, specifications correspond to columns (c) of both the panel regressions (Table 2) and the wind IV (Table 3). CO_2 coefficients were scaled by $\kappa = \frac{1}{4.5}$ as outlined in equation (3) and Table 1. Point estimates are shown as a star, while the whiskers indicate the 90% confidence interval. The bottom row shows, in percent, the share of US production over the time period that is included in the analysis.

Figure A7: Sensitivity to Time Trend

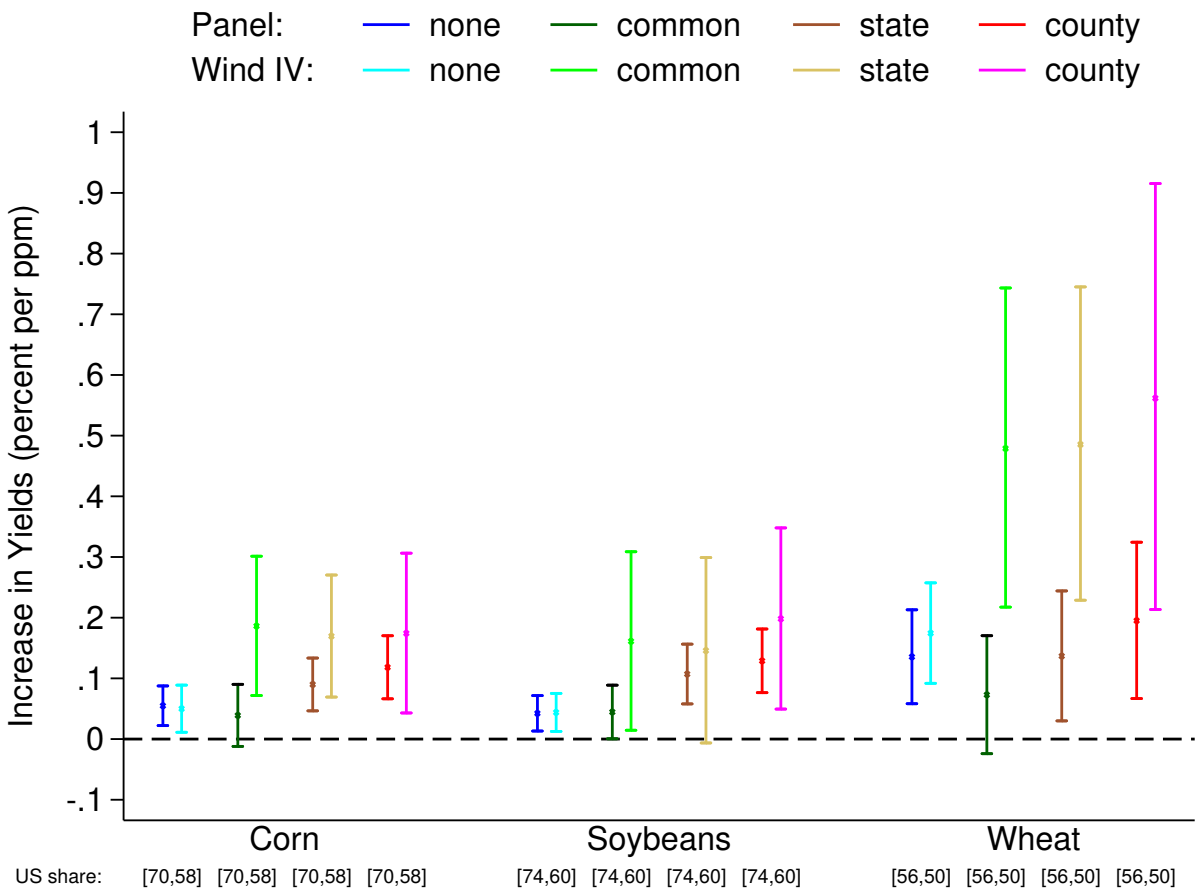

Notes: The figure displays the sensitivity of the results to the included time trend, ranging from no time trend at all, to a common time trend for all counties, a state-specific time trend, and county-specific time trends used in our baseline model. Using the baseline period from 2015–2022, all specifications include the controls from columns (c) of both the panel regressions (Table 2) and the wind IV (Table 3). CO_2 coefficients were scaled by $\kappa = \frac{1}{4.5}$ as outlined in equation (3) and Table 1. Point estimates are shown as stars, while the whiskers indicate the 90% confidence interval. The bottom row shows, in percent, the share of US production over the time period that is included in the analysis.

Figure A8: Sensitivity to Last Year in Sample

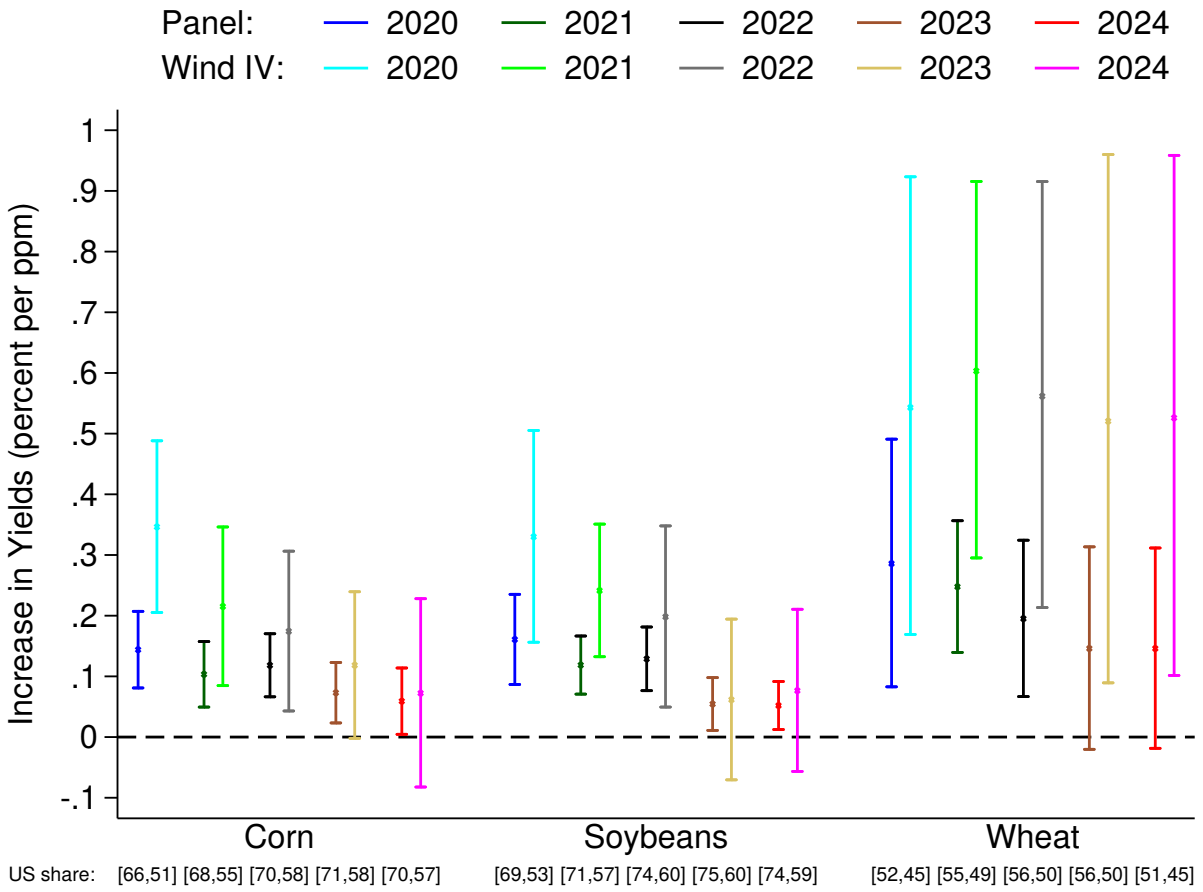

Notes: The figure displays the sensitivity of the results to the choice of end year in the analysis. The sample always begins in 2015, but the last year varies from 2020 to 2024. Specifically, blue colors represent data from 2015–2020, while red colors represent data from 2015–2024. Specifications correspond to columns (c) of both the panel regressions (Table 2) and the wind IV (Table 3). CO_2 coefficients were scaled by $\kappa = \frac{1}{4.5}$ as outlined in equation (3) and Table 1. Point estimates are shown as stars, while the whiskers indicate the 90% confidence interval. The bottom row shows, in percent, the share of US production over the time period included in the analysis.

Figure A9: Sensitivity to Functional Form

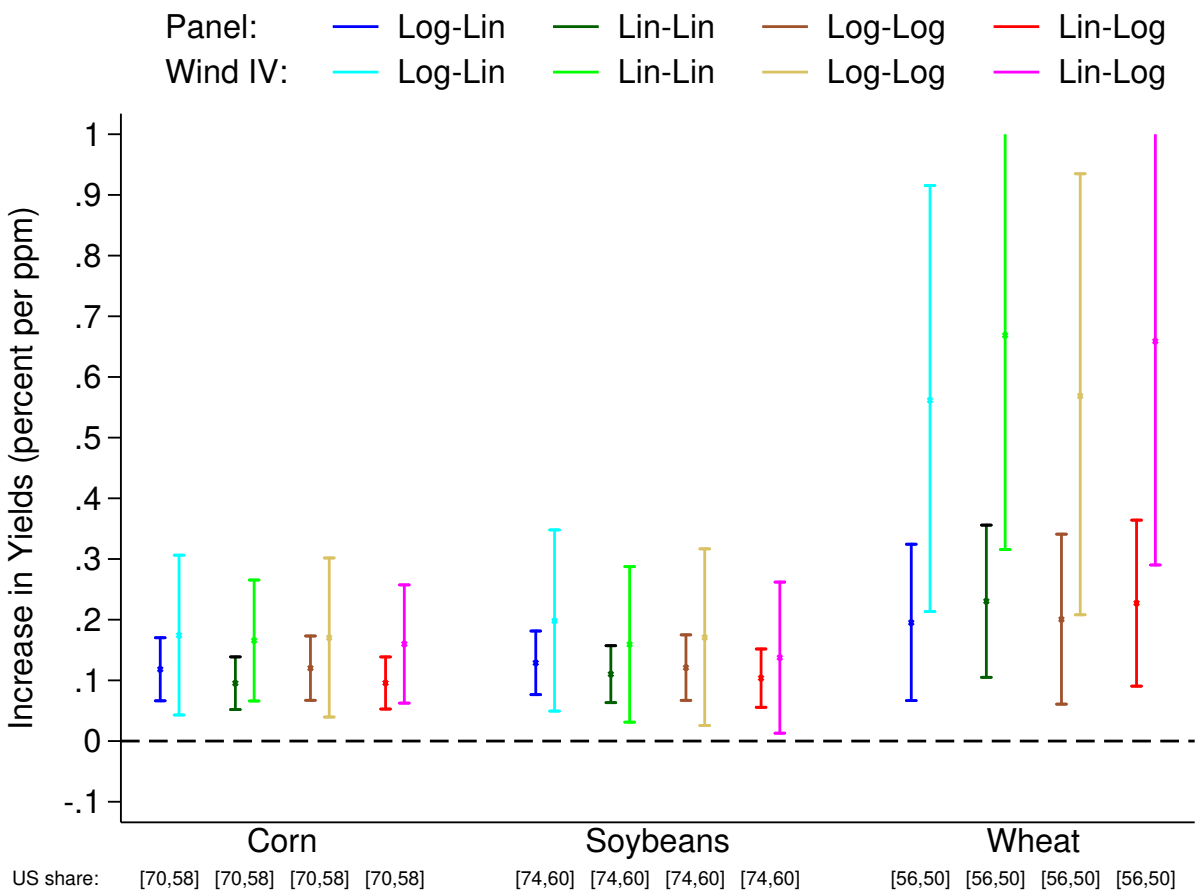

Notes: The figure displays the sensitivity of the results to the functional form. Our baseline model ("Log-Lin"; constant relative effect) regresses log yields on CO_2 levels. The "Lin-Lin" model (constant absolute effect) regresses yields on CO_2 levels, the "Log-Log" model (constant elasticity) regresses log yields on log CO_2 levels, and the "Lin-Log" model regresses yields on log CO_2 levels. Using the baseline period from 2015–2022, all specifications include the controls from columns (c) of both the panel regressions (Table 2) and the wind IV (Table 3). CO_2 coefficients were scaled by $\kappa = \frac{1}{4.5}$ as outlined in equation (3) and Table 1. Point estimates are shown as stars, while the whiskers indicate the 90% confidence interval. The bottom row shows, in percent, the share of US production over the time period included in the analysis.

Table A1: Summary Statistics of IV Setup

	Corn	Soybeans	Wheat
	Panel A: All counties		
Hours Upwind			
Mean	1461	1442	1563
Range	[615,3933]	[670,3086]	[670,3505]
Standard deviation	(1461)	(1442)	(1563)
County Upwind			
Always the same	1025	944	558
One of two counties	309	307	140
One of three or more counties	52	46	18
	Panel B: At least 1000 hours		
Hours Upwind			
Mean	1506	1483	1613
Range	[997,3933]	[997,3086]	[997,3505]
Standard deviation	(1506)	(1483)	(1613)
County Upwind			
Always the same	1012	940	550
One of two counties	260	255	112
One of three or more counties	23	23	7
	Panel C: At least 1500 hours		
Hours Upwind			
Mean	1884	1832	1955
Range	[1497,3933]	[1497,3086]	[1497,3505]
Standard deviation	(1884)	(1832)	(1955)
County Upwind			
Always the same	492	452	298
One of two counties	21	23	21
One of three or more counties	0	0	0

Notes: The table provides summary statistics for the IV setup outlined in Figure 3 using the baseline period from 2015–2022. The first three rows of each panel report the number of hours a county is upwind in the IV setup (the corresponding histogram is shown in Figure 4). Values are relative to 4,392 hours, the number of hours during the growing season April–September. The last three rows in each panel display the variation whether the upwind county changes between years or is always the same. For the majority of counties, the upwind county remains the same every year. Panel A includes all counties using the most frequent upwind neighbor, regardless of how many hours it is upwind; Panel B requires the upwind county to be upwind at least 1,000 hours; and Panel C requires the upwind county to be upwind at least 1,500 hours.

Appendix B Time Series Analysis Using Annual Data

Our baseline model used satellite measures of CO_2 anomalies throughout the US in a panel setting. We follow the recent work of Bilal and Känzig (2024) and present a time series analysis; that is, we reduce our sample size to one observation per year. While we lose coverage in space, we can extend the analysis to include additional years before the satellite began reporting. CO_2 levels are obtained from the Mauna Loa Observatory in Hawaii, which began reporting in 1958. We continue to focus on the main growing season and derive the average CO_2 from April to September for the years 1958–2024 (67 years), linking these values to annual average US crop yields for corn, soybeans, and wheat.

The revised regression equation becomes

$$y_t = \alpha_0 + \alpha_1 t + \alpha_2 t^2 + \beta\ \widehat{c_t} + \boldsymbol{\gamma}\mathbf{W}_t + \epsilon_t \tag{B1}$$

It is analogous to equation (1), except that we include an additional squared term for the time trend, α_2, given the much longer time frame of 67 years, over which the assumption of a linear trend is inadequate. Furthermore, we no longer control for pollution, as the EPA did not start reporting most pollutants until the 1980s.

We construct $\widehat{c_t} = \widehat{\epsilon_t}$ as the predicted innovations from an autoregressive process with up to L lags:

$$c_t = \alpha_0 + \sum_{k=1}^{L} \beta_k c_{t-k} + \epsilon_t \tag{B2}$$

The resulting CO_2 innovations are displayed in Figure B1. The standard deviation of these shocks ranges between 0.52 and 0.55.[B1] Note the correlation with El Niño: major El Niño events are associated with positive CO_2 innovations. This raises a potential drawback: El Niño changes weather patterns that may themselves influence yields. However, as discussed in the main paper, we would expect this effect to downward bias our estimates, as higher CO_2 levels are the result of reduced biological activity (photosynthesis), due, for example, to more extreme heat, which leads to a negative association between CO_2 and crop yields. Controlling for weather should therefore increase the predicted effect, especially for corn, a C4 crop with a lower expected CO_2 response, where we have a statistical model with great explanatory power. We derive the aggregate weather $\mathbf{W}_t$ for the US as the weighted average of all county-level weather variables.[B2]

The results are shown in Figure B2. The CO_2 fertilization effect is estimated with more noise (larger standard errors) than in our baseline results, which is not surprising given that we only have 67 observations. As hypothesized, controlling for weather increases the coeffi-

[B1] The standard deviation of these Mauna Loa-derived CO_2 shocks (σ_{MaunaLoa}) is lower than those of the OCO satellite (σ_{OCO}), hence we need to rescale by a factor $\kappa = \frac{1}{11}$ to match the variation found at 2 m in the FluxTower data as outlined in Table 1.

[B2] Weights are based on the predicted production of a county, as counties with higher output have a larger share in the overall average yield. Specifically, we fit state-specific quadratic time trends to the county-level log yield data and derive the weight as the product of the predicted yield (according to the trend) and the growing area.

cient in the case of corn, highlighting the negative correlation between CO_2 anomalies and crop yields. Once we control for weather, the results for corn are marginally significant under AR(1) and AR(2) innovations and become statistically significant under AR(3). Consistent with our baseline results, the CO_2 fertilization effect is strongest for wheat, remaining statistically significant in all models, whether we control for weather or not. On the other hand, the results are never significant for soybeans, but given the wide confidence intervals, they are also not statistically significantly different from our baseline results.

While confidence intervals are larger when we switch to the time series analysis, the findings broadly support what we found in the baseline regression, despite using a completely different source of variation, ground-level observations at Mauna Loa, rather than satellite data. This provides additional evidence for our CO_2 fertilization effects under real-world growing conditions.

Figure B1: CO_2 Innovations in Autoregressive Process

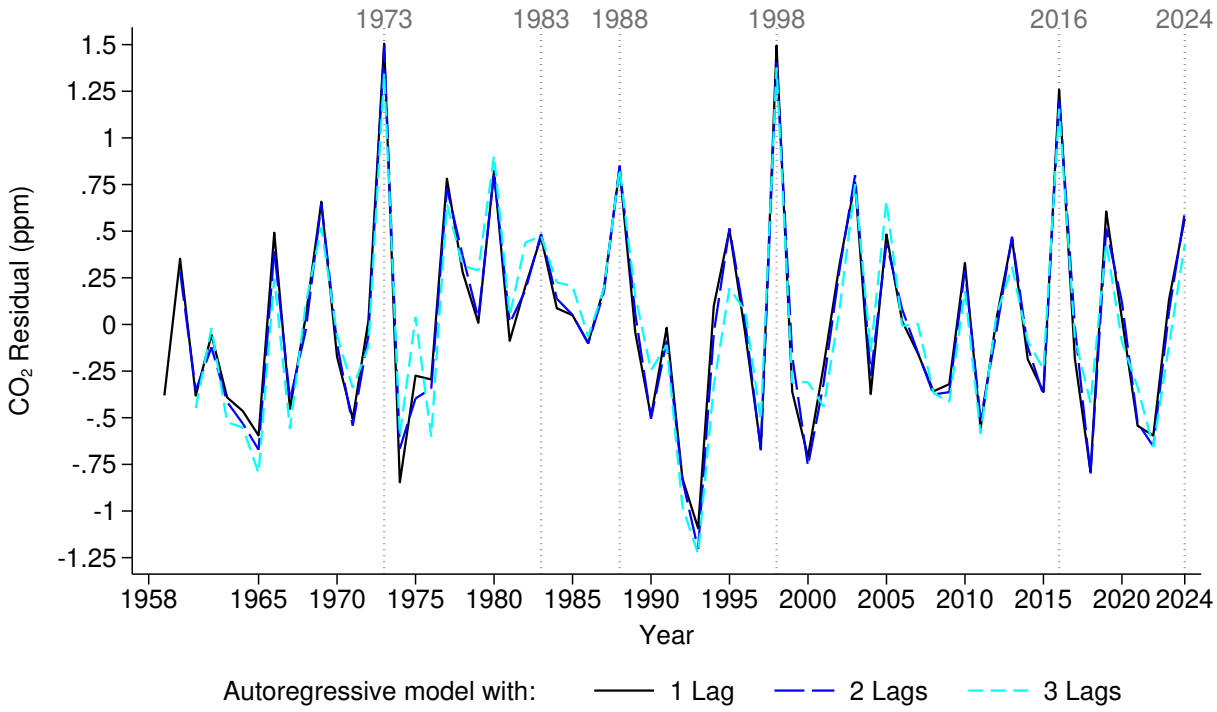

Notes: The figure displays the predicted innovations (errors) from the autoregressive process given in equation (B2), where the number of lags is varied from $L = 1$ to $L = 3$. The underlying CO_2 values are the average readings for April–September as recorded by the Mauna Loa Observatory in Hawaii. Dashed lines indicate major El Niño events: 1972–1973, 1982–1983, 1987–1988, 1997–1998, 2015–2016, and 2023–2024.

Figure B2: Time Series Regression Linking Yields to CO_2 Innovations

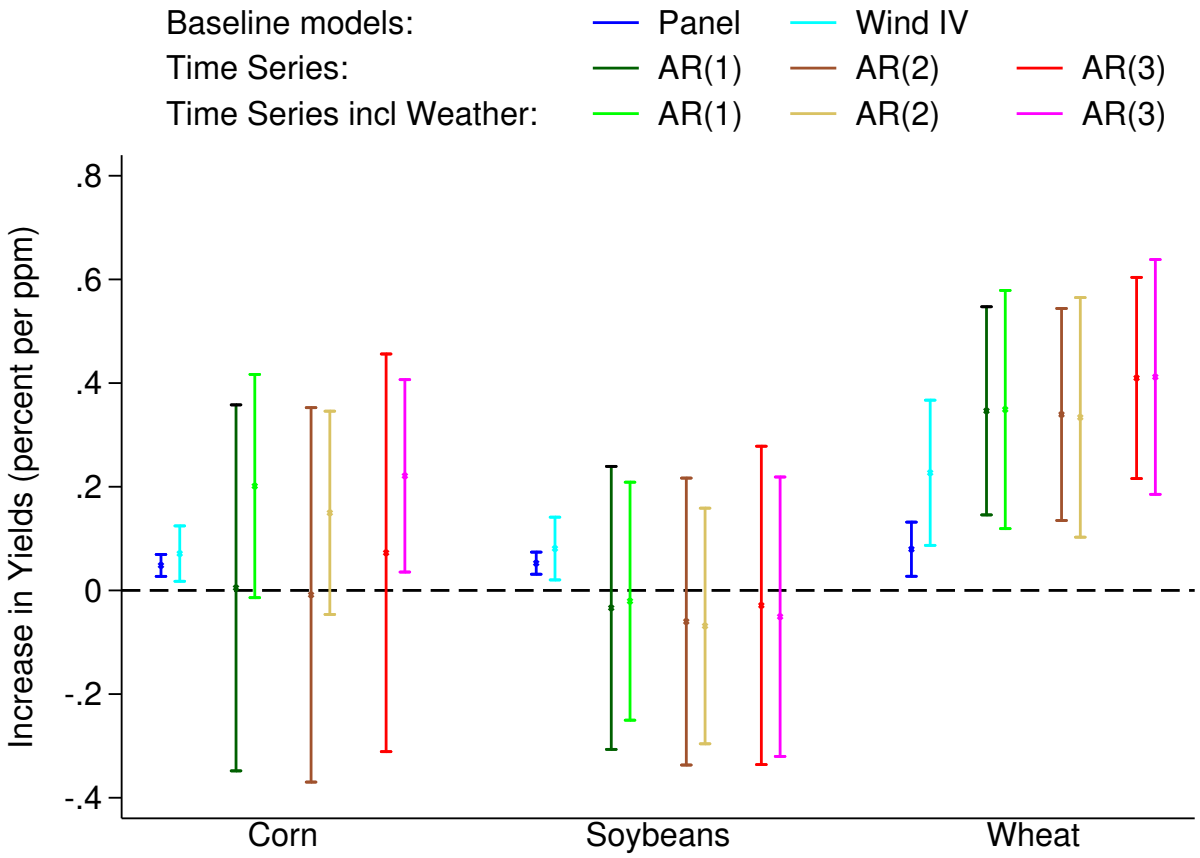

Notes: The figure displays the results when CO_2 innovations from Figure B1 are used in a time series regression linking yields to CO_2. For reference, the blue whiskers show the results from our baseline panel regression (columns (c) of Table 2) as well as the wind IV (columns (c) of Table 3). The remaining entries use the innovations from AR(1), AR(2), and AR(3) regressions, respectively. All time series regressions include quadratic time trends. For each, we present the results first without controlling for weather, and then when controlling for the same four weather variables as in columns (b) of Table 2. CO_2 coefficients were scaled by $\kappa = \frac{1}{11}$ as outlined in equation (3) and Table 1. Point estimates are shown as stars, while the whiskers indicate the 90% confidence interval.

Appendix C Flux Tower Data

Appendix C.1 Derivation of Variation in CO_2 Exposure

We downloaded all tower data from AmeriFlux to estimate how the fluctuation in CO_2 anomalies vary by height.

1) Download all data from the AmeriFlux tower network. The locations of the flux towers are shown in Figure C1.

2) Compute the average CO_2 reading over April–September of each year at each instrument.[C1] Note that most flux towers have several instruments at various heights. They generally report hourly data throughout the growing season, and we therefore do not need to perform the seasonality adjustment applied to the sparser OCO satellite data; such an adjustment would only add a constant, which is irrelevant when deriving the standard deviation of fluctuations. Seasonality patterns only matter when data are reported infrequently, as part of the year-to-year changes might otherwise be due to differences in sampling dates within the growing season.

3) Fit a model with instrument-level fixed effects and instrument-specific time trends to the annual observations from step (2), and compute the annual residuals around these time trends. Note that we estimate a separate time trend for each instrument at a flux tower, thereby allowing the trend to differ across the various heights at which the instruments are placed.

4) Calculate the standard deviation of the anomalies derived in step (3). We then fit a restricted cubic spline with three knots to model the relationship between the standard deviation of these anomalies and the height of the instrument.[C2]

5) Plot the standard deviation of the instrument-specific anomalies in Figure C2. Each x in the plot represents the standard deviation from a different instrument across years. The restricted cubic spline from step (4) is shown as a solid line, with the locations of the knots indicated by gray dashed lines. The top panel uses data from all flux towers for all available years (the earliest towers began reporting in 1993, and data through 2024 are included). The bottom panel restricts the data to instruments from flux towers located in cropland areas.[C3] The earliest flux tower began reporting in 1983, whereas the earliest flux tower located in cropland started reporting in 2001.

[C1] We exclude CO_2 readings below 300 ppm and above 1000 ppm to ensure data integrity. We deliberately keep the month span constant, even though a few towers are in the Southern Hemisphere; omitting these towers has no effect, as shown below.

[C2] We exclude one outlier instrument positioned much higher than 125 m, as it would have a disproportionate influence on the restricted cubic spline fit.

[C3] Flux towers with a vegetation class between 1 and 9.

Figure C2 shows, in all panels, that annual CO_2 fluctuations over the growing season (April–September) decrease with instrument height. Each panel displays the standard deviation at 2 m, as predicted by the fitted restricted cubic spline, as well as at the upper limit of observed heights. Since our satellites measure CO_2 over the entire atmospheric column, we need to correct for the fact that fluctuations are higher within the crop canopy (2 m) than they are for the full column.

Figure C1: Location of AmeriFlux flux towers

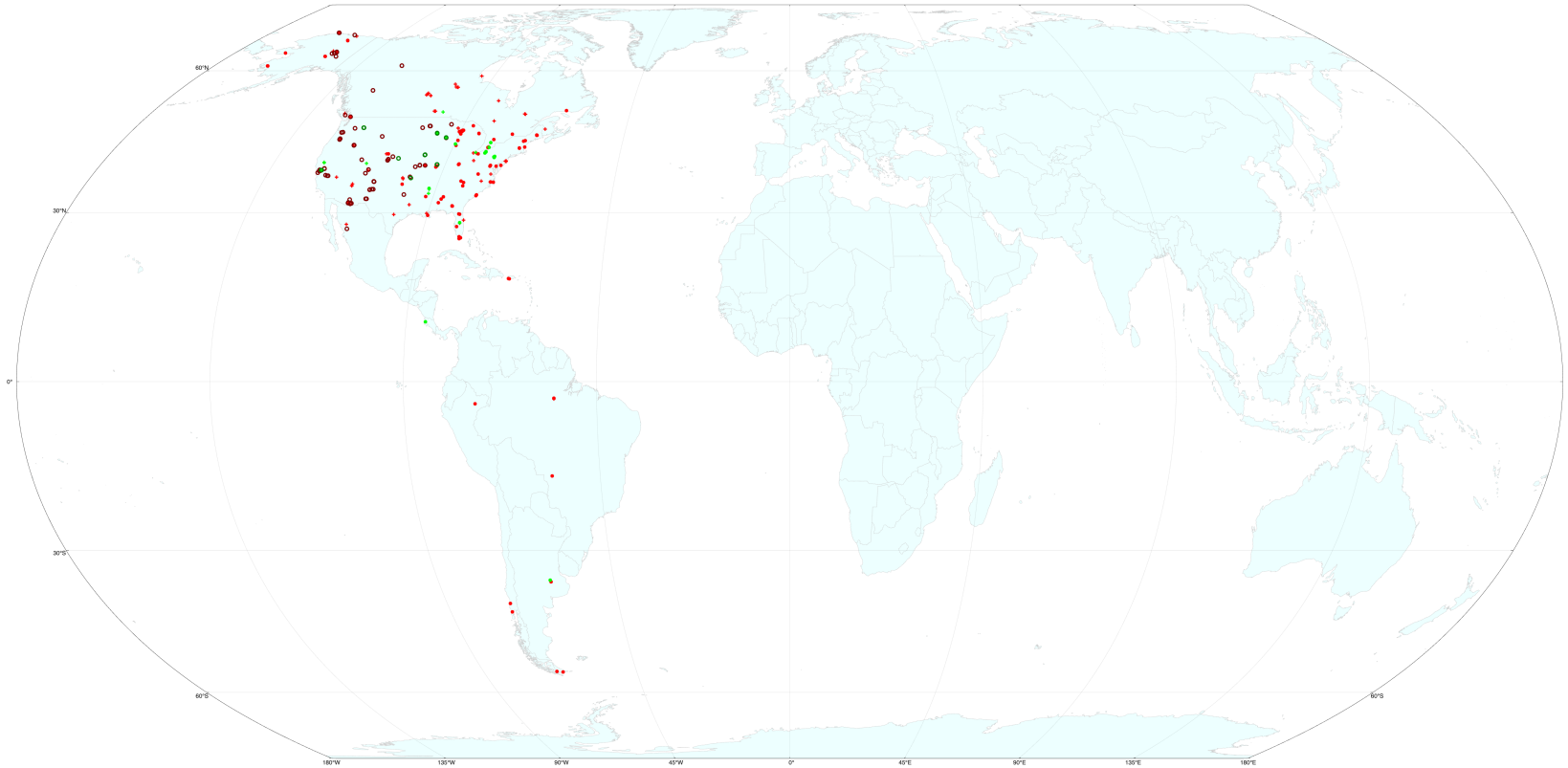

Notes: The figure displays the locations of flux towers with CO_2 data for April–September. Flux towers in cropland areas are shown in green: o indicates locations with OCO satellite readings during 2015–2022 (panel B3, column 3 in Table 1); * indicates cropland flux towers without OCO readings in 2015–2022; + indicates those with OCO readings only before 2015 or after 2022. The red markers o, *, and + show the corresponding flux tower locations outside cropland areas.

Figure C2: Annual variation in CO_2 across different heights of flux towers

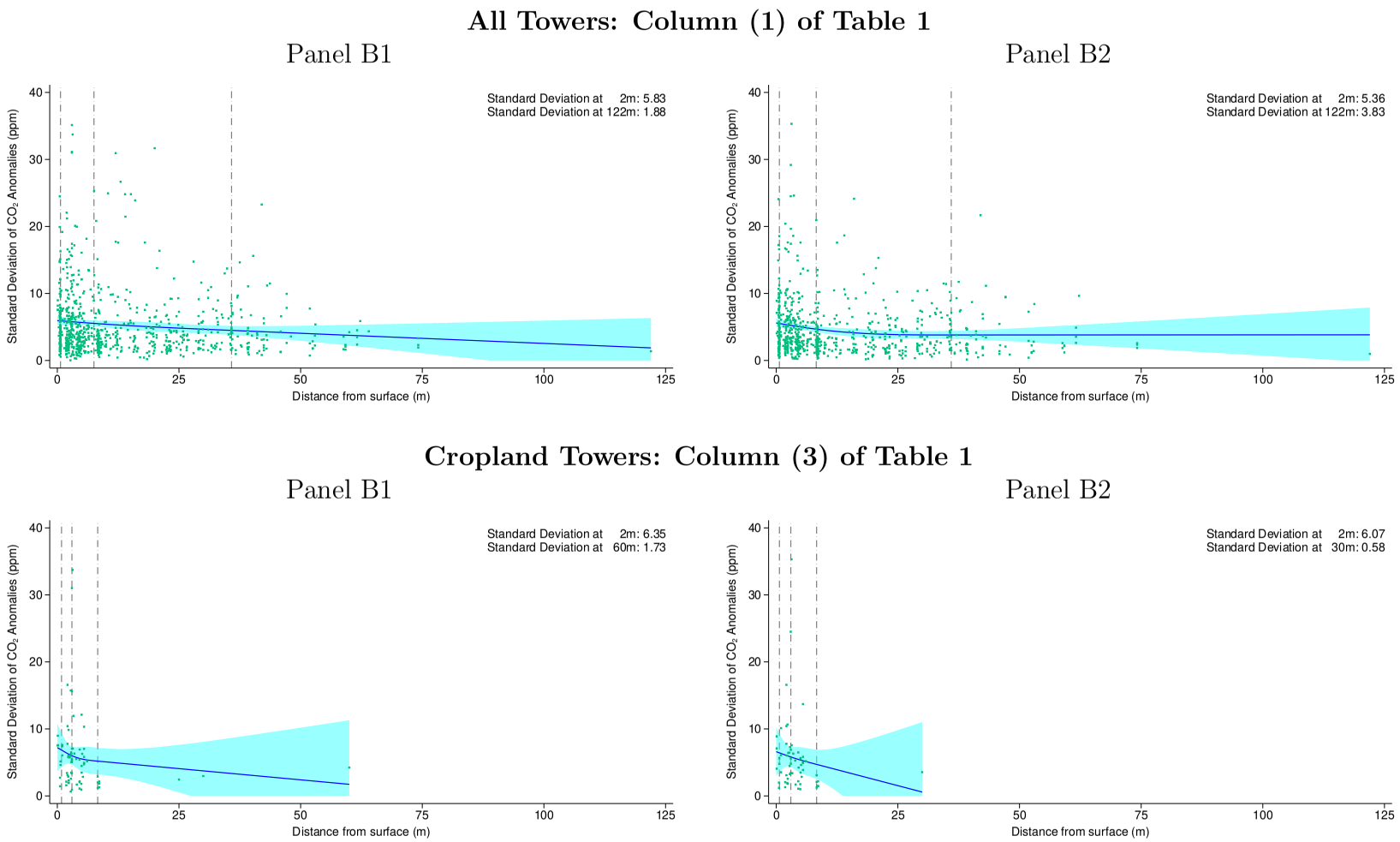

Notes: The panels use CO_2 readings from AmeriFlux flux towers (Figure C1). Each point represents the standard deviation of year-to-year anomalies around an instrument-specific time trend of average CO_2 levels over the growing season (April–September). The blue line is a restricted cubic spline with three knots (shown as gray dashed lines) that models the standard deviation in CO_2 readings as a function of instrument height.

Appendix C.2 AmeriFlux Data

We downloaded all available AmeriFlux data to conduct our analysis. Reference to particular sites is given in Table C1. We would like to acknowledge that funding for the AmeriFlux data portal was provided by the US Department of Energy Office of Science.

Table C1: Reference to AmeriFlux Data

Site ID	Citation
AR-Bal	Maria Isabel Gassmann, Natalia Edith Tonti (2024), AmeriFlux BASE AR-Bal Balcarce BA, Ver. 2-5, AmeriFlux AMP, (Dataset). https://doi.org/10.17190/AMF/2315764
AR-CCa	Gabriela Posse (2022), AmeriFlux BASE AR-CCa Carlos Casares agriculture, Ver. 1-5, AmeriFlux AMP, (Dataset). https://doi.org/10.17190/AMF/1880910
AR-CCg	Gabriela Posse (2025), AmeriFlux BASE AR-CCg Carlos Casares grassland, Ver. 5-5, AmeriFlux AMP, (Dataset). https://doi.org/10.17190/AMF/1865474
AR-TF1	Lars Kutzbach (2021), AmeriFlux BASE AR-TF1 Rio Moat bog, Ver. 2-5, AmeriFlux AMP, (Dataset). https://doi.org/10.17190/AMF/1543389
AR-TF2	Lars Kutzbach (2025), AmeriFlux BASE AR-TF2 Rio Pipo bog, Ver. 2-5, AmeriFlux AMP, (Dataset). https://doi.org/10.17190/AMF/1543388
BR-CST	Antonio Antonino (2019), AmeriFlux BASE BR-CST Caatinga Serra Talhada, Ver. 1-5, AmeriFlux AMP, (Dataset). https://doi.org/10.17190/AMF/1562386
BR-Npw	George Vourlitis, Higo Dalmagro, Jose Ì de S. Nogueira, Mark Johnson, Paulo Arruda (2019), AmeriFlux BASE BR-Npw Northern Pantanal Wetland, Ver. 1-5, AmeriFlux AMP, (Dataset). https://doi.org/10.17190/AMF/1579716
BR-Sa1	Natalia Restrepo-Coupe, Scott Saleska (2025), AmeriFlux BASE BR-Sa1 Santarem-Km67-Primary Forest, Ver. 6-5, AmeriFlux AMP, (Dataset). https://doi.org/10.17190/AMF/1245994
BR-Sa3	Mike Goulden (2019), AmeriFlux BASE BR-Sa3 Santarem-Km83-Logged Forest, Ver. 3-5, AmeriFlux AMP, (Dataset). https://doi.org/10.17190/AMF/1245995
CA-AF1	Manuel Helbig, Deirdre Spearns (2025), AmeriFlux BASE CA-AF1 Acadia Research Forest, Ver. 2-5, AmeriFlux AMP, (Dataset). https://doi.org/10.17190/AMF/2479623
CA-ARB	Aaron Todd, Elyn Humphreys (2018), AmeriFlux BASE CA-ARB Attawapiskat River Bog, Ver. 1-5, AmeriFlux AMP, (Dataset). https://doi.org/10.17190/AMF/1480319
CA-ARF	Aaron Todd, Elyn Humphreys (2018), AmeriFlux BASE CA-ARF Attawapiskat River Fen, Ver. 1-5, AmeriFlux AMP, (Dataset). https://doi.org/10.17190/AMF/1480318
CA-BOU	Michelle Garneau (2023), AmeriFlux BASE CA-BOU Bouleau Peatland, Ver. 2-5, AmeriFlux AMP, (Dataset). https://doi.org/10.17190/AMF/1987599
CA-Ca1	T. Andrew Black (2018), AmeriFlux BASE CA-Ca1 British Columbia - 1949 Douglas-fir stand, Ver. 1-5, AmeriFlux AMP, (Dataset). https://doi.org/10.17190/AMF/1480300
CA-Ca2	T. Andrew Black (2018), AmeriFlux BASE CA-Ca2 British Columbia - Clearcut Douglas-fir stand (harvested winter 1999/2000), Ver. 1-5, AmeriFlux AMP, (Dataset). https://doi.org/10.17190/AMF/1480301
CA-Ca3	T. Andrew Black (2025), AmeriFlux BASE CA-Ca3 British Columbia - Pole sapling Douglas-fir stand, Ver. 7-5, AmeriFlux AMP, (Dataset). https://doi.org/10.17190/AMF/1480302
CA-Cbo	Ralf Staebler (2022), AmeriFlux BASE CA-Cbo Ontario - Mixed Deciduous, Borden Forest Site, Ver. 6-5, AmeriFlux AMP, (Dataset). https://doi.org/10.17190/AMF/1498755
CA-CF1	Tim Papakyriakou (2023), AmeriFlux BASE CA-CF1 Churchill Fen Site 1, Ver. 2-5, AmeriFlux AMP, (Dataset). https://doi.org/10.17190/AMF/1660336
CA-CF2	Mario Tenuta (2023), AmeriFlux BASE CA-CF2 Churchill Fen Site 2, Ver. 2-5, AmeriFlux AMP, (Dataset). https://doi.org/10.17190/AMF/1634879
CA-CF3	Kyle Arndt, Susan Natali (2025), AmeriFlux BASE CA-CF3 Churchill Fen Site 3, Ver. 2-5, AmeriFlux AMP, (Dataset). https://doi.org/10.17190/AMF/2335573
CA-Cha	Charles Bourque (2018), AmeriFlux BASE CA-Cha New Brunswick - Charlie Lake site 01 (immature balsam fir forest to be thinned in year 3), Ver. 1-5, AmeriFlux AMP, (Dataset). https://doi.org/10.17190/AMF/1436317
CA-DB2	Sara Knox (2021), AmeriFlux BASE CA-DB2 Delta Burns Bog 2, Ver. 1-5, AmeriFlux AMP, (Dataset). https://doi.org/10.17190/AMF/1811362
CA-DBB	Andreas Christen, Sara Knox (2021), AmeriFlux BASE CA-DBB Delta Burns Bog, Ver. 2-5, AmeriFlux AMP, (Dataset). https://doi.org/10.17190/AMF/1543378
CA-DSM	Sara Knox (2025), AmeriFlux BASE CA-DSM Delta Salt Marsh, Ver. 2-5, AmeriFlux AMP, (Dataset). https://doi.org/10.17190/AMF/1964085
CA-EM1	Pascal Badiou (2024), AmeriFlux BASE CA-EM1 Newdale Manitoba, Ver. 1-5, AmeriFlux AMP, (Dataset). https://doi.org/10.17190/AMF/2315766
CA-EM2	Pascal Badiou (2024), AmeriFlux BASE CA-EM2 Shoal Lake Manitoba, Ver. 1-5, AmeriFlux AMP, (Dataset). https://doi.org/10.17190/AMF/2331380

Site ID	Citation
CA-ER1	Claudia Wagner-Riddle (2021), AmeriFlux BASE CA-ER1 Elora Research Station, Ver. 3-5, AmeriFlux AMP, (Dataset). https://doi.org/10.17190/AMF/1579541
CA-Gro	Harry McCaughey (2019), AmeriFlux BASE CA-Gro Ontario - Groundhog River, Boreal Mixedwood Forest, Ver. 2-5, AmeriFlux AMP, (Dataset). https://doi.org/10.17190/AMF/1245996
CA-HPC	Oliver Sonnentag, Phil Marsh (2021), AmeriFlux BASE CA-HPC Havikpak Creek, Ver. 1-5, AmeriFlux AMP, (Dataset). https://doi.org/10.17190/AMF/1773392
CA-LP1	Thomas Andrew Black (2025), AmeriFlux BASE CA-LP1 British Columbia - Mountain pine beetle-attacked lodgepole pine stand , Ver. 5-5, AmeriFlux AMP, (Dataset). https://doi.org/10.17190/AMF/1660337
CA-MA1	Brian Amiro (2023), AmeriFlux BASE CA-MA1 Manitoba Agricultural Site 1, Ver. 2-5, AmeriFlux AMP, (Dataset). https://doi.org/10.17190/AMF/1617701
CA-MA2	Brian Amiro (2023), AmeriFlux BASE CA-MA2 Manitoba Agricultural Site 2, Ver. 2-5, AmeriFlux AMP, (Dataset). https://doi.org/10.17190/AMF/1617702
CA-MA3	Brian Amiro (2023), AmeriFlux BASE CA-MA3 Manitoba Agricultural Site 3, Ver. 2-5, AmeriFlux AMP, (Dataset). https://doi.org/10.17190/AMF/1617703
CA-Man	Brian Amiro (2023), AmeriFlux BASE CA-Man Manitoba - Northern Old Black Spruce (former BOREAS Northern Study Area), Ver. 3-5, AmeriFlux AMP, (Dataset). https://doi.org/10.17190/AMF/1245997
CA-Mer	Elyn Humphreys, Peter Lafleur (2024), AmeriFlux BASE CA-Mer Ontario - Eastern Peatland, Mer Bleue, Ver. 2-5, AmeriFlux AMP, (Dataset). https://doi.org/10.17190/AMF/2448423
CA-Mtk	Kyle Arndt, Susan Natali (2025), AmeriFlux BASE CA-Mtk Mittimatalik (Pond Inlet) Tundra, Ver. 1-5, AmeriFlux AMP, (Dataset). https://doi.org/10.17190/AMF/2531141
CA-Na1	Charles P.-A. Bourque (2018), AmeriFlux BASE CA-Na1 New Brunswick - 1967 Balsam Fir - Nashwaak Lake Site 01 (Mature balsam fir forest), Ver. 1-5, AmeriFlux AMP, (Dataset). https://doi.org/10.17190/AMF/1436319
CA-NS1	Mike Goulden (2019), AmeriFlux BASE CA-NS1 UCI-1850 burn site, Ver. 3-5, AmeriFlux AMP, (Dataset). https://doi.org/10.17190/AMF/1245998
CA-NS2	Mike Goulden (2019), AmeriFlux BASE CA-NS2 UCI-1930 burn site, Ver. 3-5, AmeriFlux AMP, (Dataset). https://doi.org/10.17190/AMF/1245999
CA-NS3	Mike Goulden (2019), AmeriFlux BASE CA-NS3 UCI-1964 burn site, Ver. 3-5, AmeriFlux AMP, (Dataset). https://doi.org/10.17190/AMF/1246000
CA-NS4	Mike Goulden (2019), AmeriFlux BASE CA-NS4 UCI-1964 burn site wet, Ver. 3-5, AmeriFlux AMP, (Dataset). https://doi.org/10.17190/AMF/1246001
CA-NS5	Mike Goulden (2019), AmeriFlux BASE CA-NS5 UCI-1981 burn site, Ver. 3-5, AmeriFlux AMP, (Dataset). https://doi.org/10.17190/AMF/1246002
CA-NS6	Mike Goulden (2019), AmeriFlux BASE CA-NS6 UCI-1989 burn site, Ver. 3-5, AmeriFlux AMP, (Dataset). https://doi.org/10.17190/AMF/1246003
CA-NS7	Mike Goulden (2019), AmeriFlux BASE CA-NS7 UCI-1998 burn site, Ver. 3-5, AmeriFlux AMP, (Dataset). https://doi.org/10.17190/AMF/1246004
CA-Oas	T. Andrew Black (2016), AmeriFlux BASE CA-Oas Saskatchewan - Western Boreal, Mature Aspen, Ver. 1-1, AmeriFlux AMP, (Dataset). https://doi.org/10.17190/AMF/1375197
CA-Obs	T. Andrew Black (2016), AmeriFlux BASE CA-Obs Saskatchewan - Western Boreal, Mature Black Spruce, Ver. 1-1, AmeriFlux AMP, (Dataset). https://doi.org/10.17190/AMF/1375198
CA-Ojp	Andrew T. Black (2019), AmeriFlux BASE CA-Ojp Saskatchewan - Western Boreal, Mature Jack Pine, Ver. 2-5, AmeriFlux AMP, (Dataset). https://doi.org/10.17190/AMF/1375199
CA-Qc2	Hank Margolis (2018), AmeriFlux BASE CA-Qc2 Quebec - 1975 Harvested Black Spruce (HBS75), Ver. 1-5, AmeriFlux AMP, (Dataset). https://doi.org/10.17190/AMF/1419514
CA-Qcu	Hank A. Margolis (2016), AmeriFlux BASE CA-Qcu Quebec - Eastern Boreal, Black Spruce/Jack Pine Cutover, Ver. 1-1, AmeriFlux AMP, (Dataset). https://doi.org/10.17190/AMF/1246828
CA-Qfo	Hank A. Margolis (2019), AmeriFlux BASE CA-Qfo Quebec - Eastern Boreal, Mature Black Spruce, Ver. 2-5, AmeriFlux AMP, (Dataset). https://doi.org/10.17190/AMF/1246829
CA-RBM	Sara Knox (2025), AmeriFlux BASE CA-RBM Richmond Brackish Marsh, Ver. 1-5, AmeriFlux AMP, (Dataset). https://doi.org/10.17190/AMF/2563527
CA-RSB	Kyle Arndt, Susan Natali (2025), AmeriFlux BASE CA-RSB Resolute Bay Polar Desert, Ver. 2-5, AmeriFlux AMP, (Dataset). https://doi.org/10.17190/AMF/2563528
CA-SCB	Oliver Sonnentag, William L Quinton (2021), AmeriFlux BASE CA-SCB Scotty Creek Bog, Ver. 2-5, AmeriFlux AMP, (Dataset). https://doi.org/10.17190/AMF/1498754
CA-SCC	Oliver Sonnentag, William L Quinton (2025), AmeriFlux BASE CA-SCC Scotty Creek Landscape, Ver. 2-5, AmeriFlux AMP, (Dataset). https://doi.org/10.17190/AMF/1480303
CA-SF1	Brian Amiro (2020), AmeriFlux BASE CA-SF1 Saskatchewan - Western Boreal, forest burned in 1977, Ver. 2-5, AmeriFlux AMP, (Dataset). https://doi.org/10.17190/AMF/1246006
CA-SF2	Brian Amiro (2019), AmeriFlux BASE CA-SF2 Saskatchewan - Western Boreal, forest burned in 1989, Ver. 3-5, AmeriFlux AMP, (Dataset). https://doi.org/10.17190/AMF/1246007
CA-SF3	Brian Amiro (2020), AmeriFlux BASE CA-SF3 Saskatchewan - Western Boreal, forest burned in 1998, Ver. 2-5, AmeriFlux AMP, (Dataset). https://doi.org/10.17190/AMF/1246008

Site ID	Citation
CA-SJ1	Alan Barr (2018), AmeriFlux BASE CA-SJ1 Saskatchewan - Western Boreal, Jack Pine forest harvested in 1994, Ver. 1-5, AmeriFlux AMP, (Dataset). https://doi.org/10.17190/AMF/1436320
CA-SJ2	Alan Barr, Andrew T. Black (2018), AmeriFlux BASE CA-SJ2 Saskatchewan - Western Boreal, Jack Pine forest harvested in 2002, Ver. 2-5, AmeriFlux AMP, (Dataset). https://doi.org/10.17190/AMF/1436321
CA-SMC	Oliver Sonnentag (2021), AmeriFlux BASE CA-SMC Smith Creek, Ver. 1-5, AmeriFlux AMP, (Dataset). https://doi.org/10.17190/AMF/1767830
CA-TP1	M. Altaf Arain (2025), AmeriFlux BASE CA-TP1 Ontario - Turkey Point 2002 Plantation White Pine, Ver. 4-5, AmeriFlux AMP, (Dataset). https://doi.org/10.17190/AMF/1246009
CA-TP2	M. Altaf Arain (2018), AmeriFlux BASE CA-TP2 Ontario - Turkey Point 1989 Plantation White Pine, Ver. 2-5, AmeriFlux AMP, (Dataset). https://doi.org/10.17190/AMF/1246010
CA-TP3	M. Altaf Arain (2025), AmeriFlux BASE CA-TP3 Ontario - Turkey Point 1974 Plantation White Pine, Ver. 4-5, AmeriFlux AMP, (Dataset). https://doi.org/10.17190/AMF/1246011
CA-TP4	M. Altaf Arain (2025), AmeriFlux BASE CA-TP4 Ontario - Turkey Point 1939 Plantation White Pine, Ver. 5-5, AmeriFlux AMP, (Dataset). https://doi.org/10.17190/AMF/1246012
CA-TPA	M. Altaf Arain (2025), AmeriFlux BASE CA-TPA Ontario Turkey Point Observatory Agricultural Site, Ver. 1-5, AmeriFlux AMP, (Dataset). https://doi.org/10.17190/AMF/2563529
CA-TPD	M. Altaf Arain (2025), AmeriFlux BASE CA-TPD Ontario - Turkey Point Mature Deciduous, Ver. 3-5, AmeriFlux AMP, (Dataset). https://doi.org/10.17190/AMF/1246152
CA-TVC	Oliver Sonnentag, Philip Marsh (2025), AmeriFlux BASE CA-TVC Trail Valley Creek, Ver. 2-5, AmeriFlux AMP, (Dataset). https://doi.org/10.17190/AMF/1767831
CL-ACF	Antonio Lara (2025), AmeriFlux BASE CL-ACF Alerce Costero Forest, Ver. 1-5, AmeriFlux AMP, (Dataset). https://doi.org/10.17190/AMF/2563530
CL-SDF	Jorge Perez-Quezada, Juan J. Armesto (2022), AmeriFlux BASE CL-SDF Senda Darwin Forest, Ver. 1-5, AmeriFlux AMP, (Dataset). https://doi.org/10.17190/AMF/1902273
CL-SDP	Jorge Perez-Quezada, Juan J. Armesto (2022), AmeriFlux BASE CL-SDP Senda Darwin Peatland, Ver. 1-5, AmeriFlux AMP, (Dataset). https://doi.org/10.17190/AMF/1902274
CR-Fsc	Mark Johnson (2024), AmeriFlux BASE CR-Fsc Filadelfia sugar cane cropland, Ver. 2-5, AmeriFlux AMP, (Dataset). https://doi.org/10.17190/AMF/1829504
CR-SoC	Anthony T. Cahill, Georgianne W. Moore, Gretchen R. Miller, Jaeyoung Song (2022), AmeriFlux BASE CR-SoC Soltis Center, Ver. 1-5, AmeriFlux AMP, (Dataset). https://doi.org/10.17190/AMF/1880911
MX-Aog	Enrico A. Yepez (2020), AmeriFlux BASE MX-Aog Alamos Old-Growth tropical dry forest, Ver. 1-5, AmeriFlux AMP, (Dataset). https://doi.org/10.17190/AMF/1756414
MX-PMm	Ma. Susana Alvarado-Barrientos (2021), AmeriFlux BASE MX-PMm Puerto Morelos mangrove, Ver. 2-5, AmeriFlux AMP, (Dataset). https://doi.org/10.17190/AMF/1756415
MX-Tes	Enrico A. Yepez, Jaime Garatuza (2021), AmeriFlux BASE MX-Tes Tesopaco, secondary tropical dry forest, Ver. 2-5, AmeriFlux AMP, (Dataset). https://doi.org/10.17190/AMF/1767832
PE-QFR	Tyler Roman, Timothy Griffis, Randy Kolka, Craig Wayson, Erik Lilleskov, Dennis del Castillo, Lizardo FachÃn, Jhon Rengifo (2025), AmeriFlux BASE PE-QFR Quistococha Forest Reserve, Ver. 3-5, AmeriFlux AMP, (Dataset). https://doi.org/10.17190/AMF/1671889
PR-xGU	NEON (National Ecological Observatory Network) (2025), AmeriFlux BASE PR-xGU NEON Guanica Forest (GUAN), Ver. 8-5, AmeriFlux AMP, (Dataset). https://doi.org/10.17190/AMF/1773393
PR-xLA	NEON (National Ecological Observatory Network) (2025), AmeriFlux BASE PR-xLA NEON Lajas Experimental Station (LAJA), Ver. 8-5, AmeriFlux AMP, (Dataset). https://doi.org/10.17190/AMF/1773394
US-A03	Ryan Sullivan, Dave Billesbach, David Cook, Sebastien Biraud (2025), AmeriFlux BASE US-A03 ARM-AMF3-Oliktok, Ver. 6-5, AmeriFlux AMP, (Dataset). https://doi.org/10.17190/AMF/1498752
US-A10	Ryan Sullivan, Dave Billesbach, David Cook, Sebastien Biraud (2025), AmeriFlux BASE US-A10 ARM-NSA-Barrow, Ver. 5-5, AmeriFlux AMP, (Dataset). https://doi.org/10.17190/AMF/1498753
US-A32	Dave Billesbach, Lara Kueppers, Margaret Torn, Sebastien Biraud (2018), AmeriFlux BASE US-A32 ARM-SGP Medford hay pasture, Ver. 1-5, AmeriFlux AMP, (Dataset). https://doi.org/10.17190/AMF/1436327
US-A37	Ryan Sullivan, Evan Keeler, Jenni Kyrouac, Sujan Pal (2025), AmeriFlux BASE US-A37 ARM-SGP-Waukomis, Ver. 2-5, AmeriFlux AMP, (Dataset). https://doi.org/10.17190/AMF/2531140
US-A39	Ryan Sullivan, Dave Billesbach, David Cook, Evan Keeler, Jenni Kyrouac, Sebastien Biraud, Sujan Pal (2025), AmeriFlux BASE US-A39 ARM-SGP-Morrison, Ver. 1-5, AmeriFlux AMP, (Dataset). https://doi.org/10.17190/AMF/2563531
US-A74	Dave Billesbach, Lara Kueppers, Margaret Torn, Sebastien Biraud (2018), AmeriFlux BASE US-A74 ARM SGP milo field, Ver. 1-5, AmeriFlux AMP, (Dataset). https://doi.org/10.17190/AMF/1436328
US-Act	Sarah Waldo (2022), AmeriFlux BASE US-Act Acton Lake Flux Tower Site, Ver. 1-5, AmeriFlux AMP, (Dataset). https://doi.org/10.17190/AMF/1846660
US-ADR	Michael Moreo (2018), AmeriFlux BASE US-ADR Amargosa Desert Research Site (ADRS), Ver. 1-5, AmeriFlux AMP, (Dataset). https://doi.org/10.17190/AMF/1418680
US-Akn	Monique Leclerc (2023), AmeriFlux BASE US-Akn Savannah River Site, Ver. 6-5, AmeriFlux AMP, (Dataset). https://doi.org/10.17190/AMF/1246141

Site ID	Citation
US-ALQ	Brent Olson (2025), AmeriFlux BASE US-ALQ Allequash Creek Site, Ver. 21-5, AmeriFlux AMP, (Dataset). https://doi.org/10.17190/AMF/1480323
US-AMS	Gavin McNicol, Roser Matamala (2025), AmeriFlux BASE US-AMS Argonne Testbed for Multiscale Observational Science (ATMOS), Ver. 1-5, AmeriFlux AMP, (Dataset). https://doi.org/10.17190/AMF/2531142
US-An1	Adrian Rocha, Gaius Shaver, John Hobbie (2020), AmeriFlux BASE US-An1 Anaktuvuk River Severe Burn, Ver. 2-5, AmeriFlux AMP, (Dataset). https://doi.org/10.17190/AMF/1246142
US-An2	Adrian Rocha, Gaius Shaver, John Hobbie (2020), AmeriFlux BASE US-An2 Anaktuvuk River Moderate Burn, Ver. 2-5, AmeriFlux AMP, (Dataset). https://doi.org/10.17190/AMF/1246143
US-An3	Adrian Rocha, Gaius Shaver, John Hobbie (2020), AmeriFlux BASE US-An3 Anaktuvuk River Unburned, Ver. 2-5, AmeriFlux AMP, (Dataset). https://doi.org/10.17190/AMF/1246144
US-AR1	Dave Billesbach, James Bradford, Margaret Torn (2019), AmeriFlux BASE US-AR1 ARM USDA UNL OSU Woodward Switchgrass 1, Ver. 3-5, AmeriFlux AMP, (Dataset). https://doi.org/10.17190/AMF/1246137
US-AR2	Dave Billesbach, James Bradford, Margaret Torn (2019), AmeriFlux BASE US-AR2 ARM USDA UNL OSU Woodward Switchgrass 2, Ver. 3-5, AmeriFlux AMP, (Dataset). https://doi.org/10.17190/AMF/1246138
US-ARb	Margaret Torn (2019), AmeriFlux BASE US-ARb ARM Southern Great Plains burn site- Lamont, Ver. 3-5, AmeriFlux AMP, (Dataset). https://doi.org/10.17190/AMF/1246025
US-ARc	Margaret Torn (2019), AmeriFlux BASE US-ARc ARM Southern Great Plains control site- Lamont, Ver. 3-5, AmeriFlux AMP, (Dataset). https://doi.org/10.17190/AMF/1246026
US-ARM	Sebastien Biraud, Marc Fischer, Stephen Chan, Margaret Torn (2025), AmeriFlux BASE US-ARM ARM Southern Great Plains site- Lamont, Ver. 14-5, AmeriFlux AMP, (Dataset). https://doi.org/10.17190/AMF/1246027
US-ASH	Ray G. Anderson (2020), AmeriFlux BASE US-ASH USSL San Joaquin Valley Almond High Salinity, Ver. 1-5, AmeriFlux AMP, (Dataset). https://doi.org/10.17190/AMF/1634880
US-ASL	Ray G. Anderson (2020), AmeriFlux BASE US-ASL USSL San Joaquin Valley Almond Low Salinity, Ver. 1-5, AmeriFlux AMP, (Dataset). https://doi.org/10.17190/AMF/1617706
US-ASM	Ray G. Anderson (2020), AmeriFlux BASE US-ASM USSL San Joaquin Valley Almond Medium Salinity, Ver. 1-5, AmeriFlux AMP, (Dataset). https://doi.org/10.17190/AMF/1617709
US-Aud	Tilden Meyers (2016), AmeriFlux BASE US-Aud Audubon Research Ranch, Ver. 4-1, AmeriFlux AMP, (Dataset). https://doi.org/10.17190/AMF/1246028
US-Bar	Andrew Richardson, David Hollinger (2025), AmeriFlux BASE US-Bar Bartlett Experimental Forest, Ver. 7-5, AmeriFlux AMP, (Dataset). https://doi.org/10.17190/AMF/1246030
US-Bi1	Camilo Rey-Sanchez, Carlos Tianxin Wang, Daphne Szutu, Robert Shortt, Samuel D. Chamberlain, Joseph Verfaillie, Dennis Baldocchi (2025), AmeriFlux BASE US-Bi1 Bouldin Island Alfalfa, Ver. 14-5, AmeriFlux AMP, (Dataset). https://doi.org/10.17190/AMF/1480317
US-Bi2	Camilo Rey-Sanchez, Carlos Tianxin Wang, Daphne Szutu, Kyle Hemes, Joseph Verfaillie, Dennis Baldocchi (2025), AmeriFlux BASE US-Bi2 Bouldin Island corn, Ver. 19-5, AmeriFlux AMP, (Dataset). https://doi.org/10.17190/AMF/1419513
US-Blo	Allen Goldstein (2019), AmeriFlux BASE US-Blo Blodgett Forest, Ver. 4-5, AmeriFlux AMP, (Dataset). https://doi.org/10.17190/AMF/1246032
US-BMM	Paul Stoy, E. N. J. Brookshire (2022), AmeriFlux BASE US-BMM Bangtail Mountain Meadow, Ver. 3-5, AmeriFlux AMP, (Dataset). https://doi.org/10.17190/AMF/1660338
US-Bo1	Tilden Meyers (2016), AmeriFlux BASE US-Bo1 Bondville, Ver. 2-1, AmeriFlux AMP, (Dataset). https://doi.org/10.17190/AMF/1246036
US-Bo2	Carl Bernacchi (2016), AmeriFlux BASE US-Bo2 Bondville (companion site), Ver. 2-1, AmeriFlux AMP, (Dataset). https://doi.org/10.17190/AMF/1246037
US-BRG	Kimberly Novick (2020), AmeriFlux BASE US-BRG Bayles Road Grassland Tower, Ver. 1-5, AmeriFlux AMP, (Dataset). https://doi.org/10.17190/AMF/1756416
US-Bsg	Chris Still (2022), AmeriFlux BASE US-Bsg Burns Sagebrush, Ver. 1-5, AmeriFlux AMP, (Dataset). https://doi.org/10.17190/AMF/1846661
US-BWa	Kenneth Davis (2023), AmeriFlux BASE US-BWa INFLUX - NIST Turfgrass Site, Ver. 1-5, AmeriFlux AMP, (Dataset). https://doi.org/10.17190/AMF/2229153
US-BWb	Kenneth Davis (2023), AmeriFlux BASE US-BWb INFLUX - Montgomery County pasture site, Ver. 1-5, AmeriFlux AMP, (Dataset). https://doi.org/10.17190/AMF/2229154
US-BZB	Eugenie Euskirchen (2025), AmeriFlux BASE US-BZB Bonanza Creek Thermokarst Bog, Ver. 5-5, AmeriFlux AMP, (Dataset). https://doi.org/10.17190/AMF/1773401
US-BZF	Eugenie Euskirchen (2025), AmeriFlux BASE US-BZF Bonanza Creek Rich Fen, Ver. 5-5, AmeriFlux AMP, (Dataset). https://doi.org/10.17190/AMF/1756433
US-BZo	Eugenie Euskirchen (2025), AmeriFlux BASE US-BZo Bonanza Creek Old Thermokarst Bog, Ver. 4-5, AmeriFlux AMP, (Dataset). https://doi.org/10.17190/AMF/1846662
US-BZS	Eugenie Euskirchen (2025), AmeriFlux BASE US-BZS Bonanza Creek Black Spruce, Ver. 4-5, AmeriFlux AMP, (Dataset). https://doi.org/10.17190/AMF/1756434
US-CAK	Kyle Arndt, Susan Natali (2025), AmeriFlux BASE US-CAK Council Alaska Tundra, Ver. 1-5, AmeriFlux AMP, (Dataset). https://doi.org/10.17190/AMF/2563532

Site ID	Citation
US-CC1	Paul Stoy, Sharifa Brevert (2022), AmeriFlux BASE US-CC1 Coloma Corn 1, Ver. 1-5, AmeriFlux AMP, (Dataset). https://doi.org/10.17190/AMF/1865475
US-CC2	Paul Stoy, Sharifa Brevert, Anam Khan (2022), AmeriFlux BASE US-CC2 Coloma Corn 2, Ver. 2-5, AmeriFlux AMP, (Dataset). https://doi.org/10.17190/AMF/1865476
US-CdM	David Bowling, Steve Kannenberg, William Anderegg (2025), AmeriFlux BASE US-CdM Cedar Mesa, Ver. 3-5, AmeriFlux AMP, (Dataset). https://doi.org/10.17190/AMF/1865477
US-Ced	Ken Clark (2025), AmeriFlux BASE US-Ced Cedar Bridge, Ver. 8-5, AmeriFlux AMP, (Dataset). https://doi.org/10.17190/AMF/1246043
US-CF1	Claire L. Phillips, Dave Huggins (2022), AmeriFlux BASE US-CF1 CAF-LTAR Cook East, Ver. 3-5, AmeriFlux AMP, (Dataset). https://doi.org/10.17190/AMF/1543382
US-CF2	Dave Huggins (2021), AmeriFlux BASE US-CF2 CAF-LTAR Cook West, Ver. 2-5, AmeriFlux AMP, (Dataset). https://doi.org/10.17190/AMF/1543383
US-CF3	Dave Huggins (2022), AmeriFlux BASE US-CF3 CAF-LTAR Boyd North, Ver. 3-5, AmeriFlux AMP, (Dataset). https://doi.org/10.17190/AMF/1543385
US-CF4	Dave Huggins (2022), AmeriFlux BASE US-CF4 CAF-LTAR Boyd South, Ver. 3-5, AmeriFlux AMP, (Dataset). https://doi.org/10.17190/AMF/1543384
US-CGG	Patty Oikawa (2025), AmeriFlux BASE US-CGG Concord Grazed Grassland, Ver. 2-5, AmeriFlux AMP, (Dataset). https://doi.org/10.17190/AMF/1987600
US-ChR	Tilden Meyers (2016), AmeriFlux BASE US-ChR Chestnut Ridge, Ver. 2-1, AmeriFlux AMP, (Dataset). https://doi.org/10.17190/AMF/1246044
US-CLF	Kenneth J. Davis (2023), AmeriFlux BASE US-CLF Cole Farm, Ver. 1-5, AmeriFlux AMP, (Dataset). https://doi.org/10.17190/AMF/1987601
US-Cms	Akira Miyata, Yoshinobu Harazono (2025), AmeriFlux BASE US-Cms Central Marsh, Ver. 2-5, AmeriFlux AMP, (Dataset). https://doi.org/10.17190/AMF/1987602
US-CMW	Russell Scott (2022), AmeriFlux BASE US-CMW Charleston Mesquite Woodland, Ver. 2-5, AmeriFlux AMP, (Dataset). https://doi.org/10.17190/AMF/1660339
US-Cop	David Bowling (2019), AmeriFlux BASE US-Cop Corral Pocket, Ver. 2-5, AmeriFlux AMP, (Dataset). https://doi.org/10.17190/AMF/1246129
US-CPk	Brent Ewers, Mario Bretfeld, Elise Pendall (2016), AmeriFlux BASE US-CPk Chimney Park, Ver. 2-1, AmeriFlux AMP, (Dataset). https://doi.org/10.17190/AMF/1246150
US-CRK	Asko Noormets (2025), AmeriFlux BASE US-CRK Davy Crockett National Forest, Ver. 6-5, AmeriFlux AMP, (Dataset). https://doi.org/10.17190/AMF/2204055
US-CRT	Jiquan Chen, Housen Chu (2021), AmeriFlux BASE US-CRT Curtice Walter-Berger cropland, Ver. 5-5, AmeriFlux AMP, (Dataset). https://doi.org/10.17190/AMF/1246156
US-CS1	Ankur Desai (2023), AmeriFlux BASE US-CS1 Central Sands Irrigated Agricultural Field, Ver. 3-5, AmeriFlux AMP, (Dataset). https://doi.org/10.17190/AMF/1617710
US-CS2	Ankur Desai (2023), AmeriFlux BASE US-CS2 Tri county school Pine Forest, Ver. 5-5, AmeriFlux AMP, (Dataset). https://doi.org/10.17190/AMF/1617711
US-CS3	Ankur Desai (2023), AmeriFlux BASE US-CS3 Central Sands Irrigated Agricultural Field, Ver. 4-5, AmeriFlux AMP, (Dataset). https://doi.org/10.17190/AMF/1617713
US-CS4	Ankur Desai (2023), AmeriFlux BASE US-CS4 Central Sands Irrigated Agricultural Field, Ver. 4-5, AmeriFlux AMP, (Dataset). https://doi.org/10.17190/AMF/1756417
US-CS5	Ankur Desai (2022), AmeriFlux BASE US-CS5 Central Sands Irrigated Agricultural Field, Ver. 1-5, AmeriFlux AMP, (Dataset). https://doi.org/10.17190/AMF/1846663
US-CS6	Ankur Desai (2023), AmeriFlux BASE US-CS6 Central Sands Irrigated Agricultural Field, Ver. 1-5, AmeriFlux AMP, (Dataset). https://doi.org/10.17190/AMF/2001297
US-CS8	Ankur Desai (2023), AmeriFlux BASE US-CS8 Central Sands Irrigated Agricultural Field, Ver. 2-5, AmeriFlux AMP, (Dataset). https://doi.org/10.17190/AMF/2001298
US-Cst	Kim Novick (2022), AmeriFlux BASE US-Cst Crossett Experimental Forest, Ver. 1-5, AmeriFlux AMP, (Dataset). https://doi.org/10.17190/AMF/1902275
US-CU1	Bhupendra Raut, Sujan Pal, Paytsar Muradyan, Joseph R. O'Brien, Max Berkelhammer, Matthew Tuftedal, Max Grover, Scott Collis, Robert C. Jackson (2025), AmeriFlux BASE US-CU1 UIC Plant Research Laboratory Chicago, Ver. 1-5, AmeriFlux AMP, (Dataset). https://doi.org/10.17190/AMF/2531143
US-Cwt	A. Christopher Oishi (2025), AmeriFlux BASE US-Cwt Coweeta, Ver. 2-5, AmeriFlux AMP, (Dataset). https://doi.org/10.17190/AMF/1671890
US-DBk	Allen Goldstein, Joshua Apte (2025), AmeriFlux BASE US-DBk Berkeley Way West, Ver. 1-5, AmeriFlux AMP, (Dataset). https://doi.org/10.17190/AMF/2567980
US-DFC	Alison Duff, Ankur Desai (2025), AmeriFlux BASE US-DFC US Dairy Forage Research Center, Prairie du Sac, Ver. 3-5, AmeriFlux AMP, (Dataset). https://doi.org/10.17190/AMF/1660340
US-DFK	Alison Duff, Ankur Desai, Valentin Picasso Risso (2021), AmeriFlux BASE US-DFK Dairy Forage Research Center - Kernza, Ver. 1-5, AmeriFlux AMP, (Dataset). https://doi.org/10.17190/AMF/1825937
US-Dia	Sonia Wharton (2016), AmeriFlux BASE US-Dia Diablo, Ver. 1-1, AmeriFlux AMP, (Dataset). https://doi.org/10.17190/AMF/1246146

Site ID	Citation
US-Dix	Ken Clark (2025), AmeriFlux BASE US-Dix Fort Dix, Ver. 3-5, AmeriFlux AMP, (Dataset). https://doi.org/10.17190/AMF/1246045
US-Dk1	Chris Oishi, Kim Novick, Paul Stoy (2018), AmeriFlux BASE US-Dk1 Duke Forest-open field, Ver. 4-5, AmeriFlux AMP, (Dataset). https://doi.org/10.17190/AMF/1246046
US-Dk2	Chris Oishi, Kim Novick, Paul Stoy (2018), AmeriFlux BASE US-Dk2 Duke Forest-hardwoods, Ver. 4-5, AmeriFlux AMP, (Dataset). https://doi.org/10.17190/AMF/1246047
US-Dk3	Chris Oishi, Kim Novick, Paul Stoy (2018), AmeriFlux BASE US-Dk3 Duke Forest - loblolly pine, Ver. 4-5, AmeriFlux AMP, (Dataset). https://doi.org/10.17190/AMF/1246048
US-Dmg	Ariane Arias-Ortiz, Dennis Baldocchi (2025), AmeriFlux BASE US-Dmg Dutch Slough Marsh Gilbert Tract, Ver. 5-5, AmeriFlux AMP, (Dataset). https://doi.org/10.17190/AMF/1964086
US-DPW	Charles Ross Hinkle, Rosvel Bracho (2019), AmeriFlux BASE US-DPW Disney Wilderness Preserve Wetland, Ver. 1-5, AmeriFlux AMP, (Dataset). https://doi.org/10.17190/AMF/1562387
US-DS1	Nick Christen (2024), AmeriFlux BASE US-DS1 Staten Corn 1, Ver. 1-5, AmeriFlux AMP, (Dataset). https://doi.org/10.17190/AMF/2407202
US-DS2	Steve Deverel (2024), AmeriFlux BASE US-DS2 Staten Corn 2, Ver. 1-5, AmeriFlux AMP, (Dataset). https://doi.org/10.17190/AMF/2407203
US-DS3	Michael R. Schuppenhauer, Sebastien C. Biraud, Steve Deverel, Stephen Chan (2025), AmeriFlux BASE US-DS3 Staten Rice 1, Ver. 3-5, AmeriFlux AMP, (Dataset). https://doi.org/10.17190/AMF/1890490
US-DUF	John Frank (2025), AmeriFlux BASE US-DUF Denver Urban Field Station, Ver. 1-5, AmeriFlux AMP, (Dataset). https://doi.org/10.17190/AMF/2567981
US-EA4	Tyson McKinney (2025), AmeriFlux BASE US-EA4 EAA Field Research Park Woodland, Ver. 2-5, AmeriFlux AMP, (Dataset). https://doi.org/10.17190/AMF/2315767
US-EA5	Tyson McKinney (2024), AmeriFlux BASE US-EA5 Uvalde Ranch Mesquite Woodland, Ver. 2-5, AmeriFlux AMP, (Dataset). https://doi.org/10.17190/AMF/2204056
US-EA6	Preston Fleck (2024), AmeriFlux BASE US-EA6 Camp Wood Shield Ranch Oak Savannah, Ver. 1-5, AmeriFlux AMP, (Dataset). https://doi.org/10.17190/AMF/2315768
US-EDN	Patty Oikawa (2025), AmeriFlux BASE US-EDN Eden Landing Ecological Reserve, Ver. 4-5, AmeriFlux AMP, (Dataset). https://doi.org/10.17190/AMF/1543381
US-EKH	Adina Paytan (2025), AmeriFlux BASE US-EKH Elkhorn Slough Hester Marsh, Ver. 2-5, AmeriFlux AMP, (Dataset). https://doi.org/10.17190/AMF/2479624
US-EKN	Adina Paytan (2025), AmeriFlux BASE US-EKN Elkhorn Slough North Marsh, Ver. 1-5, AmeriFlux AMP, (Dataset). https://doi.org/10.17190/AMF/2531144
US-EKP	Adina Paytan (2025), AmeriFlux BASE US-EKP Elkhorn Slough Porter Marsh, Ver. 2-5, AmeriFlux AMP, (Dataset). https://doi.org/10.17190/AMF/2479625
US-Elm	Gregory Starr, Steve Oberbauer (2025), AmeriFlux BASE US-Elm Everglades (long hydroperiod marsh), Ver. 7-5, AmeriFlux AMP, (Dataset). https://doi.org/10.17190/AMF/1246118
US-EML	Rosvel Bracho, Gerardo Celis, Heidi Rodenhizer, Craig See, Edward A. Schuur (2021), AmeriFlux BASE US-EML Eight Mile Lake Permafrost thaw gradient, Healy Alaska., Ver. 4-5, AmeriFlux AMP, (Dataset). https://doi.org/10.17190/AMF/1418678
US-Esm	Gregory Starr, Steve Oberbauer (2025), AmeriFlux BASE US-Esm Everglades (short hydroperiod marsh), Ver. 7-5, AmeriFlux AMP, (Dataset). https://doi.org/10.17190/AMF/1246119
US-EvM	Gregory Starr, Steven F. Oberbuer (2024), AmeriFlux BASE US-EvM Everglades Saltwater intrusion marsh, Ver. 2-5, AmeriFlux AMP, (Dataset). https://doi.org/10.17190/AMF/2229155
US-Fcr	Masahito Ueyama, Hiroki Iwata, Yoshinobu Harazono (2023), AmeriFlux BASE US-Fcr Cascaden Ridge Fire Scar, Ver. 3-5, AmeriFlux AMP, (Dataset). https://doi.org/10.17190/AMF/1562388
US-Fmf	Sabina Dore, Thomas Kolb (2019), AmeriFlux BASE US-Fmf Flagstaff - Managed Forest, Ver. 6-5, AmeriFlux AMP, (Dataset). https://doi.org/10.17190/AMF/1246050
US-Fo1	John Kochendorfer, Praveena Krishnan, Mark Heuer (2025), AmeriFlux BASE US-Fo1 Flux Observations of Carbon from an Airborne Laboratory (FOCAL) Campaign Site 1, Ver. 1-5, AmeriFlux AMP, (Dataset). https://doi.org/10.17190/AMF/2531145
US-Fo2	Praveena Krishnan, Mark Heuer (2025), AmeriFlux BASE US-Fo2 Flux Observations of Carbon from an Airborne Laboratory (FOCAL) Campaign Site 2, Ver. 1-5, AmeriFlux AMP, (Dataset). https://doi.org/10.17190/AMF/2531146
US-Fuf	Sabina Dore, Thomas Kolb (2019), AmeriFlux BASE US-Fuf Flagstaff - Unmanaged Forest, Ver. 6-5, AmeriFlux AMP, (Dataset). https://doi.org/10.17190/AMF/1246051
US-Fwf	Sabina Dore, Thomas Kolb (2019), AmeriFlux BASE US-Fwf Flagstaff - Wildfire, Ver. 8-5, AmeriFlux AMP, (Dataset). https://doi.org/10.17190/AMF/1246052
US-GBT	Bill Massman (2016), AmeriFlux BASE US-GBT GLEES Brooklyn Tower, Ver. 1-1, AmeriFlux AMP, (Dataset). https://doi.org/10.17190/AMF/1375200
US-GL1	Chris Spence (2024), AmeriFlux BASE US-GL1 Stannard Rock, Ver. 3-5, AmeriFlux AMP, (Dataset). https://doi.org/10.17190/AMF/2204057
US-GLE	John Frank, George Valentine, Bill Massman (2021), AmeriFlux BASE US-GLE GLEES, Ver. 8-5, AmeriFlux AMP, (Dataset). https://doi.org/10.17190/AMF/1246056

Site ID	Citation
US-Ha1	J. William Munger (2025), AmeriFlux BASE US-Ha1 Harvard Forest EMS Tower (HFR1), Ver. 25-5, AmeriFlux AMP, (Dataset). https://doi.org/10.17190/AMF/1246059
US-Ha2	Julian Hadley, J. William Munger (2025), AmeriFlux BASE US-Ha2 Harvard Forest Hemlock Site, Ver. 14-5, AmeriFlux AMP, (Dataset). https://doi.org/10.17190/AMF/1246060
US-HB1	Jeremy D. Forsythe, Michael A. Kline, Thomas L. O'Halloran (2023), AmeriFlux BASE US-HB1 North Inlet Crab Haul Creek, Ver. 3-5, AmeriFlux AMP, (Dataset). https://doi.org/10.17190/AMF/1660341
US-HB2	Jeremy D. Forsythe, Michael A. Kline, Thomas L. O'Halloran (2020), AmeriFlux BASE US-HB2 Hobcaw Barony Mature Longleaf Pine, Ver. 1-5, AmeriFlux AMP, (Dataset). https://doi.org/10.17190/AMF/1660342
US-HB3	Jeremy D. Forsythe, Michael A. Kline, Thomas L. O'Halloran (2023), AmeriFlux BASE US-HB3 Hobcaw Barony Longleaf Pine Restoration, Ver. 2-5, AmeriFlux AMP, (Dataset). https://doi.org/10.17190/AMF/1660343
US-HB4	Tom O'Halloran (2025), AmeriFlux BASE US-HB4 Minim Creek Brackish Impoundment, Ver. 2-5, AmeriFlux AMP, (Dataset). https://doi.org/10.17190/AMF/2001299
US-HBK	Eric Kelsey, Mark Green (2023), AmeriFlux BASE US-HBK Hubbard Brook Experimental Forest, Ver. 2-5, AmeriFlux AMP, (Dataset). https://doi.org/10.17190/AMF/1634881
US-Hn2	Heping Liu, Maoyi Huang, Xingyuan Chen (2019), AmeriFlux BASE US-Hn2 Hanford 100H grassland, Ver. 1-5, AmeriFlux AMP, (Dataset). https://doi.org/10.17190/AMF/1562389
US-Hn3	Heping Liu, Maoyi Huang, Xingyuan Chen (2019), AmeriFlux BASE US-Hn3 Hanford 100H sagebrush, Ver. 1-5, AmeriFlux AMP, (Dataset). https://doi.org/10.17190/AMF/1543379
US-Ho1	David Hollinger (2025), AmeriFlux BASE US-Ho1 Howland Forest (main tower), Ver. 11-5, AmeriFlux AMP, (Dataset). https://doi.org/10.17190/AMF/1246061
US-Ho2	David Hollinger (2025), AmeriFlux BASE US-Ho2 Howland Forest (west tower), Ver. 8-5, AmeriFlux AMP, (Dataset). https://doi.org/10.17190/AMF/1246062
US-Ho3	David Hollinger (2025), AmeriFlux BASE US-Ho3 Howland Forest (harvest site), Ver. 3-5, AmeriFlux AMP, (Dataset). https://doi.org/10.17190/AMF/1246063
US-HRA	Benjamin R. K. Runkle (2021), AmeriFlux BASE US-HRA Humnoke Farm Rice Field â€“ Field A, Ver. 3-5, AmeriFlux AMP, (Dataset). https://doi.org/10.17190/AMF/1543376
US-HRC	Michele L. Reba (2021), AmeriFlux BASE US-HRC Humnoke Farm Rice Field â€“ Field C, Ver. 3-5, AmeriFlux AMP, (Dataset). https://doi.org/10.17190/AMF/1543375
US-Hsm	Ariane Arias-Ortiz, Daphne Szutu, Joseph Verfaillie, Dennis Baldocchi (2025), AmeriFlux BASE US-Hsm Hill Slough Marsh, Ver. 5-5, AmeriFlux AMP, (Dataset). https://doi.org/10.17190/AMF/1890483
US-HVs	Akira Miyata, Yoshinobu Harazono (2023), AmeriFlux BASE US-HVs Happy Valley Wet Sedge Tundra, Ver. 1-5, AmeriFlux AMP, (Dataset). https://doi.org/10.17190/AMF/1964087
US-HWB	Sarah Goslee (2023), AmeriFlux BASE US-HWB USDA ARS Pasture Sytems and Watershed Management Research Unit- Hawbecker Site, Ver. 2-5, AmeriFlux AMP, (Dataset). https://doi.org/10.17190/AMF/1811363
US-IAB	Vanloocke Andy (2025), AmeriFlux BASE US-IAB Iowa State University NE tower, Ver. 1-5, AmeriFlux AMP, (Dataset). https://doi.org/10.17190/AMF/2567982
US-IAM	Vanloocke Andy (2025), AmeriFlux BASE US-IAM Iowa State University Miscanthus, Ver. 1-5, AmeriFlux AMP, (Dataset). https://doi.org/10.17190/AMF/2567983
US-IB1	Roser Matamala (2019), AmeriFlux BASE US-IB1 Fermi National Accelerator Laboratory- Batavia (Agricultural site), Ver. 8-5, AmeriFlux AMP, (Dataset). https://doi.org/10.17190/AMF/1246065
US-IB2	Roser Matamala (2019), AmeriFlux BASE US-IB2 Fermi National Accelerator Laboratory- Batavia (Prairie site), Ver. 8-5, AmeriFlux AMP, (Dataset). https://doi.org/10.17190/AMF/1246066
US-ICh	Eugenie Euskirchen, Gaius Shaver, Syndonia Bret-Harte (2025), AmeriFlux BASE US-ICh Imnavait Creek Watershed Heath Tundra, Ver. 6-5, AmeriFlux AMP, (Dataset). https://doi.org/10.17190/AMF/1246133
US-ICs	Eugenie Euskirchen, Gaius Shaver, Syndonia Bret-Harte (2025), AmeriFlux BASE US-ICs Imnavait Creek Watershed Wet Sedge Tundra, Ver. 10-5, AmeriFlux AMP, (Dataset). https://doi.org/10.17190/AMF/1246130
US-ICt	Eugenie Euskirchen, Gaius Shaver, Syndonia Bret-Harte (2025), AmeriFlux BASE US-ICt Imnavait Creek Watershed Tussock Tundra, Ver. 7-5, AmeriFlux AMP, (Dataset). https://doi.org/10.17190/AMF/1246131
US-INa	Kenneth Davis (2025), AmeriFlux BASE US-INa INFLUX - Cemetery Turfgrass Tower, Ver. 2-5, AmeriFlux AMP, (Dataset). https://doi.org/10.17190/AMF/2001300
US-INb	Kenneth Davis (2025), AmeriFlux BASE US-INb INFLUX - Golf Course, Ver. 2-5, AmeriFlux AMP, (Dataset). https://doi.org/10.17190/AMF/2001301
US-INc	Kenneth Davis (2025), AmeriFlux BASE US-INc INFLUX - Downtown Indianapolis (Site-3), Ver. 3-5, AmeriFlux AMP, (Dataset). https://doi.org/10.17190/AMF/1987603
US-INd	Kenneth Davis (2023), AmeriFlux BASE US-INd INFLUX - Agricultural Site East near Pittsboro, Ver. 1-5, AmeriFlux AMP, (Dataset). https://doi.org/10.17190/AMF/2001302
US-INe	Kenneth Davis (2023), AmeriFlux BASE US-INe INFLUX - Agricultural Site West near Pittsboro, Ver. 1-5, AmeriFlux AMP, (Dataset). https://doi.org/10.17190/AMF/2001303
US-INf	Kenneth Davis (2023), AmeriFlux BASE US-INf INFLUX - East 21st St (Site 2), Ver. 1-5, AmeriFlux AMP, (Dataset). https://doi.org/10.17190/AMF/2001304
US-INg	Brandon R Forsythe, Jason Horne, Kenneth Davis (2025), AmeriFlux BASE US-INg INFLUX - Wayne Twp Comm (Site-7), Ver. 2-5, AmeriFlux AMP, (Dataset). https://doi.org/10.17190/AMF/2001305

Site ID	Citation
US-INi	Kenneth Davis (2023), AmeriFlux BASE US-INi INFLUX - Agricultural Site East of Indianapolis (Site-9a), Ver. 1-5, AmeriFlux AMP, (Dataset). https://doi.org/10.17190/AMF/2001306
US-INj	Kenneth Davis (2023), AmeriFlux BASE US-INj INFLUX - Agricultural Site East of Indianapolis (Site-9b), Ver. 1-5, AmeriFlux AMP, (Dataset). https://doi.org/10.17190/AMF/2001307
US-INn	Kenneth Davis (2023), AmeriFlux BASE US-INn INFLUX - Agricultural Site West of Indianapolis (Site-14a), Ver. 1-5, AmeriFlux AMP, (Dataset). https://doi.org/10.17190/AMF/2001308
US-INp	Kenneth Davis (2023), AmeriFlux BASE US-INp INFLUX - Agricultural Site West of Indianapolis (Site-14b) , Ver. 1-5, AmeriFlux AMP, (Dataset). https://doi.org/10.17190/AMF/2001309
US-Jo1	Craig Tweedie (2024), AmeriFlux BASE US-Jo1 Jornada Experimental Range Bajada Site, Ver. 4-5, AmeriFlux AMP, (Dataset). https://doi.org/10.17190/AMF/1767833
US-Jo2	Enrique R. Vivoni, Eli R. Perez-Ruiz (2022), AmeriFlux BASE US-Jo2 Jornada Experimental Range Mixed Shrubland, Ver. 2-5, AmeriFlux AMP, (Dataset). https://doi.org/10.17190/AMF/1617696
US-JRn	Derek Johnson, Gil Bohrer, Jaclyn Hatala Matthes (2020), AmeriFlux BASE US-JRn WV Jacks Run, Ver. 1-5, AmeriFlux AMP, (Dataset). https://doi.org/10.17190/AMF/1617714
US-KFS	Nathaniel Brunsell (2020), AmeriFlux BASE US-KFS Kansas Field Station, Ver. 7-5, AmeriFlux AMP, (Dataset). https://doi.org/10.17190/AMF/1246132
US-KL1	G. Philip Robertson, Jiquan Chen (2022), AmeriFlux BASE US-KL1 KBS Lux Arbor Reserve Corn, Ver. 3-5, AmeriFlux AMP, (Dataset). https://doi.org/10.17190/AMF/1660344
US-KL2	G. Philip Robertson, Jiquan Chen (2022), AmeriFlux BASE US-KL2 KBS Lux Arbor Reserve Switchgrass, Ver. 4-5, AmeriFlux AMP, (Dataset). https://doi.org/10.17190/AMF/1644212
US-KL3	G. Philip Robertson, Jiquan Chen (2022), AmeriFlux BASE US-KL3 KBS Lux Arbor Reserve Prairie, Ver. 4-5, AmeriFlux AMP, (Dataset). https://doi.org/10.17190/AMF/1647438
US-KLS	Nathaniel Brunsell (2021), AmeriFlux BASE US-KLS Kansas Land Institute, Ver. 2-5, AmeriFlux AMP, (Dataset). https://doi.org/10.17190/AMF/1498745
US-KM1	G. Philip Robertson, Jiquan Chen (2022), AmeriFlux BASE US-KM1 KBS Marshall Farms Corn, Ver. 4-5, AmeriFlux AMP, (Dataset). https://doi.org/10.17190/AMF/1647439
US-KM2	G. Philip Robertson, Jiquan Chen (2022), AmeriFlux BASE US-KM2 KBS Marshall Farms Prairie, Ver. 4-5, AmeriFlux AMP, (Dataset). https://doi.org/10.17190/AMF/1647440
US-KM3	G. Philip Robertson, Jiquan Chen (2022), AmeriFlux BASE US-KM3 KBS Marshall Farms Switchgrass, Ver. 3-5, AmeriFlux AMP, (Dataset). https://doi.org/10.17190/AMF/1660345
US-KM4	G. Philip Robertson, Jiquan Chen (2022), AmeriFlux BASE US-KM4 KBS Marshall Farms Smooth Brome Grass (Ref), Ver. 5-5, AmeriFlux AMP, (Dataset). https://doi.org/10.17190/AMF/1634882
US-Kon	Nathaniel Brunsell (2020), AmeriFlux BASE US-Kon Konza Prairie LTER (KNZ), Ver. 5-5, AmeriFlux AMP, (Dataset). https://doi.org/10.17190/AMF/1246068
US-KPL	Patrick Sullivan (2023), AmeriFlux BASE US-KPL Lily Lake Fen, Ver. 2-5, AmeriFlux AMP, (Dataset). https://doi.org/10.17190/AMF/1865478
US-KS1	Bert Drake, Ross Hinkle, Rosvel Bracho, Thomas Powell, Sabina Dore (2019), AmeriFlux BASE US-KS1 Kennedy Space Center (slash pine), Ver. 3-5, AmeriFlux AMP, (Dataset). https://doi.org/10.17190/AMF/1246069
US-KS2	Bert Drake, Ross Hinkle, Rosvel Bracho, Sabina Dore, Thomas Powell (2019), AmeriFlux BASE US-KS2 Kennedy Space Center (scrub oak), Ver. 3-5, AmeriFlux AMP, (Dataset). https://doi.org/10.17190/AMF/1246070
US-KS3	Rosvel Bracho, Charles Ross Hinkle (2019), AmeriFlux BASE US-KS3 Kennedy Space Center (salt marsh), Ver. 1-5, AmeriFlux AMP, (Dataset). https://doi.org/10.17190/AMF/1562390
US-KUT	Joe McFadden (2016), AmeriFlux BASE US-KUT KUOM Turfgrass Field, Ver. 1-1, AmeriFlux AMP, (Dataset). https://doi.org/10.17190/AMF/1246145
US-LA1	Ken Krauss (2019), AmeriFlux BASE US-LA1 Pointe-aux-Chenes Brackish Marsh, Ver. 2-5, AmeriFlux AMP, (Dataset). https://doi.org/10.17190/AMF/1543386
US-LA2	Eric Ward, Sergio Merino, Camille Stagg, Ken Krauss (2025), AmeriFlux BASE US-LA2 Salvador WMA Freshwater Marsh, Ver. 4-5, AmeriFlux AMP, (Dataset). https://doi.org/10.17190/AMF/1543387
US-LA3	Eric Ward, Sergio Merino, Camille Stagg, Ken Krauss (2025), AmeriFlux BASE US-LA3 Barataria Bay Saline Marsh, Ver. 2-5, AmeriFlux AMP, (Dataset). https://doi.org/10.17190/AMF/2229156
US-Lin	Silvano Fares (2019), AmeriFlux BASE US-Lin Lindcove Orange Orchard, Ver. 2-5, AmeriFlux AMP, (Dataset). https://doi.org/10.17190/AMF/1246830
US-LL1	Gregory Starr (2021), AmeriFlux BASE US-LL1 Longleaf Pine - Baker (Mesic site), Ver. 2-5, AmeriFlux AMP, (Dataset). https://doi.org/10.17190/AMF/1773395
US-LL2	Gregory Starr (2021), AmeriFlux BASE US-LL2 Longleaf Pine - Dubignion (Intermediate site), Ver. 1-5, AmeriFlux AMP, (Dataset). https://doi.org/10.17190/AMF/1773396
US-LL3	Gregory Starr (2021), AmeriFlux BASE US-LL3 Longleaf Pine - Red Dirt (Xeric site), Ver. 1-5, AmeriFlux AMP, (Dataset). https://doi.org/10.17190/AMF/1773397
US-Los	Ankur Desai (2025), AmeriFlux BASE US-Los Lost Creek, Ver. 32-5, AmeriFlux AMP, (Dataset). https://doi.org/10.17190/AMF/1246071

Site ID	Citation
US-LS1	Russell Scott (2020), AmeriFlux BASE US-LS1 San Pedro River Lewis Springs Sacaton Grassland, Ver. 1-5, AmeriFlux AMP, (Dataset). https://doi.org/10.17190/AMF/1660346
US-LS2	Russell Scott (2020), AmeriFlux BASE US-LS2 San Pedro River Lewis Springs Savanna, Ver. 1-5, AmeriFlux AMP, (Dataset). https://doi.org/10.17190/AMF/1660347
US-MBP	Tyler Roman, Andrew C. Hill, Randy Kolka, Timothy Griffis, Julian Deventer (2025), AmeriFlux BASE US-MBP Marcell Bog Lake Peatland, Ver. 5-5, AmeriFlux AMP, (Dataset). https://doi.org/10.17190/AMF/1767835
US-MC1	Paul Stoy, Jessica Torrion (2020), AmeriFlux BASE US-MC1 Creston, Montana pivot-irrigated spring wheat, Ver. 1-5, AmeriFlux AMP, (Dataset). https://doi.org/10.17190/AMF/1660348
US-MC2	Paul Stoy, Jessica Torrion (2021), AmeriFlux BASE US-MC2 Creston, Montana pivot-irrigated spring wheat 2, Ver. 1-5, AmeriFlux AMP, (Dataset). https://doi.org/10.17190/AMF/1829506
US-Me1	Bev Law (2019), AmeriFlux BASE US-Me1 Metolius - Eyerly burn, Ver. 3-5, AmeriFlux AMP, (Dataset). https://doi.org/10.17190/AMF/1246074
US-Me2	Bev Law (2025), AmeriFlux BASE US-Me2 Metolius mature ponderosa pine, Ver. 21-5, AmeriFlux AMP, (Dataset). https://doi.org/10.17190/AMF/1246076
US-Me3	Bev Law (2018), AmeriFlux BASE US-Me3 Metolius-second young aged pine, Ver. 4-5, AmeriFlux AMP, (Dataset). https://doi.org/10.17190/AMF/1246077
US-Me4	Bev Law (2025), AmeriFlux BASE US-Me4 Metolius-old aged ponderosa pine, Ver. 7-5, AmeriFlux AMP, (Dataset). https://doi.org/10.17190/AMF/1246078
US-Me5	Bev Law (2021), AmeriFlux BASE US-Me5 Metolius-first young aged pine, Ver. 3-5, AmeriFlux AMP, (Dataset). https://doi.org/10.17190/AMF/1246079
US-Me6	Bev Law (2025), AmeriFlux BASE US-Me6 Metolius Young Pine Burn, Ver. 18-5, AmeriFlux AMP, (Dataset). https://doi.org/10.17190/AMF/1246128
US-Me7	Chad Hanson, Chris Still (2024), AmeriFlux BASE US-Me7 Metolius Low Burn Severity Subcanopy, Ver. 1-5, AmeriFlux AMP, (Dataset). https://doi.org/10.17190/AMF/2331381
US-MEF	John Frank (2025), AmeriFlux BASE US-MEF Manitou Experimental Forest, Ver. 1-5, AmeriFlux AMP, (Dataset). https://doi.org/10.17190/AMF/2567984
US-Men	Ankur Desai (2018), AmeriFlux BASE US-Men Lake Mendota, Center for Limnology Site, Ver. 3-5, AmeriFlux AMP, (Dataset). https://doi.org/10.17190/AMF/1433375
US-MH1	Paul Stoy, Kent McVay (2020), AmeriFlux BASE US-MH1 Huntley, Montana irrigated barley site 1, Ver. 1-5, AmeriFlux AMP, (Dataset). https://doi.org/10.17190/AMF/1660349
US-MH2	Paul Stoy, Kent McVay (2021), AmeriFlux BASE US-MH2 Huntley, Montana irrigated barley site 2, Ver. 1-5, AmeriFlux AMP, (Dataset). https://doi.org/10.17190/AMF/1825938
US-Mi1	Sarah Goslee (2022), AmeriFlux BASE US-Mi1 LTAR UCB (Upper Chesapeake Bay) Miscanthus 1, Ver. 1-5, AmeriFlux AMP, (Dataset). https://doi.org/10.17190/AMF/1865479
US-Mi2	Sarah Goslee (2022), AmeriFlux BASE US-Mi2 LTAR UCB (Upper Chesapeake Bay) Miscanthus 2, Ver. 1-5, AmeriFlux AMP, (Dataset). https://doi.org/10.17190/AMF/1865480
US-Mi3	Sarah Goslee (2022), AmeriFlux BASE US-Mi3 LTAR UCB (Upper Chesapeake Bay) Miscanthus 3, Ver. 1-5, AmeriFlux AMP, (Dataset). https://doi.org/10.17190/AMF/1865481
US-Mj1	Paul C. Stoy, Elizabeth Vick (2020), AmeriFlux BASE US-Mj1 Montana Judith Basin wheat field, Ver. 1-5, AmeriFlux AMP, (Dataset). https://doi.org/10.17190/AMF/1617715
US-Mj2	Paul C. Stoy, Elizabeth Vick (2020), AmeriFlux BASE US-Mj2 Montana Judith Basin summer fallow field, Ver. 1-5, AmeriFlux AMP, (Dataset). https://doi.org/10.17190/AMF/1617716
US-MMS	Kim Novick, Rich Phillips (2025), AmeriFlux BASE US-MMS Morgan Monroe State Forest, Ver. 29-5, AmeriFlux AMP, (Dataset). https://doi.org/10.17190/AMF/1246080
US-MN1	Christina Helseth, Jane Johnson (2025), AmeriFlux BASE US-MN1 Morris: Corn-Soybean with Cover Crops, Strip Tillage, Ver. 2-5, AmeriFlux AMP, (Dataset). https://doi.org/10.17190/AMF/2407204
US-MN2	Christina Helseth, Jane Johnson (2025), AmeriFlux BASE US-MN2 Morris: Corn-Soybean-Wheat with Cover Crops, Minimal Tillage, Ver. 2-5, AmeriFlux AMP, (Dataset). https://doi.org/10.17190/AMF/2407205
US-MN3	Christina Helseth, Jane Johnson (2025), AmeriFlux BASE US-MN3 Morris: Corn-Soybean, Conventional Tillage, Ver. 2-5, AmeriFlux AMP, (Dataset). https://doi.org/10.17190/AMF/2407206
US-Mo1	Adam Schreiner-McGraw (2025), AmeriFlux BASE US-Mo1 LTAR CMRB Field 1 (CMRB ASP), Ver. 4-5, AmeriFlux AMP, (Dataset). https://doi.org/10.17190/AMF/1870588
US-Mo2	Adam Schreiner-McGraw (2025), AmeriFlux BASE US-Mo2 LTAR CMRB Tucker Prairie (CMRB TP), Ver. 4-5, AmeriFlux AMP, (Dataset). https://doi.org/10.17190/AMF/1902276
US-Mo3	Adam Schreiner-McGraw (2024), AmeriFlux BASE US-Mo3 LTAR CMRB Field 3 (CMRB BAU), Ver. 3-5, AmeriFlux AMP, (Dataset). https://doi.org/10.17190/AMF/1870589
US-MOz	Jeffrey Wood, Lianhong Gu (2022), AmeriFlux BASE US-MOz Missouri Ozark Site, Ver. 11-5, AmeriFlux AMP, (Dataset). https://doi.org/10.17190/AMF/1246081
US-Mpj	Marcy Litvak (2024), AmeriFlux BASE US-Mpj Mountainair Pinyon-Juniper Woodland, Ver. 25-5, AmeriFlux AMP, (Dataset). https://doi.org/10.17190/AMF/1246123
US-MSR	Paul Stoy (2022), AmeriFlux BASE US-MSR Montana Sun River winter wheat , Ver. 3-5, AmeriFlux AMP, (Dataset). https://doi.org/10.17190/AMF/1617717

Site ID	Citation
US-MtB	Greg Barron-Gafford (2025), AmeriFlux BASE US-MtB Mt Bigelow, Ver. 5-5, AmeriFlux AMP, (Dataset). https://doi.org/10.17190/AMF/1579717
US-MVF	Paul Stoy (2021), AmeriFlux BASE US-MVF Montana Vaughn Fallow, Ver. 1-5, AmeriFlux AMP, (Dataset). https://doi.org/10.17190/AMF/1829507
US-MVW	Paul Stoy (2021), AmeriFlux BASE US-MVW Montana Vaughn Wheat, Ver. 1-5, AmeriFlux AMP, (Dataset). https://doi.org/10.17190/AMF/1829508
US-Myb	Jaclyn Hatala Matthes, Cove Sturtevant, Patty Oikawa, Samuel D Chamberlain, Daphne Szutu, Ariane Arias-Ortiz, Joseph Verfaillie, Dennis Baldocchi (2025), AmeriFlux BASE US-Myb Mayberry Wetland, Ver. 15-5, AmeriFlux AMP, (Dataset). https://doi.org/10.17190/AMF/1246139
US-NC1	Asko Noormets, Ge Sun, Michael Gavazzi, Steve McNulty, Jean-Christophe Domec, John King (2018), AmeriFlux BASE US-NC1 NC_Clearcut, Ver. 3-5, AmeriFlux AMP, (Dataset). https://doi.org/10.17190/AMF/1246082
US-NC2	Asko Noormets, Ge Sun, Michael Gavazzi, Jean-Christophe Domec, Steve McNulty, Guofang Miao, Maricar Aguilos, Bhaskar Mitra, Kevan Minick, John King, Linqing Yang, Prajaya Prajapati (2025), AmeriFlux BASE US-NC2 NC_Loblolly Plantation, Ver. 18-5, AmeriFlux AMP, (Dataset). https://doi.org/10.17190/AMF/1246083
US-NC3	Asko Noormets, Michael Gavazzi, Maricar Aguilos, John King, Bhaskar Mitra, Jean-Christophe Domec (2022), AmeriFlux BASE US-NC3 NC_Clearcut#3, Ver. 4-5, AmeriFlux AMP, (Dataset). https://doi.org/10.17190/AMF/1419506
US-NC4	Asko Noormets, John King, Bhaskar Mitra, Guofang Miao, Maricar Aguilos, Kevan Minick, Prajaya Prajapati, Jean-Christophe Domec (2025), AmeriFlux BASE US-NC4 NC_AlligatorRiver, Ver. 7-5, AmeriFlux AMP, (Dataset). https://doi.org/10.17190/AMF/1480314
US-Ne1	Andy Suyker (2025), AmeriFlux BASE US-Ne1 Mead - irrigated continuous maize site, Ver. 19-5, AmeriFlux AMP, (Dataset). https://doi.org/10.17190/AMF/1246084
US-Ne2	Andy Suyker (2024), AmeriFlux BASE US-Ne2 Mead - irrigated maize-soybean rotation site, Ver. 18-5, AmeriFlux AMP, (Dataset). https://doi.org/10.17190/AMF/1246085
US-Ne3	Andy Suyker (2025), AmeriFlux BASE US-Ne3 Mead - rainfed maize-soybean rotation site, Ver. 19-5, AmeriFlux AMP, (Dataset). https://doi.org/10.17190/AMF/1246086
US-NGB	Margaret Torn, Sigrid Dengel (2023), AmeriFlux BASE US-NGB NGEE Arctic Barrow, Ver. 5-5, AmeriFlux AMP, (Dataset). https://doi.org/10.17190/AMF/1436326
US-NGC	Margaret Torn, Sigrid Dengel (2023), AmeriFlux BASE US-NGC NGEE Arctic Council, Ver. 3-5, AmeriFlux AMP, (Dataset). https://doi.org/10.17190/AMF/1634883
US-NMj	Jiquan Chen (2019), AmeriFlux BASE US-NMj Northern Michigan Jack Pine Stand, Ver. 3-5, AmeriFlux AMP, (Dataset). https://doi.org/10.17190/AMF/1246087
US-NR1	Peter D. Blanken, Russel K. Monson, Sean P. Burns, David R. Bowling, Andrew A. Turnipseed (2025), AmeriFlux BASE US-NR1 Niwot Ridge Forest (LTER NWT1), Ver. 23-5, AmeriFlux AMP, (Dataset). https://doi.org/10.17190/AMF/1246088
US-NR3	John Knowles (2025), AmeriFlux BASE US-NR3 Niwot Ridge Alpine (T-Van West), Ver. 6-5, AmeriFlux AMP, (Dataset). https://doi.org/10.17190/AMF/1804491
US-NR4	John Knowles (2025), AmeriFlux BASE US-NR4 Niwot Ridge Alpine (T-Van East), Ver. 6-5, AmeriFlux AMP, (Dataset). https://doi.org/10.17190/AMF/1804492
US-Oho	Jiquan Chen, Housen Chu, Asko Noormets (2021), AmeriFlux BASE US-Oho Oak Openings, Ver. 7-5, AmeriFlux AMP, (Dataset). https://doi.org/10.17190/AMF/1246089
US-ONA	Maria L. Silveira, Rosvel Bracho (2024), AmeriFlux BASE US-ONA Florida pine flatwoods, Ver. 4-5, AmeriFlux AMP, (Dataset). https://doi.org/10.17190/AMF/1660350
US-OPE	Joe Alfieri (2024), AmeriFlux BASE US-OPE Optimizing Production Inputs for Economic and Environmental Enhancement (OPE3), Ver. 1-5, AmeriFlux AMP, (Dataset). https://doi.org/10.17190/AMF/2315769
US-ORv	Gil Bohrer (2020), AmeriFlux BASE US-ORv Olentangy River Wetland Research Park, Ver. 3-5, AmeriFlux AMP, (Dataset). https://doi.org/10.17190/AMF/1246135
US-OWC	Gil Bohrer, Janice Kerns (2024), AmeriFlux BASE US-OWC Old Woman Creek, Ver. 5-5, AmeriFlux AMP, (Dataset). https://doi.org/10.17190/AMF/1418679
US-PAS	Rosvel Bracho, Maria L. Silveira (2023), AmeriFlux BASE US-PAS Florida, Paspalum notatum pasture, Ver. 2-5, AmeriFlux AMP, (Dataset). https://doi.org/10.17190/AMF/1870590
US-PFa	Ankur Desai (2025), AmeriFlux BASE US-PFa Park Falls/WLEF, Ver. 31-5, AmeriFlux AMP, (Dataset). https://doi.org/10.17190/AMF/1246090
US-PFb	Ankur Desai, Brian Butterworth, Steven Oncley (2020), AmeriFlux BASE US-PFb NW1 Pine-1 CHEESEHEAD 2019, Ver. 1-5, AmeriFlux AMP, (Dataset). https://doi.org/10.17190/AMF/1717850
US-PFc	Ankur Desai, Brian Butterworth, Steven Oncley (2020), AmeriFlux BASE US-PFc NW2 Aspen-1 CHEESEHEAD 2019, Ver. 1-5, AmeriFlux AMP, (Dataset). https://doi.org/10.17190/AMF/1717851
US-PFd	Ankur Desai, Brian Butterworth, Steven Oncley (2020), AmeriFlux BASE US-PFd NW3 Tussock-1 CHEESEHEAD 2019, Ver. 1-5, AmeriFlux AMP, (Dataset). https://doi.org/10.17190/AMF/1717852
US-PFe	Ankur Desai, Brian Butterworth, Steven Oncley (2020), AmeriFlux BASE US-PFe NW4 Lake-1 CHEESEHEAD 2019, Ver. 1-5, AmeriFlux AMP, (Dataset). https://doi.org/10.17190/AMF/1717853

Site ID	Citation
US-PFf	Ankur Desai, Brian Butterworth, Jonathan Thom, Paul Stoy (2025), AmeriFlux BASE US-PFf NW5 Grass-1 CHEESEHEAD 2019, Ver. 2-5, AmeriFlux AMP, (Dataset). https://doi.org/10.17190/AMF/1890484
US-PFg	Ankur Desai, Brian Butterworth, Steven Oncley (2020), AmeriFlux BASE US-PFg NE1 Pine-2 CHEESEHEAD 2019, Ver. 1-5, AmeriFlux AMP, (Dataset). https://doi.org/10.17190/AMF/1717854
US-PFh	Ankur Desai, Brian Butterworth, Steven Oncley (2020), AmeriFlux BASE US-PFh NE2 Pine-3 CHEESEHEAD 2019, Ver. 1-5, AmeriFlux AMP, (Dataset). https://doi.org/10.17190/AMF/1717855
US-PFi	Ankur Desai, Brian Butterworth, Steven Oncley (2020), AmeriFlux BASE US-PFi NE3 Hardwood-1 CHEESEHEAD 2019, Ver. 1-5, AmeriFlux AMP, (Dataset). https://doi.org/10.17190/AMF/1717856
US-PFj	Ankur Desai, Brian Butterworth, Steven Oncley (2020), AmeriFlux BASE US-PFj NE4 Maple-1 CHEESEHEAD 2019, Ver. 1-5, AmeriFlux AMP, (Dataset). https://doi.org/10.17190/AMF/1717857
US-PFk	Ankur Desai, Brian Butterworth, Steven Oncley (2020), AmeriFlux BASE US-PFk SW1 Aspen-2 CHEESEHEAD 2019, Ver. 1-5, AmeriFlux AMP, (Dataset). https://doi.org/10.17190/AMF/1717858
US-PFL	Ankur Desai, Brian Butterworth, Steven Oncley (2020), AmeriFlux BASE US-PFL SW2 Aspen-3 CHEESEHEAD 2019, Ver. 1-5, AmeriFlux AMP, (Dataset). https://doi.org/10.17190/AMF/1717859
US-PFm	Ankur Desai, Brian Butterworth, Steven Oncley (2020), AmeriFlux BASE US-PFm SW3 Hardwood-2 CHEESEHEAD 2019, Ver. 1-5, AmeriFlux AMP, (Dataset). https://doi.org/10.17190/AMF/1717860
US-PFn	Ankur Desai, Brian Butterworth, Steven Oncley (2020), AmeriFlux BASE US-PFn SW4 Hardwood-3 CHEESEHEAD 2019, Ver. 1-5, AmeriFlux AMP, (Dataset). https://doi.org/10.17190/AMF/1717861
US-PFo	Ankur Desai, Brian Butterworth, Jonathan Thom, Paul Stoy (2022), AmeriFlux BASE US-PFo SE1 Lake-2 CHEESEHEAD 2019, Ver. 1-5, AmeriFlux AMP, (Dataset). https://doi.org/10.17190/AMF/1880912
US-PFp	Ankur Desai, Brian Butterworth, Steven Oncley (2020), AmeriFlux BASE US-PFp SE2 Hardwood-4 CHEESEHEAD 2019, Ver. 1-5, AmeriFlux AMP, (Dataset). https://doi.org/10.17190/AMF/1717862
US-PFq	Ankur Desai, Brian Butterworth, Steven Oncley (2020), AmeriFlux BASE US-PFq SE3 Aspen-4 CHEESEHEAD 2019, Ver. 1-5, AmeriFlux AMP, (Dataset). https://doi.org/10.17190/AMF/1717863
US-PFr	Ankur Desai, Brian Butterworth, Steven Oncley (2020), AmeriFlux BASE US-PFr SE4 Tussock-2 CHEESEHEAD 2019, Ver. 1-5, AmeriFlux AMP, (Dataset). https://doi.org/10.17190/AMF/1717864
US-PFs	Ankur Desai, Brian Butterworth, Steven Oncley (2020), AmeriFlux BASE US-PFs SE5 Aspen-5 CHEESEHEAD 2019, Ver. 1-5, AmeriFlux AMP, (Dataset). https://doi.org/10.17190/AMF/1717865
US-PFt	Ankur Desai, Brian Butterworth, Steven Oncley (2020), AmeriFlux BASE US-PFt SE6 Pine-4 CHEESEHEAD 2019, Ver. 1-5, AmeriFlux AMP, (Dataset). https://doi.org/10.17190/AMF/1717866
US-PHM	Anne Giblin (2021), AmeriFlux BASE US-PHM Plum Island High Marsh, Ver. 3-5, AmeriFlux AMP, (Dataset). https://doi.org/10.17190/AMF/1543377
US-Pnp	Ankur Desai (2023), AmeriFlux BASE US-Pnp Lake Mendota, Picnic Point Site, Ver. 8-5, AmeriFlux AMP, (Dataset). https://doi.org/10.17190/AMF/1433376
US-Prr	Go Iwahana, Hideki Kobayashi, Hiroki Ikawa, Rikie Suzuki (2023), AmeriFlux BASE US-Prr Poker Flat Research Range Black Spruce Forest, Ver. 4-5, AmeriFlux AMP, (Dataset). https://doi.org/10.17190/AMF/1246153
US-PSH	Ray G. Anderson (2020), AmeriFlux BASE US-PSH USSL San Joaquin Valley Pistachio High, Ver. 1-5, AmeriFlux AMP, (Dataset). https://doi.org/10.17190/AMF/1617719
US-PSL	Ray G. Anderson (2020), AmeriFlux BASE US-PSL USSL San Joaquin Valley Pistachio Low, Ver. 1-5, AmeriFlux AMP, (Dataset). https://doi.org/10.17190/AMF/1617720
US-RC1	Jinshu Chi, Brian Lamb, Shelley Pressley (2021), AmeriFlux BASE US-RC1 Cook Agronomy Farm - No Till, Ver. 2-5, AmeriFlux AMP, (Dataset). https://doi.org/10.17190/AMF/1498748
US-RC2	Jinshu Chi, Brian Lamb, Shelley Pressley (2021), AmeriFlux BASE US-RC2 Cook Agronomy Farm - Conventional Till, Ver. 2-5, AmeriFlux AMP, (Dataset). https://doi.org/10.17190/AMF/1498747
US-RC3	Jinshu Chi, Brian Lamb, Shelley Pressley (2021), AmeriFlux BASE US-RC3 WSU Lind Dryland Research Station, Ver. 2-5, AmeriFlux AMP, (Dataset). https://doi.org/10.17190/AMF/1498749
US-RC4	Jinshu Chi, Brian Lamb, Shelley Pressley (2021), AmeriFlux BASE US-RC4 Moscow Mountain on-farm site, Ver. 2-5, AmeriFlux AMP, (Dataset). https://doi.org/10.17190/AMF/1498750
US-RC5	Jinshu Chi, Brian Lamb, Shelley Pressley (2021), AmeriFlux BASE US-RC5 Moses Lake on-farm site, Ver. 2-5, AmeriFlux AMP, (Dataset). https://doi.org/10.17190/AMF/1498751
US-RGA	Michael R. Schuppenhauer, Sebastien C. Biraud, Stephen Chan (2025), AmeriFlux BASE US-RGA Arkansas Corn Farm, Ver. 4-5, AmeriFlux AMP, (Dataset). https://doi.org/10.17190/AMF/1880913
US-RGB	Michael Schuppenhauer, Sebastien C. Biraud, Stephen Chan (2025), AmeriFlux BASE US-RGB Butte County Rice Farm, Ver. 5-5, AmeriFlux AMP, (Dataset). https://doi.org/10.17190/AMF/1870591
US-RGF	Michael R. Schuppenhauer, Sebastien C. Biraud, Stephen Chan (2025), AmeriFlux BASE US-RGF Stanislaus County Forage Farm, Ver. 3-5, AmeriFlux AMP, (Dataset). https://doi.org/10.17190/AMF/2001310
US-RGo	Michael R. Schuppenhauer, Sebastien C. Biraud, Stephen Chan (2025), AmeriFlux BASE US-RGo Glenn County Organic Rice Farm, Ver. 4-5, AmeriFlux AMP, (Dataset). https://doi.org/10.17190/AMF/1880914
US-RGW	Michael R. Schuppenhauer, Sebastien C. Biraud, Stephen Chan (2025), AmeriFlux BASE US-RGW Desha County Rice Farm, Ver. 4-5, AmeriFlux AMP, (Dataset). https://doi.org/10.17190/AMF/1880915
US-Rls	Gerald Flerchinger (2025), AmeriFlux BASE US-Rls RCEW Low Sagebrush, Ver. 7-5, AmeriFlux AMP, (Dataset). https://doi.org/10.17190/AMF/1418682

Site ID	Citation
US-Rms	Gerald Flerchinger (2025), AmeriFlux BASE US-Rms RCEW Mountain Big Sagebrush, Ver. 7-5, AmeriFlux AMP, (Dataset). https://doi.org/10.17190/AMF/1375202
US-Ro1	John Baker, Tim Griffis, Timothy Griffis (2018), AmeriFlux BASE US-Ro1 Rosemount- G21, Ver. 5-5, AmeriFlux AMP, (Dataset). https://doi.org/10.17190/AMF/1246092
US-Ro2	John Baker, Tim Griffis (2023), AmeriFlux BASE US-Ro2 Rosemount- C7, Ver. 2-5, AmeriFlux AMP, (Dataset). https://doi.org/10.17190/AMF/1418683
US-Ro3	John Baker, Tim Griffis (2019), AmeriFlux BASE US-Ro3 Rosemount- G19, Ver. 4-5, AmeriFlux AMP, (Dataset). https://doi.org/10.17190/AMF/1246093
US-Ro4	John Baker, Tim Griffis (2024), AmeriFlux BASE US-Ro4 Rosemount Prairie, Ver. 26-5, AmeriFlux AMP, (Dataset). https://doi.org/10.17190/AMF/1419507
US-Ro5	John Baker, Tim Griffis (2024), AmeriFlux BASE US-Ro5 Rosemount I18_South, Ver. 26-5, AmeriFlux AMP, (Dataset). https://doi.org/10.17190/AMF/1419508
US-Ro6	John Baker, Tim Griffis (2024), AmeriFlux BASE US-Ro6 Rosemount I18_North, Ver. 26-5, AmeriFlux AMP, (Dataset). https://doi.org/10.17190/AMF/1419509
US-Rpf	Masahito Ueyama, Hiroki Iwata, Yoshinobu Harazono (2025), AmeriFlux BASE US-Rpf Poker Flat Research Range: Succession from fire scar to deciduous forest, Ver. 11-5, AmeriFlux AMP, (Dataset). https://doi.org/10.17190/AMF/1579540
US-RRC	Lisa Haber, Katrina Poppe (2024), AmeriFlux BASE US-RRC Rice Rivers Center Marsh, Ver. 2-5, AmeriFlux AMP, (Dataset). https://doi.org/10.17190/AMF/2331382
US-Rwe	Gerald Flerchinger, Michele L. Reba (2020), AmeriFlux BASE US-Rwe RCEW Reynolds Mountain East, Ver. 1-5, AmeriFlux AMP, (Dataset). https://doi.org/10.17190/AMF/1617721
US-Rwf	Gerald Flerchinger (2025), AmeriFlux BASE US-Rwf RCEW Upper Sheep Prescibed Fire, Ver. 5-5, AmeriFlux AMP, (Dataset). https://doi.org/10.17190/AMF/1617724
US-Rws	Gerald Flerchinger (2025), AmeriFlux BASE US-Rws Reynolds Creek Wyoming big sagebrush, Ver. 7-5, AmeriFlux AMP, (Dataset). https://doi.org/10.17190/AMF/1375201
US-Sag	Akira Miyata, Yoshinobu Harazono (2023), AmeriFlux BASE US-Sag Sag River, Ver. 1-5, AmeriFlux AMP, (Dataset). https://doi.org/10.17190/AMF/1987604
US-SdH	Dave Billesbach, Tim J. Arkebauer (2016), AmeriFlux BASE US-SdH Nebraska SandHills Dry Valley, Ver. 1-1, AmeriFlux AMP, (Dataset). https://doi.org/10.17190/AMF/1246136
US-Seg	Marcy Litvak (2025), AmeriFlux BASE US-Seg Sevilleta grassland, Ver. 26-5, AmeriFlux AMP, (Dataset). https://doi.org/10.17190/AMF/1246124
US-Ses	Marcy Litvak (2025), AmeriFlux BASE US-Ses Sevilleta shrubland, Ver. 26-5, AmeriFlux AMP, (Dataset). https://doi.org/10.17190/AMF/1246125
US-SHC	Sebastian Wolf (2025), AmeriFlux BASE US-SHC Sagehen Creek Field Station, Ver. 1-5, AmeriFlux AMP, (Dataset). https://doi.org/10.17190/AMF/2567985
US-Slt	Ken Clark (2025), AmeriFlux BASE US-Slt Silas Little- New Jersey, Ver. 6-5, AmeriFlux AMP, (Dataset). https://doi.org/10.17190/AMF/1246096
US-Snd	Matteo Detto, Cove Sturtevant, Patty Oikawa, Joseph Verfaillie, Dennis Baldocchi (2016), AmeriFlux BASE US-Snd Sherman Island, Ver. 2-1, AmeriFlux AMP, (Dataset). https://doi.org/10.17190/AMF/1246094
US-Sne	Robert Shortt, Kyle Hemes, Daphne Szutu, Joseph Verfaillie, Dennis Baldocchi (2021), AmeriFlux BASE US-Sne Sherman Island Restored Wetland, Ver. 7-5, AmeriFlux AMP, (Dataset). https://doi.org/10.17190/AMF/1418684
US-Snf	Kuno Kusak, Camilo Rey Sanchez, Daphne Szutu, Dennis Baldocchi (2020), AmeriFlux BASE US-Snf Sherman Barn, Ver. 3-5, AmeriFlux AMP, (Dataset). https://doi.org/10.17190/AMF/1579718
US-SP1	Rosvel Bracho, Timothy A. Martin (2023), AmeriFlux BASE US-SP1 Slashpine-Austin Cary- 65yrs nat regen, Ver. 5-5, AmeriFlux AMP, (Dataset). https://doi.org/10.17190/AMF/1246100
US-SP2	Rosvel Bracho, Timothy Martin (2016), AmeriFlux BASE US-SP2 Slashpine-Mize-clearcut-3yr,regen, Ver. 3-1, AmeriFlux AMP, (Dataset). https://doi.org/10.17190/AMF/1246101
US-SP3	Rosvel Bracho, Timothy Martin (2016), AmeriFlux BASE US-SP3 Slashpine-Donaldson-mid-rot- 12yrs, Ver. 3-1, AmeriFlux AMP, (Dataset). https://doi.org/10.17190/AMF/1246102
US-SP4	Rosvel Bracho, Timothy A. Martin (2019), AmeriFlux BASE US-SP4 Slashpine-Rayonier-mid-rot- 12yrs, Ver. 3-5, AmeriFlux AMP, (Dataset). https://doi.org/10.17190/AMF/1246103
US-SRC	Shirley Kurc (2019), AmeriFlux BASE US-SRC Santa Rita Creosote, Ver. 6-5, AmeriFlux AMP, (Dataset). https://doi.org/10.17190/AMF/1246127
US-SRG	Russell Scott (2025), AmeriFlux BASE US-SRG Santa Rita Grassland, Ver. 18-5, AmeriFlux AMP, (Dataset). https://doi.org/10.17190/AMF/1246154
US-SRM	Russell Scott (2025), AmeriFlux BASE US-SRM Santa Rita Mesquite, Ver. 29-5, AmeriFlux AMP, (Dataset). https://doi.org/10.17190/AMF/1246104
US-Srr	Brian Bergamaschi, Lisamarie Windham-Myers (2018), AmeriFlux BASE US-Srr Suisun marsh - Rush Ranch, Ver. 1-5, AmeriFlux AMP, (Dataset). https://doi.org/10.17190/AMF/1418685
US-SRS	Enrique R. Vivoni (2022), AmeriFlux BASE US-SRS Santa Rita Savanna, Ver. 3-5, AmeriFlux AMP, (Dataset). https://doi.org/10.17190/AMF/1660351

Site ID	Citation
US-SSH	Brandon R. Forsythe, Jason Horne, Kenneth J. Davis (2022), AmeriFlux BASE US-SSH Susquehanna Shale Hills Critical Zone Observatory, Ver. 1-5, AmeriFlux AMP, (Dataset). https://doi.org/10.17190/AMF/1880916
US-Sta	Brent Ewers, Elise Pendall (2019), AmeriFlux BASE US-Sta Saratoga, Ver. 2-5, AmeriFlux AMP, (Dataset). https://doi.org/10.17190/AMF/1246831
US-StJ	Rodrigo Vargas (2020), AmeriFlux BASE US-StJ St Jones Reserve, Ver. 2-5, AmeriFlux AMP, (Dataset). https://doi.org/10.17190/AMF/1480316
US-SuM	Dong Wang, Ray Anderson (2019), AmeriFlux BASE US-SuM Maui Sugarcane Middle, Ver. 2-5, AmeriFlux AMP, (Dataset). https://doi.org/10.17190/AMF/1246158
US-SuS	Dong Wang, Ray Anderson (2019), AmeriFlux BASE US-SuS Maui Sugarcane Lee/Sheltered, Ver. 2-5, AmeriFlux AMP, (Dataset). https://doi.org/10.17190/AMF/1246159
US-SuW	Dong Wang, Ray Anderson (2019), AmeriFlux BASE US-SuW Maui Sugarcane Windy, Ver. 2-5, AmeriFlux AMP, (Dataset). https://doi.org/10.17190/AMF/1246157
US-Syv	Ankur Desai (2025), AmeriFlux BASE US-Syv Sylvania Wilderness Area, Ver. 30-5, AmeriFlux AMP, (Dataset). https://doi.org/10.17190/AMF/1246106
US-TaS	Sparkle Malone, Tiffany Troxler (2024), AmeriFlux BASE US-TaS Taylor Slough/Panhandle, Ver. 1-5, AmeriFlux AMP, (Dataset). https://doi.org/10.17190/AMF/2331383
US-TEF	Paul Stoy (2024), AmeriFlux BASE US-TEF Tenderfoot Creek Experimental Forest, Ver. 1-5, AmeriFlux AMP, (Dataset). https://doi.org/10.17190/AMF/2315770
US-TLR	Camilo Rey-Sanchez (2025), AmeriFlux BASE US-TLR Timberlake Observatory for Wetland Restoration (TOWeR), Ver. 1-5, AmeriFlux AMP, (Dataset). https://doi.org/10.17190/AMF/2531147
US-Ton	Siyan Ma, Liukang Xu, Joseph Verfaillie, Dennis Baldocchi (2025), AmeriFlux BASE US-Ton Tonzi Ranch, Ver. 23-5, AmeriFlux AMP, (Dataset). https://doi.org/10.17190/AMF/1245971
US-TrB	Paul Stoy, Ankur Desai, Hilary Dugan, Paul Schramm (2025), AmeriFlux BASE US-TrB Trout Bog, Ver. 2-5, AmeriFlux AMP, (Dataset). https://doi.org/10.17190/AMF/1804493
US-TrS	Paul Stoy, Ankur Desai, Hilary Dugan, Paul Schramm (2025), AmeriFlux BASE US-TrS Trout Lake Area South Sparkling Bog, Ver. 2-5, AmeriFlux AMP, (Dataset). https://doi.org/10.17190/AMF/1825939
US-Tur	Paul Stoy, Adam Cook, John Dore (2025), AmeriFlux BASE US-Tur Turner Ranch, Ver. 2-5, AmeriFlux AMP, (Dataset). https://doi.org/10.17190/AMF/1825940
US-Tw1	Alex Valach, Robert Shortt, Daphne Szutu, Elke Eichelmann, Sara Knox, Kyle Hemes, Joseph Verfaillie, Dennis Baldocchi (2024), AmeriFlux BASE US-Tw1 Twitchell Wetland West Pond, Ver. 11-5, AmeriFlux AMP, (Dataset). https://doi.org/10.17190/AMF/1246147
US-Tw2	Cove Sturtevant, Joseph Verfaillie, Dennis Baldocchi (2019), AmeriFlux BASE US-Tw2 Twitchell Corn, Ver. 2-5, AmeriFlux AMP, (Dataset). https://doi.org/10.17190/AMF/1246148
US-Tw3	Samuel D Chamberlain, Patty Oikawa, Cove Sturtevant, Daphne Szutu, Joseph Verfaillie, Dennis Baldocchi (2018), AmeriFlux BASE US-Tw3 Twitchell Alfalfa, Ver. 5-5, AmeriFlux AMP, (Dataset). https://doi.org/10.17190/AMF/1246149
US-Tw4	Elke Eichelmann, Robert Shortt, Sara Knox, Camilo Rey Sanchez, Alex Valach, Cove Sturtevant, Daphne Szutu, Joseph Verfaillie, Dennis Baldocchi (2024), AmeriFlux BASE US-Tw4 Twitchell East End Wetland, Ver. 14-5, AmeriFlux AMP, (Dataset). https://doi.org/10.17190/AMF/1246151
US-Tw5	Alex Valach, Kuno Kasak, Daphne Szutu, Joseph Verfaillie, Dennis Baldocchi (2020), AmeriFlux BASE US-Tw5 East Pond Wetland, Ver. 3-5, AmeriFlux AMP, (Dataset). https://doi.org/10.17190/AMF/1543380
US-Twt	Sara Knox, Jaclyn Hatala Matthes, Joseph Verfaillie, Dennis Baldocchi (2023), AmeriFlux BASE US-Twt Twitchell Island, Ver. 7-5, AmeriFlux AMP, (Dataset). https://doi.org/10.17190/AMF/1246140
US-Uaf	Masahito Ueyama, Hiroki Iwata, Yoshinobu Harazono (2025), AmeriFlux BASE US-Uaf University of Alaska, Fairbanks, Ver. 13-5, AmeriFlux AMP, (Dataset). https://doi.org/10.17190/AMF/1480322
US-UC1	Sarah Goslee (2025), AmeriFlux BASE US-UC1 LTAR UCB (Upper Chesapeake Bay) EC1, Ver. 5-5, AmeriFlux AMP, (Dataset). https://doi.org/10.17190/AMF/1865482
US-UC2	Sarah Goslee (2025), AmeriFlux BASE US-UC2 LTAR UCB (Upper Chesapeake Bay) EC2, Ver. 5-5, AmeriFlux AMP, (Dataset). https://doi.org/10.17190/AMF/1865483
US-UiA	Carl Bernacchi, Bethany Blakely, Caitlin Moore, Taylor Pederson (2025), AmeriFlux BASE US-UiA University of Illinois Switchgrass, Ver. 3-5, AmeriFlux AMP, (Dataset). https://doi.org/10.17190/AMF/1617725
US-UiB	Carl J Bernacchi, Bethany Blakely, Caitlin Moore, Taylor Pederson (2025), AmeriFlux BASE US-UiB University of Illinois Miscanthus, Ver. 3-5, AmeriFlux AMP, (Dataset). https://doi.org/10.17190/AMF/1846664
US-UiC	Carl J Bernacchi, Bethany Blakely, Caitlin Moore, Taylor Pederson (2022), AmeriFlux BASE US-UiC University of Illinois Maize-Soy, Ver. 1-5, AmeriFlux AMP, (Dataset). https://doi.org/10.17190/AMF/1846665
US-UiD	Carl Bernacchi, Bethany Blakely, Caitlin Moore, Taylor Pederson (2025), AmeriFlux BASE US-UiD University of Illinois Restored Native Prairie, Ver. 2-5, AmeriFlux AMP, (Dataset). https://doi.org/10.17190/AMF/1987605
US-UiE	Carl J Bernacchi (2025), AmeriFlux BASE US-UiE University of Illinois Sorghum-Soy, Ver. 1-5, AmeriFlux AMP, (Dataset). https://doi.org/10.17190/AMF/2567986
US-UM3	Gil Bohrer (2018), AmeriFlux BASE US-UM3 Douglas Lake, Ver. 1-5, AmeriFlux AMP, (Dataset). https://doi.org/10.17190/AMF/1480315

Site ID	Citation
US-UMB	Christopher Gough, Gil Bohrer, Peter Curtis (2025), AmeriFlux BASE US-UMB Univ. of Mich. Biological Station, Ver. 22-5, AmeriFlux AMP, (Dataset). https://doi.org/10.17190/AMF/1246107
US-UMd	Christopher Gough, Gil Bohrer, Peter Curtis (2025), AmeriFlux BASE US-UMd UMBS Disturbance, Ver. 17-5, AmeriFlux AMP, (Dataset). https://doi.org/10.17190/AMF/1246134
US-UTB	Kathryn Ladig, Paul Inkenbrandt (2024), AmeriFlux BASE US-UTB UFLUX Bonneville Salt Flats, Ver. 2-5, AmeriFlux AMP, (Dataset). https://doi.org/10.17190/AMF/2001311
US-UTD	Paul Inkenbrandt (2025), AmeriFlux BASE US-UTD UFLUX Dugout Ranch, Ver. 1-5, AmeriFlux AMP, (Dataset). https://doi.org/10.17190/AMF/2531148
US-UTE	Paul Inkenbrandt (2025), AmeriFlux BASE US-UTE UFLUX Escalante, Ver. 1-5, AmeriFlux AMP, (Dataset). https://doi.org/10.17190/AMF/2531149
US-UTJ	Paul Inkenbrandt (2025), AmeriFlux BASE US-UTJ UFLUX Bluff, Ver. 1-5, AmeriFlux AMP, (Dataset). https://doi.org/10.17190/AMF/2531150
US-UTM	Kathryn Ladig, Paul Inkenbrandt (2025), AmeriFlux BASE US-UTM UFLUX Matheson, Ver. 1-5, AmeriFlux AMP, (Dataset). https://doi.org/10.17190/AMF/2507521
US-UTN	Paul Inkenbrandt (2023), AmeriFlux BASE US-UTN UFLUX Nephi, Ver. 1-5, AmeriFlux AMP, (Dataset). https://doi.org/10.17190/AMF/2204058
US-UTP	Paul Inkenbrandt (2025), AmeriFlux BASE US-UTP UFLUX Great Salt Lake Phragmites, Ver. 1-5, AmeriFlux AMP, (Dataset). https://doi.org/10.17190/AMF/2531151
US-UTV	Kathryn Ladig, Paul Inkenbrandt (2025), AmeriFlux BASE US-UTV UFLUX Desert View, Ver. 1-5, AmeriFlux AMP, (Dataset). https://doi.org/10.17190/AMF/2531152
US-UTW	Kathryn Ladig, Paul Inkenbrandt (2025), AmeriFlux BASE US-UTW UFLUX Wellington, Ver. 1-5, AmeriFlux AMP, (Dataset). https://doi.org/10.17190/AMF/2507522
US-Var	Siyan Ma, Liukang Xu, Joseph Verfaillie, Dennis Baldocchi (2025), AmeriFlux BASE US-Var Vaira Ranch-Ione, Ver. 23-5, AmeriFlux AMP, (Dataset). https://doi.org/10.17190/AMF/1245984
US-Vcm	Marcy Litvak (2024), AmeriFlux BASE US-Vcm Valles Caldera Mixed Conifer, Ver. 26-5, AmeriFlux AMP, (Dataset). https://doi.org/10.17190/AMF/1246121
US-Vcp	Marcy Litvak (2025), AmeriFlux BASE US-Vcp Valles Caldera Ponderosa Pine, Ver. 25-5, AmeriFlux AMP, (Dataset). https://doi.org/10.17190/AMF/1246122
US-Vcs	Marcy Litvak (2025), AmeriFlux BASE US-Vcs Valles Caldera Sulphur Springs Mixed Conifer, Ver. 18-5, AmeriFlux AMP, (Dataset). https://doi.org/10.17190/AMF/1418681
US-VT1	Kesondra Key, Kim Novick (2025), AmeriFlux BASE US-VT1 Vermillion Tributary Paired Cropland â€“ Site 1 (Corn/Soy; No Cover Crops), Ver. 1-5, AmeriFlux AMP, (Dataset). https://doi.org/10.17190/AMF/2567994
US-VT2	Kesondra Key, Kim Novick (2025), AmeriFlux BASE US-VT2 Vermillion Tributary Paired Cropland â€“ Site 2 (Corn/Soy; Cover Crops), Ver. 1-5, AmeriFlux AMP, (Dataset). https://doi.org/10.17190/AMF/2567995
US-WCr	Ankur Desai (2025), AmeriFlux BASE US-WCr Willow Creek, Ver. 32-5, AmeriFlux AMP, (Dataset). https://doi.org/10.17190/AMF/1246111
US-Whs	Russ Scott (2025), AmeriFlux BASE US-Whs Walnut Gulch Lucky Hills Shrub, Ver. 25-5, AmeriFlux AMP, (Dataset). https://doi.org/10.17190/AMF/1246113
US-Wi0	Jiquan Chen (2020), AmeriFlux BASE US-Wi0 Young red pine (YRP), Ver. 3-5, AmeriFlux AMP, (Dataset). https://doi.org/10.17190/AMF/1246016
US-Wi1	Jiquan Chen (2020), AmeriFlux BASE US-Wi1 Intermediate hardwood (IHW), Ver. 3-5, AmeriFlux AMP, (Dataset). https://doi.org/10.17190/AMF/1246015
US-Wi2	Jiquan Chen (2020), AmeriFlux BASE US-Wi2 Intermediate red pine (IRP), Ver. 3-5, AmeriFlux AMP, (Dataset). https://doi.org/10.17190/AMF/1246017
US-Wi3	Jiquan Chen (2020), AmeriFlux BASE US-Wi3 Mature hardwood (MHW), Ver. 3-5, AmeriFlux AMP, (Dataset). https://doi.org/10.17190/AMF/1246018
US-Wi4	Jiquan Chen (2020), AmeriFlux BASE US-Wi4 Mature red pine (MRP), Ver. 3-5, AmeriFlux AMP, (Dataset). https://doi.org/10.17190/AMF/1246019
US-Wi5	Jiquan Chen (2020), AmeriFlux BASE US-Wi5 Mixed young jack pine (MYJP), Ver. 3-5, AmeriFlux AMP, (Dataset). https://doi.org/10.17190/AMF/1246020
US-Wi6	Jiquan Chen (2020), AmeriFlux BASE US-Wi6 Pine barrens #1 (PB1), Ver. 3-5, AmeriFlux AMP, (Dataset). https://doi.org/10.17190/AMF/1246021
US-Wi7	Jiquan Chen (2020), AmeriFlux BASE US-Wi7 Red pine clearcut (RPCC), Ver. 3-5, AmeriFlux AMP, (Dataset). https://doi.org/10.17190/AMF/1246022
US-Wi8	Jiquan Chen (2020), AmeriFlux BASE US-Wi8 Young hardwood clearcut (YHW), Ver. 3-5, AmeriFlux AMP, (Dataset). https://doi.org/10.17190/AMF/1246023
US-Wi9	Jiquan Chen (2020), AmeriFlux BASE US-Wi9 Young Jack pine (YJP), Ver. 3-5, AmeriFlux AMP, (Dataset). https://doi.org/10.17190/AMF/1246024
US-Wjs	Marcy Litvak (2025), AmeriFlux BASE US-Wjs Willard Juniper Savannah, Ver. 25-5, AmeriFlux AMP, (Dataset). https://doi.org/10.17190/AMF/1246120
US-Wkg	Russell Scott (2025), AmeriFlux BASE US-Wkg Walnut Gulch Kendall Grasslands, Ver. 25-5, AmeriFlux AMP, (Dataset). https://doi.org/10.17190/AMF/1246112

Site ID	Citation
US-Wlr	David Cook, Richard L. Coulter (2018), AmeriFlux BASE US-Wlr Walnut River Watershed (Smileyburg), Ver. 4-5, AmeriFlux AMP, (Dataset). https://doi.org/10.17190/AMF/1246115
US-WPT	Jiquan Chen, Housen Chu (2019), AmeriFlux BASE US-WPT Winous Point North Marsh, Ver. 4-5, AmeriFlux AMP, (Dataset). https://doi.org/10.17190/AMF/1246155
US-Wrc	Sonia Wharton (2016), AmeriFlux BASE US-Wrc Wind River Crane Site, Ver. 8-1, AmeriFlux AMP, (Dataset). https://doi.org/10.17190/AMF/1246114
US-WT1	Craig Bednarz (2025), AmeriFlux BASE US-WT1 Kress, TX no-till cotton and grain sorghum production, Ver. 2-5, AmeriFlux AMP, (Dataset). https://doi.org/10.17190/AMF/2407207
US-xAB	NEON (National Ecological Observatory Network) (2025), AmeriFlux BASE US-xAB NEON Abby Road (ABBY), Ver. 10-5, AmeriFlux AMP, (Dataset). https://doi.org/10.17190/AMF/1617726
US-xAE	NEON (National Ecological Observatory Network) (2025), AmeriFlux BASE US-xAE NEON Klemme Range Research Station (OAES), Ver. 9-5, AmeriFlux AMP, (Dataset). https://doi.org/10.17190/AMF/1671891
US-xBA	NEON (National Ecological Observatory Network) (2025), AmeriFlux BASE US-xBA NEON Barrow Environmental Observatory (BARR), Ver. 9-5, AmeriFlux AMP, (Dataset). https://doi.org/10.17190/AMF/1671892
US-xBL	NEON (National Ecological Observatory Network) (2025), AmeriFlux BASE US-xBL NEON Blandy Experimental Farm (BLAN), Ver. 9-5, AmeriFlux AMP, (Dataset). https://doi.org/10.17190/AMF/1671893
US-xBN	NEON (National Ecological Observatory Network) (2025), AmeriFlux BASE US-xBN NEON Caribou Creek - Poker Flats Watershed (BONA), Ver. 10-5, AmeriFlux AMP, (Dataset). https://doi.org/10.17190/AMF/1617727
US-xBR	NEON (National Ecological Observatory Network) (2025), AmeriFlux BASE US-xBR NEON Bartlett Experimental Forest (BART), Ver. 10-5, AmeriFlux AMP, (Dataset). https://doi.org/10.17190/AMF/1579542
US-xCL	NEON (National Ecological Observatory Network) (2025), AmeriFlux BASE US-xCL NEON LBJ National Grassland (CLBJ), Ver. 9-5, AmeriFlux AMP, (Dataset). https://doi.org/10.17190/AMF/1671894
US-xCP	NEON (National Ecological Observatory Network) (2025), AmeriFlux BASE US-xCP NEON Central Plains Experimental Range (CPER), Ver. 10-5, AmeriFlux AMP, (Dataset). https://doi.org/10.17190/AMF/1579720
US-xDC	NEON (National Ecological Observatory Network) (2025), AmeriFlux BASE US-xDC NEON Dakota Coteau Field School (DCFS), Ver. 10-5, AmeriFlux AMP, (Dataset). https://doi.org/10.17190/AMF/1617728
US-xDJ	NEON (National Ecological Observatory Network) (2025), AmeriFlux BASE US-xDJ NEON Delta Junction (DEJU), Ver. 10-5, AmeriFlux AMP, (Dataset). https://doi.org/10.17190/AMF/1634884
US-xDL	NEON (National Ecological Observatory Network) (2025), AmeriFlux BASE US-xDL NEON Dead Lake (DELA), Ver. 10-5, AmeriFlux AMP, (Dataset). https://doi.org/10.17190/AMF/1579721
US-xDS	NEON (National Ecological Observatory Network) (2025), AmeriFlux BASE US-xDS NEON Disney Wilderness Preserve (DSNY), Ver. 9-5, AmeriFlux AMP, (Dataset). https://doi.org/10.17190/AMF/1671895
US-xGR	NEON (National Ecological Observatory Network) (2025), AmeriFlux BASE US-xGR NEON Great Smoky Mountains National Park, Twin Creeks (GRSM), Ver. 10-5, AmeriFlux AMP, (Dataset). https://doi.org/10.17190/AMF/1634885
US-xHA	NEON (National Ecological Observatory Network) (2025), AmeriFlux BASE US-xHA NEON Harvard Forest (HARV), Ver. 11-5, AmeriFlux AMP, (Dataset). https://doi.org/10.17190/AMF/1562391
US-xHE	NEON (National Ecological Observatory Network) (2025), AmeriFlux BASE US-xHE NEON Healy (HEAL), Ver. 10-5, AmeriFlux AMP, (Dataset). https://doi.org/10.17190/AMF/1617729
US-xJE	NEON (National Ecological Observatory Network) (2025), AmeriFlux BASE US-xJE NEON Jones Ecological Research Center (JERC), Ver. 10-5, AmeriFlux AMP, (Dataset). https://doi.org/10.17190/AMF/1617730
US-xJR	NEON (National Ecological Observatory Network) (2025), AmeriFlux BASE US-xJR NEON Jornada LTER (JORN), Ver. 10-5, AmeriFlux AMP, (Dataset). https://doi.org/10.17190/AMF/1617731
US-xKA	NEON (National Ecological Observatory Network) (2025), AmeriFlux BASE US-xKA NEON Konza Prairie Biological Station - Relocatable (KONA), Ver. 10-5, AmeriFlux AMP, (Dataset). https://doi.org/10.17190/AMF/1579722
US-xKZ	NEON (National Ecological Observatory Network) (2025), AmeriFlux BASE US-xKZ NEON Konza Prairie Biological Station (KONZ), Ver. 11-5, AmeriFlux AMP, (Dataset). https://doi.org/10.17190/AMF/1562392
US-xLE	NEON (National Ecological Observatory Network) (2025), AmeriFlux BASE US-xLE NEON Lenoir Landing (LENO), Ver. 8-5, AmeriFlux AMP, (Dataset). https://doi.org/10.17190/AMF/1773398
US-xMB	NEON (National Ecological Observatory Network) (2025), AmeriFlux BASE US-xMB NEON Moab (MOAB), Ver. 9-5, AmeriFlux AMP, (Dataset). https://doi.org/10.17190/AMF/1671896
US-xML	NEON (National Ecological Observatory Network) (2025), AmeriFlux BASE US-xML NEON Mountain Lake Biological Station (MLBS), Ver. 9-5, AmeriFlux AMP, (Dataset). https://doi.org/10.17190/AMF/1671897
US-xNG	NEON (National Ecological Observatory Network) (2025), AmeriFlux BASE US-xNG NEON Northern Great Plains Research Laboratory (NOGP), Ver. 10-5, AmeriFlux AMP, (Dataset). https://doi.org/10.17190/AMF/1617732
US-xNQ	NEON (National Ecological Observatory Network) (2025), AmeriFlux BASE US-xNQ NEON Onaqui-Ault (ONAQ), Ver. 10-5, AmeriFlux AMP, (Dataset). https://doi.org/10.17190/AMF/1617733

Site ID	Citation
US-xNW	NEON (National Ecological Observatory Network) (2025), AmeriFlux BASE US-xNW NEON Niwot Ridge Mountain Research Station (NIWO), Ver. 9-5, AmeriFlux AMP, (Dataset). https://doi.org/10.17190/AMF/1671898
US-xPU	NEON (National Ecological Observatory Network) (2025), AmeriFlux BASE US-xPU NEON Pu'u Maka'ala Natural Area Reserve (PUUM), Ver. 8-5, AmeriFlux AMP, (Dataset). https://doi.org/10.17190/AMF/1773399
US-xRM	NEON (National Ecological Observatory Network) (2025), AmeriFlux BASE US-xRM NEON Rocky Mountain National Park, CASTNET (RMNP), Ver. 10-5, AmeriFlux AMP, (Dataset). https://doi.org/10.17190/AMF/1579723
US-xRN	NEON (National Ecological Observatory Network) (2025), AmeriFlux BASE US-xRN NEON Oak Ridge National Lab (ORNL), Ver. 8-5, AmeriFlux AMP, (Dataset). https://doi.org/10.17190/AMF/1773400
US-xSB	NEON (National Ecological Observatory Network) (2025), AmeriFlux BASE US-xSB NEON Ordway-Swisher Biological Station (OSBS), Ver. 9-5, AmeriFlux AMP, (Dataset). https://doi.org/10.17190/AMF/1671899
US-xSC	NEON (National Ecological Observatory Network) (2025), AmeriFlux BASE US-xSC NEON Smithsonian Conservation Biology Institute (SCBI), Ver. 9-5, AmeriFlux AMP, (Dataset). https://doi.org/10.17190/AMF/1671900
US-xSE	NEON (National Ecological Observatory Network) (2025), AmeriFlux BASE US-xSE NEON Smithsonian Environmental Research Center (SERC), Ver. 10-5, AmeriFlux AMP, (Dataset). https://doi.org/10.17190/AMF/1617734
US-xSJ	NEON (National Ecological Observatory Network) (2025), AmeriFlux BASE US-xSJ NEON San Joaquin Experimental Range (SJER), Ver. 9-5, AmeriFlux AMP, (Dataset). https://doi.org/10.17190/AMF/1671901
US-xSL	NEON (National Ecological Observatory Network) (2025), AmeriFlux BASE US-xSL NEON North Sterling, CO (STER), Ver. 10-5, AmeriFlux AMP, (Dataset). https://doi.org/10.17190/AMF/1617735
US-xSP	NEON (National Ecological Observatory Network) (2025), AmeriFlux BASE US-xSP NEON Soaproot Saddle (SOAP), Ver. 10-5, AmeriFlux AMP, (Dataset). https://doi.org/10.17190/AMF/1617736
US-xSR	NEON (National Ecological Observatory Network) (2025), AmeriFlux BASE US-xSR NEON Santa Rita Experimental Range (SRER), Ver. 10-5, AmeriFlux AMP, (Dataset). https://doi.org/10.17190/AMF/1579543
US-xST	NEON (National Ecological Observatory Network) (2025), AmeriFlux BASE US-xST NEON Steigerwaldt Land Services (STEI), Ver. 10-5, AmeriFlux AMP, (Dataset). https://doi.org/10.17190/AMF/1617737
US-xTA	NEON (National Ecological Observatory Network) (2025), AmeriFlux BASE US-xTA NEON Talladega National Forest (TALL), Ver. 9-5, AmeriFlux AMP, (Dataset). https://doi.org/10.17190/AMF/1671902
US-xTE	NEON (National Ecological Observatory Network) (2025), AmeriFlux BASE US-xTE NEON Lower Teakettle (TEAK), Ver. 10-5, AmeriFlux AMP, (Dataset). https://doi.org/10.17190/AMF/1617738
US-xTL	NEON (National Ecological Observatory Network) (2025), AmeriFlux BASE US-xTL NEON Toolik (TOOL), Ver. 10-5, AmeriFlux AMP, (Dataset). https://doi.org/10.17190/AMF/1617739
US-xTR	NEON (National Ecological Observatory Network) (2025), AmeriFlux BASE US-xTR NEON Treehaven (TREE), Ver. 10-5, AmeriFlux AMP, (Dataset). https://doi.org/10.17190/AMF/1634886
US-xUK	NEON (National Ecological Observatory Network) (2025), AmeriFlux BASE US-xUK NEON The University of Kansas Field Station (UKFS), Ver. 10-5, AmeriFlux AMP, (Dataset). https://doi.org/10.17190/AMF/1617740
US-xUN	NEON (National Ecological Observatory Network) (2025), AmeriFlux BASE US-xUN NEON University of Notre Dame Environmental Research Center (UNDE), Ver. 10-5, AmeriFlux AMP, (Dataset). https://doi.org/10.17190/AMF/1617741
US-xWD	NEON (National Ecological Observatory Network) (2025), AmeriFlux BASE US-xWD NEON Woodworth (WOOD), Ver. 10-5, AmeriFlux AMP, (Dataset). https://doi.org/10.17190/AMF/1579724
US-xWR	NEON (National Ecological Observatory Network) (2025), AmeriFlux BASE US-xWR NEON Wind River Experimental Forest (WREF), Ver. 10-5, AmeriFlux AMP, (Dataset). https://doi.org/10.17190/AMF/1617742
US-xYE	NEON (National Ecological Observatory Network) (2025), AmeriFlux BASE US-xYE NEON Yellowstone Northern Range (Frog Rock) (YELL), Ver. 10-5, AmeriFlux AMP, (Dataset). https://doi.org/10.17190/AMF/1617743
US-YK1	Susan Natali (2024), AmeriFlux BASE US-YK1 Yukon-Kuskokwim Delta, Izaviknek-Kingaglia uplands, Burned 2015, Ver. 1-5, AmeriFlux AMP, (Dataset). https://doi.org/10.17190/AMF/2331384
US-YK2	Sue Natali (2025), AmeriFlux BASE US-YK2 Yukon-Kuskokwim Delta, Izaviknek-Kingaglia uplands, Unburned, Ver. 2-5, AmeriFlux AMP, (Dataset). https://doi.org/10.17190/AMF/2331385

Appendix D Other Figures and Charts

Figure D1: Spatial Variation in CO_2 Anomalies within a Growing Season, 2019

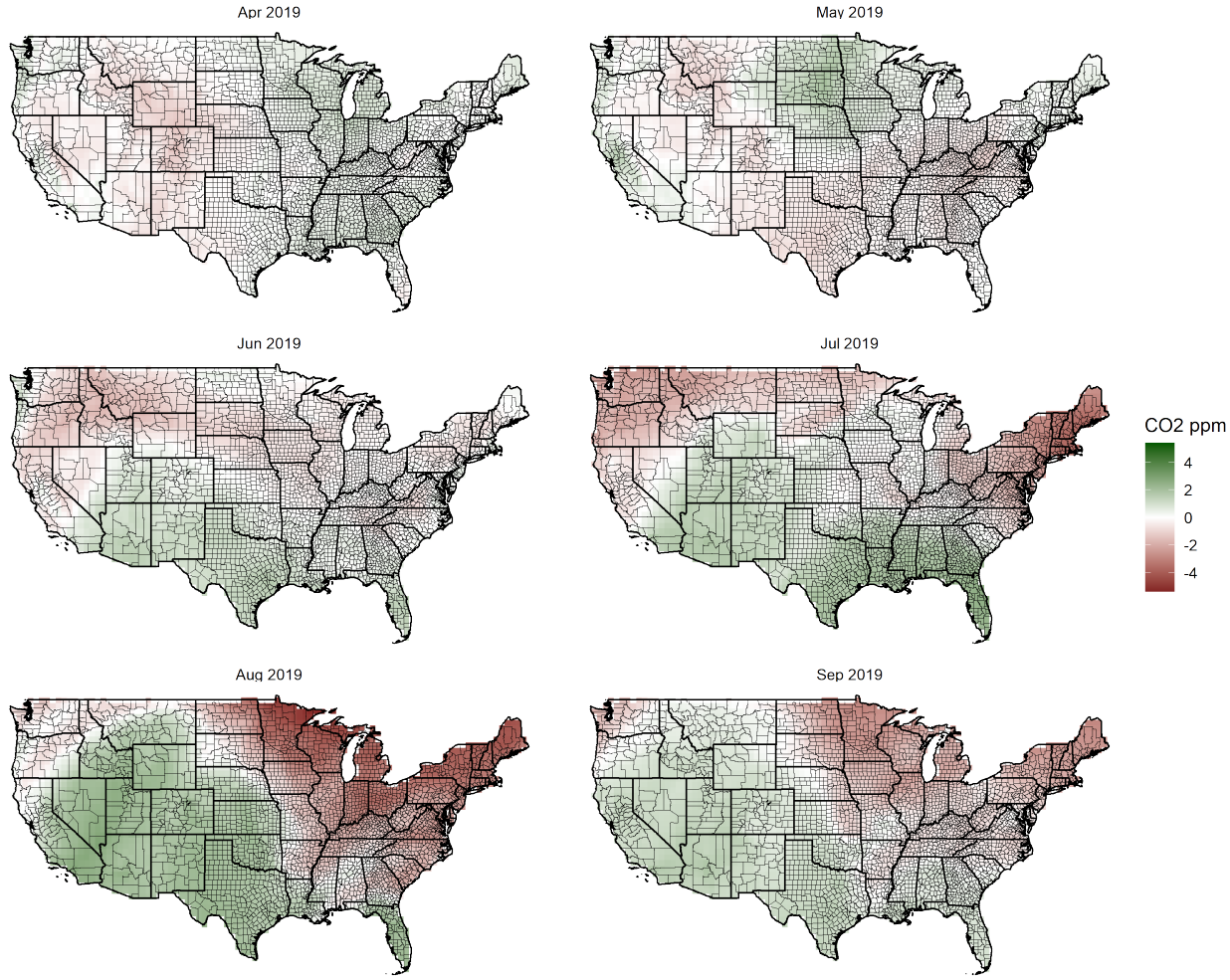

Notes: The figure displays CO_2 anomalies relative to the mean value on the first day of each month during the 2019 growing season, using OCO-2's GEOS Level 3 daily modeled product (Weir and Ott, 2022). While our analysis uses the non-interpolated Level 2 satellite measurements, this figure shows the smoothed spatial extent of the anomalies using the Level 3 product.

Figure D2: Annual Trends in NDVI Vegetation from the AVHRR Satellite, 1982-2013

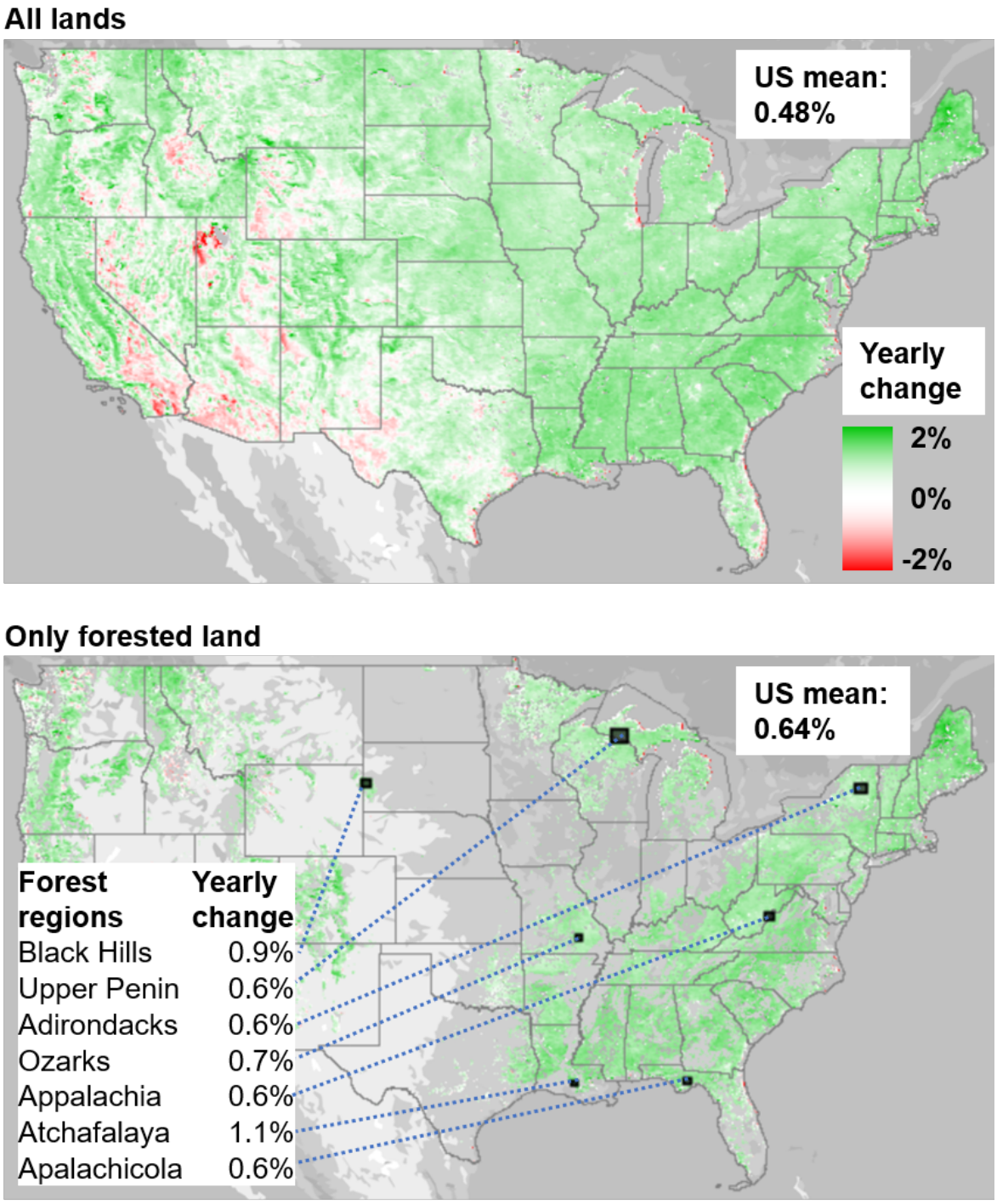

Notes: The figure displays 30 m pixel-level linear trends in log NDVI values by year for the six months of the growing season (April to September) over 31 years from 1982 to 2013, using AVHRR satellite data (Vermote et al., 2014). Map visualization and calculations were produced using Google Earth Engine.